A Nonlinear Magnetic Controller for Three-Axis Stability of Nanosatellites

Kristin L. Makovec

Thesis submitted to the Faculty of the
Virginia Polytechnic Institute and State University
in partial fulfillment of the requirements for the degree of

Master of Science
in
Aerospace Engineering

Dr. Christopher Hall, Chair
Dr. Frederick Lutze, Committee Member
Dr. Mary Kasarda, Committee Member

July 23, 2001
Blacksburg, Virginia

Keywords: Spacecraft Attitude Dynamics, Magnetic Control, Three-Axis Stability

A Nonlinear Magnetic Controller for Three-Axis Stability of Nanosatellites

Kristin L. Makovec

(ABSTRACT)

The problem of magnetic control for three-axis stability of a spacecraft is examined. Two controllers, a proportional-derivative controller and a constant coefficient linear quadratic regulator, are applied to the system of equations describing the motion of the spacecraft. The stability of each is checked for different spacecraft configurations through simulations, and the results for gravity-gradient stable and non gravity-gradient stable spacecraft are compared. An optimization technique is implemented in an attempt to obtain the best performance from the controller. For every spacecraft configuration, a set of gains can be chosen for implementation in the controller that stabilizes the linear and nonlinear equations of motion for the spacecraft.

Contents

Abstract **ii**

Table of Contents **iii**

List of Figures **viii**

List of Tables **xi**

Nomenclature **xii**

1 Introduction **1**

1.1 Problem Statement 1

1.2 Prior Work in Magnetic Attitude Control 1

1.3 Approach and Results 4

1.4 Outline of Thesis 5

2 Earth's Magnetic Field **6**

2.1 Magnetic Fields 6

2.1.1 Origin and Equations 6

2.1.2 Characteristics 8

2.2 Origin and Effects of the Earth's Magnetic Field 10

2.2.1 Geomagnetic Field 10

2.2.2 Origin of the Magnetic Field 14

2.2.3 Variations in the Magnetic Field 14

2.2.4 Effects of the Earth's Magnetic Field on Spacecraft 19
2.3 Theory and Mathematical Models 20
2.3.1 Coordinate Systems 20
2.3.2 Analytic Models 21
2.3.3 Accuracy of Models 26
2.4 Measuring Magnetic Fields 27
2.4.1 Measurement Hardware 27
2.4.2 Magnetic Field Measurement of Celestial Bodies 31
2.4.3 Data Collection for the IGRF 32
2.5 Magnetic Fields of Other Bodies 32
2.5.1 Reasons for Examination 33
2.5.2 Interstellar Magnetic Field 33
2.5.3 Celestial Bodies 33
2.6 Summary 38

3 Spacecraft Dynamics **39**
3.1 Orbit Dynamics 39
3.1.1 Keplerian Orbits 39
3.1.2 Coordinate Systems 45
3.2 Attitude Dynamics 48
3.2.1 Reference Frames 48
3.2.2 Rotations 49
3.2.3 Angular Velocity 50
3.3 Equations of Motion 51
3.3.1 Dynamic Equations of Motion 51
3.3.2 Kinematic Equations of Motion 52
3.4 Environmental Disturbance Torques 53
3.4.1 Gravity-Gradient Torque 54
3.4.2 Magnetic Torque 54

3.5 Attitude Determination 54
3.5.1 Magnetometers 55
3.5.2 Earth Sensors 56
3.5.3 Sun Sensors 56
3.5.4 Star Trackers 56
3.5.5 Gyroscopes 56
3.6 Attitude Control 56
3.6.1 Spin Stabilization 57
3.6.2 Three-axis Stabilization 57
3.6.3 Passive Control 58
3.7 Summary 59

4 Spacecraft Magnetic Field Interactions 60
4.1 Magnetic Torques 60
4.1.1 Magnetic Torque Origins 60
4.1.2 Magnetic Disturbance Torques 63
4.1.3 Magnetic Control Torques 66
4.2 Magnetic Control Hardware 68
4.2.1 Torque Coils 68
4.2.2 Torque Rods 68
4.2.3 Permanent Magnets 68
4.3 Magnetic Field and Orbit Interaction 68
4.3.1 Equatorial Orbits 69
4.3.2 Polar Orbits 69
4.3.3 Circular Orbits 69
4.4 Time to Slew 71
4.5 Summary 72

5 Control Laws 73

5.1 Equations of Motion . . . 73
5.1.1 Nonlinear Equations of Motion . . . 73
5.1.2 Desired Equilibrium Attitude . . . 74
5.1.3 Linearized Equations of Motion Using Euler Angles . . . 74
5.1.4 Linearized Equations of Motion Using Quaternions . . . 76
5.1.5 Quasi-Periodic Nature of Equations of Motion . . . 78
5.1.6 Average Value Linearized Equations of Motion . . . 79
5.1.7 Summary . . . 80
5.2 Control Laws . . . 80
5.2.1 Proportional-Derivative Controller . . . 80
5.2.2 Constant Coefficient Linear Quadratic Regulator . . . 80
5.2.3 Application of Floquet Theory . . . 81
5.2.4 Optimization of Q . . . 82
5.2.5 Implementation of Gains in Nonlinear System . . . 82
5.3 Summary . . . 83

6 Simulation Results **84**

6.1 Simulation Parameters . . . 84
6.1.1 Inputs . . . 84
6.1.2 Outputs . . . 85
6.2 System With No Magnetic Control . . . 85
6.3 Magnetic Control with Gravity Gradient Stability . . . 87
6.3.1 P-D Controller . . . 87
6.3.2 Constant Coefficient Linear Quadratic Regulator . . . 89
6.4 Magnetic Control Without Gravity Gradient Stability . . . 91
6.4.1 P-D Controller . . . 91
6.4.2 Constant Coefficient Linear Quadratic Regulator . . . 93
6.5 Optimization of Q . . . 97
6.5.1 Gravity-Gradient Stable . . . 97

6.5.2 Non Gravity-Gradient Stable . . . 98
6.6 Inverted Spacecraft . . . 104
6.7 Summary . . . 105

7 Conclusion **107**
7.1 Summary . . . 107
7.2 Contributions . . . 107
7.3 Recommended Future Work . . . 108

A HokieSat ADCS **109**
A.1 Project Background . . . 109
A.1.1 ION-F . . . 109
A.1.2 HokieSat . . . 110
A.2 ADCS System Requirements . . . 110
A.3 Attitude Determination . . . 110
A.3.1 Magnetometer . . . 110
A.3.2 Cameras . . . 111
A.3.3 Rate Gyro . . . 112
A.3.4 Sun Sensor . . . 112
A.4 Attitude Control . . . 113
A.4.1 Torque Coil Sizing . . . 114
A.4.2 Torque Coil Composition . . . 115

B International Geomagnetic Reference Field **117**

References **122**

Vita **126**

List of Figures

2.1 Magnetic Field of a Bar Magnet 8
2.2 Magnetic Field Model 10
2.3 Geomagnetic Coordinates 11
2.4 The Magnetosphere 12
2.5 Appearance and Evolution of a Magnetic Bottle 16
2.6 Movement of the North Pole over Time 18
2.7 Movement of the South Pole over Time 19
2.8 Magnetic Field Coordinates 21
2.9 Spherical Harmonic Model 23
2.10 Air Core Loop Antenna 29
2.11 Rod Antenna 29
2.12 Sunspot Activity 34
2.13 Archimedes Spiral 35

3.1 Relative Motion of Two Bodies 41
3.2 Elliptical Orbit 43
3.3 Orbital Elements 44
3.4 Heliocentric-Ecliptic Coordinate System 46
3.5 Earth-Centered Inertial Reference Frame 47
3.6 Earth-Centered Earth-Fixed Reference Frame 47
3.7 Earth-Centered Inertial and Orbital Reference Frames 49
3.8 Comparison of Environmental Torques 53

4.1 Forces on the Moving Charges in a Current-Carrying Conductor 61
4.2 Forces on a Current-Carrying Loop in a Magnetic Field 62
4.3 Magnetic Torque Direction 66
4.4 Magnetic Control Torques 67
4.5 Equatorial Orbit in Magnetic Field 69
4.6 Polar Orbit in Magnetic Field 70

5.1 $\mathbf{G}(t)$ Elements 79
5.2 Summary of LQR Method 82

6.1 Quaternions with No Magnetic Torque, Initial Angle=14° 86
6.2 Quaternions with No Magnetic Torque, Initial Angle=6° 87
6.3 Quaternion for Linear, P-D Controller with Gravity-Gradient Stability . . . 88
6.4 Quaternion for Nonlinear, P-D Controller with Gravity-Gradient Stability . . 88
6.5 Eigenvalues of $\mathcal{X}(t)$ with Gravity-Gradient Stability 89
6.6 Quaternion for Linear, LQR Controller with Gravity-Gradient Stability . . . 90
6.7 Quaternion for Nonlinear, LQR Controller with Gravity-Gradient Stability . 90
6.8 Magnetic Moment for Gravity-Gradient Stable Spacecraft 91
6.9 Magnetic Moment for Gravity-Gradient Stable Spacecraft Over a Long Period of Time 92
6.10 Quaternion for Linear, P-D Controller without Gravity-Gradient Stability . . 92
6.11 Quaternion for Nonlinear, P-D Controller without Gravity-Gradient Stability 93
6.12 Quaternion for Linear, LQR Controller Without Gravity-Gradient Stability, Case 1 94
6.13 Quaternion for Nonlinear, LQR Controller Without Gravity-Gradient Stability, Case 1 95
6.14 Magnetic Moment for Non Gravity-Gradient Stable Spacecraft 95
6.15 Quaternion for Linear, LQR Controller Without Gravity-Gradient Stability, Case 2 96
6.16 Quaternion for Nonlinear, LQR Controller Without Gravity-Gradient Stability, Case 2 96

6.17 Optimized Linear Gravity-Gradient Stable Quaternion 98
6.18 Optimized Nonlinear Gravity-Gradient Stable Quaternion 99
6.19 Optimized Nonlinear Gravity-Gradient Stable Magnetic Moment 99
6.20 Optimized Linear Non Gravity-Gradient Stable Quaternion 100
6.21 Eigenvalue Comparison for Optimization 101
6.22 Optimized Nonlinear Non Gravity-Gradient Stable Quaternion 101
6.23 Optimized Nonlinear Non Gravity-Gradient Stable Magnetic Moment 102
6.24 Optimized Linear Non Gravity-Gradient Stable Quaternion, Alternate Example 103
6.25 Optimized Nonlinear Non Gravity-Gradient Stable Quaternion, Alternate Example 104
6.26 Nonlinear Quaternions for Non Gravity-Gradient Stable Inverted Spacecraft 105
6.27 Magnetic Moment for Inverted Spacecraft 106

A.1 HMC2003 Honeywell Magnetometer 111
A.2 Fuga 15d Camera 111
A.3 QRS11 Systron Donner Rate Gyro 112
A.4 Sun Sensor Detection 112
A.5 Sun Sensor Cone of Possibilities 113

B.1 Variation in the IGRF Coefficient g_1^0 121

List of Tables

2.1 Magnetic Field Units 9

2.2 Magnetic Field Strengths 9

2.3 Field Strength Instrument Characteristics 28

3.1 Ranges of Sensor Accuracy 55

A.1 Magnet Wire Characteristics 115

A.2 HokieSat Torque Coil Characteristics 115

B.1 Spherical Harmonic Coefficients of the IGRF-DGRF models over the 20^{th} Century 117

Nomenclature

a	Semi-major axis
$\mathbf{a}$	Euler axis vector
A	Area of current loop
A_w	Cross-sectional area of wire
$\mathbf{B}$	Magnetic field
d_w	Diameter of wire
e	Eccentricity
$\mathbf{E}$	Electric Field
$\mathcal{F}$	Frame
$\mathbf{F}$	System matrix of linear equations
$\mathbf{g}$	Torque
g_n^m	Gaussian coefficient
$\mathbf{g}_g$	Gravity-gradient torque
$\mathbf{g}_m$	Magnetic torque
$\mathbf{g}_{m_i}$	Ideal magnetic torque
G	Universal gravitational constant
$\mathbf{G}$	Input matrix for control
h	Angular momentum
h_n^m	Gaussian coefficient
$\mathbf{H}$	Magnetic Field
i	Inclination
I	Current
$\mathbf{I}$	Moment of inertia

J	Current density
K	Sun intensity
$\mathbf{K}$	Gain matrix
$\mathbf{K}_d$	Derivative gain matrix
$\mathbf{K}_p$	Proportional gain matrix
ℓ_w	Length of wire
m	Mass
$\hat{\mathbf{m}}$	Magnetic dipole axis
m_c	Mass of coil
$\mathbf{M}$	Magnetic dipole moment
$\tilde{\mathbf{M}}$	Mapped magnetic moment
$\mathcal{M}$	Magnetization
$\hat{\mathbf{n}}$	Normal unit vector
N	Number of coil turns
p_c	Perimeter of coil
P	Power
P_n^m	Legendre function
$\bar{\mathbf{q}}$	Quaternion
$\mathbf{Q}$	Weight matrix
r	Geocentric distance
$\mathbf{r}$, $\mathbf{R}$	Position vector
R	Resistance
$\mathbf{R}$	Rotation matrix
$\hat{R}$	Resistivity
$R_\oplus$	Radius of the Earth
t	Time
T	Time of periapsis passage
$\mathcal{T}$	Period of orbit
u	Argument of latitude
$\mathbf{u}$	Applied control

v	Velocity
V	Scalar potential function
$\mathbf{x}$	State vector
$\mathcal{X}$	Monodromy matrix
α	Right ascension
α	Sun angle
δ	Declination
ϵ	Oblateness
θ	Co-elevation
$\boldsymbol{\theta}$	Euler Angles
θ_g	Greenwich sidereal time
θ_{g0}	Greenwich sidereal time at epoch
θ'_m	Co-elevation of dipole
λ	Geodetic latitude
μ	Gravitational parameter
μ	Permeability of core material
μ_0	Permeability of free space
ν	True anomaly
Υ	Vernal equinox
ϕ	Longitude
ϕ_f	Flight path angle
ϕ'_m	East longitude of dipole
Φ	Angle of rotation
ω	Argument of periapsis
$\boldsymbol{\omega}$	Angular velocity
ω_c	Orbital angular velocity
$\omega_\oplus$	Average rotation rate of Earth
Ω	Right ascension of ascending node

Chapter 1

Introduction

In this thesis, the problem of using magnetic control to stabilize a spacecraft on three axes is examined. In this chapter, the advantages and disadvantages of magnetic control are presented for three-axis stabilized spacecraft. The prior work in magnetic control is discussed through a literature review. In addition, the approach taken to obtain magnetic control in this thesis is described.

1.1 Problem Statement

Magnetic control is a favorable way to stabilize spacecraft. Often, the hardware is simple and lightweight, and does not degrade or change mass over time.

However, a magnetic control system does have some disadvantages and limitations. The control, which is in the form of magnetic moment, can only be applied perpendicular to the local magnetic field. In addition, there is uncertainty in the Earth magnetic field models due to the complicated dynamic nature of the field. Also, the magnetic hardware and the spacecraft can interact, causing both to behave in undesirable ways.

In this thesis, control laws are developed to stabilize spacecraft on three axes. The motivation for this project is the HokieSat satellite, which is a nanosatellite developed at Virginia Tech. A description of the HokieSat attitude determination and control system is available in Appendix A.

1.2 Prior Work in Magnetic Attitude Control

White, Shigemoto, and Bourquin[49] were among the first to mention using magnetic torques for spacecraft control in 1961. Their analysis examined the feasibility of using the interaction

of the Earth's magnetic field and current-carrying coils in a fine-control attitude system. This research developed control laws to track the spin axis of the Orbiting Astronomical Observatory. They determined that it is possible to obtain torque about all three axes of a spacecraft on an intermittent basis, which changes the angular velocity of the spacecraft, and can be used to change the orientation.

The first implementation of magnetic control was in spin-stabilized spacecraft. In 1965, Ergin and Wheeler[9] developed control laws for spin orientation control using a magnetic torque coil and discussed advantages of magnetic control. The control laws aligned the spin axis normal to the orbit plane. A similar analysis was conducted by Wheeler[48] for active nutation damping, as well as spin-axis precession of rigid, axially symmetric, spinning satellites in circular Earth orbits. The feasibility of a single magnetic dipole aligned with the spin axis was investigated. Wheeler determined that theoretical stability is provided by control laws that direct the spin axis of any axially symmetric spinning satellite in a circular Earth orbit to any direction in space.

Renard[33] developed control laws for magnetic attitude control using an averaging method. This work examined having a control coil axis parallel to the spin axis and inverting the polarity of the control torque every quarter of the orbit period. He determined that any desired orientation is obtainable using this method, although for certain motions it may be necessary to wait and take advantage of the orbital eccentricity at certain times of the day.

Sorenson[39] examined a magnetic attitude control system to point the spin axis of a spacecraft in a highly eccentric orbit and maintain a constant spin speed. The control is based on minimum energy considerations, and uses a Kalman filter to decrease energy requirements and provide active damping. This method is effective for full control of spinning spacecraft in Earth orbits between 20° and 70°, and eccentricities of up to 0.7.

Shigehara[36] further examined the problem of magnetic control of spinning spacecraft by developing a control law which used a switching function instead of averaging techniques. The switching function, which is derived from the condition of asymptotic stability, selects the pattern of the magnetic dipole achieving the maximum effective torque and minimum transverse torque at every instant. The switching point is different from the averaged quarter orbit point, and attains the desired attitude direction faster. This method is proven through simulation runs, and has an increase in performance over averaging methods.

In 1975, Schmidt[22] described using magnetic attitude control on three-axis stabilized, momentum-biased satellites. Here, a momentum wheel was mounted along the pitch axis to provide bias, or nominal angular momentum that is not zero. Schmidt showed that this system required minimum switching of the closed loop controller, and thus was reliable for long duration missions. This work was used towards the RCA Satcom geosynchronous satellite, which was three-axis stabilized using air core coils.

Stickler and Alfriend[40] further examined using magnetic control with momentum bias. They developed a three-axis closed-loop attitude control system which was fully autonomous.

Analytical expressions of system response were compared with numerical solutions of the governing equations. The two solutions of equations were in agreement, suggesting a feasible three-axis control system.

Goel and Rajaram[15] developed a closed-loop control law which performed both attitude corrections and nutation damping for three-axis stabilized spacecraft with momentum bias. In this system, a magnetic torquer was placed along the roll axis of the spacecraft, and yaw control was obtained by the roll/yaw coupling from the momentum wheel. Simulation results matched with analytical results, and indicated that there was adequate damping of the system.

Junkins, Carrington, and Williams[23] discussed the use of time-optimal magnetic attitude maneuvers with spin-stabilized spacecraft. They suggested a nonlinear bang-bang switching function used with a single electromagnet aligned with the spin axis, and determined that their method was practical for rapidly determining maneuvers for a spacecraft. This method was used to determine optimal maneuvers for the NOVA navigational satellite.

Martel, Pal, and Psiaki[26] examined using magnetic control for gravity-gradient stabilized spacecraft in 1988. Whereas previous spacecraft used momentum wheels to augment the magnetic control, Martel, Pal, and Psiaki claimed that the proper ratio of moments of inertia, causing gravity-gradient stabilization, along with magnetic control could provide three-axis stabilization. Simulations showed that the algorithms performed well over a large range of orbital inclinations and attitude angles.

In 1989, Musser and Ebert[30] were among the first to attempt to use a fully magnetic attitude control system for three-axis stability. They claim that this became possible due to the increase in computer computational power onboard spacecraft. Musser and Ebert developed linear feedback control laws which use a linear quadratic regulator to obtain the value of the magnetic control torque. The equations of motion are in the form

$$\dot{\mathbf{x}} = \mathbf{F}\mathbf{x} + \mathbf{G}(t)\mathbf{M}(t) \tag{1.1}$$

where $\mathbf{M}$ is the control magnetic moment and is computed by

$$\mathbf{M}(t) = -\mathbf{B}^{-1}\mathbf{G}^{T}(t)\mathbf{S}(t)\mathbf{x}(t) \tag{1.2}$$

using a linear quadratic regulator. The control laws as a function of time were replaced with laws that were a function of orbital position. Musser and Ebert performed simulations showing that their technique was a good candidate for onboard attitude control systems.

Wiśniewski[50,51] further developed the ideas of Musser and Ebert. He used a combination of linear and nonlinear system theory to develop control laws for three-axis stabilization of the spacecraft. Linear theory was used to obtain both time varying and constant gain controllers for a satellite with a gravity gradient boom. His analysis used the fact that the geomagnetic field varies nearly periodically at high inclination orbits. In addition, he developed a nonlinear controller for a satellite without appendages based on sliding mode

control theory. He showed that three-axis control can be achieved with magnetic torquers only, and implemented this idea on the Danish Ørsted satellite.

Grassi[16] developed a three-axis, fully autonomous, magnetic control system for use on a small remote sensing satellite. This control could be carried out solely with magnetometer measurements and orbital location information. The magnetic dipole moment for control is

$$\mathbf{M} = \mathbf{K}_p(\mathbf{B}_o - \mathbf{B}_r) + \mathbf{K}_d(\dot{\mathbf{B}}_o - \dot{\mathbf{B}}_r) \tag{1.3}$$

where $\mathbf{B}_o$ is the measured magnetic field, $\mathbf{B}_r$ is the reference magnetic field, and $\mathbf{K}_p$ and $\mathbf{K}_d$ are the control position and rate gains. Control laws were numerically tested to show that the magnetic control system works within resolution limits.

Arduini and Baiocco[3] examined control laws for magnetic control of a gravity-gradient stabilized spacecraft. They discussed the challenges that exist due to magnetic torques only applied perpendicular to the magnetic field. Their control algorithm was based on first determining the ideal torque, and then generating the actual torque through a series of suggested approaches. They also discussed the relationship between stability and the change in energy of the system. They discovered a good agreement between the analytical approximations and numerical solutions.

1.3 Approach and Results

This thesis develops control laws based on the methods of Musser and Ebert, and Wiśniewski. First, nonlinear equations of motion are developed and then linearized in a time varying form. The equations are reduced to linear time invariant using the periodic nature of the equations in an orbit. Magnetic control laws are developed using both a proportional-derivative controller and a constant coefficient linear quadratic regulator.

The control laws are tested by performing simulations with various spacecraft configurations and initial conditions. The gains are varied for each case such that the system damps to the desired equilibrium.

When a gravity-gradient stable spacecraft is simulated, the proportional-derivative and linear quadratic regulator both result in stable systems from simply selected gains. However, non gravity-gradient stable spacecraft yield different results. The proportional-derivative controller only provides stable results for linear equations, and is unstable for nonlinear equations with simple gains. The linear quadratic regulator controller, however, stabilizes non gravity-gradient spacecraft using both linear and nonlinear equations.

An optimization technique is implemented with the linear quadratic regulator to determine a set of gains that maximize the performance of the controller. This optimization works for linear equations, but obtains mixed results with nonlinear equations.

1.4 Outline of Thesis

Chapter 2 introduces magnetic field basics and discusses specifics of the Earth's magnetic field. Mathematical models of the geomagnetic field are presented for use in later simulations. Methods of measuring magnetic fields are mentioned, along with the hardware used for the task. The chapter ends with a discussion of the magnetic fields of other celestial bodies and how they differ from the geomagnetic field.

Chapter 3 discusses spacecraft dynamics. First, equations for orbit dynamics are described. Then, attitude dynamic equations are developed, and a description of reference frames and rotations is included. Environmental disturbance torques are explained. Finally, there is a description of attitude determination, as well as attitude control.

Chapter 4 concentrates on the interaction of spacecraft and magnetic fields. Magnetic torques are described in detail by first explaining disturbance torques, and then control torques. The hardware for magnetic control is detailed, and the interaction between the orbit and the magnetic field is explained.

Chapter 5 develops control laws to magnetically control the spacecraft on three axes. Equations of motion are first developed and linearized. Then, two controllers are implemented. The first is a proportional-derivative controller, and the other is a constant coefficient linear quadratic regulator controller. A technique to optimize the performance of the linear quadratic regulator controller is described.

Chapter 6 details the results from simulations performed with the control laws. The results are compared for both types of controllers with the linear and nonlinear equations. The differences in results for gravity-gradient and non gravity-gradient stable spacecraft are described. The gains in the system are optimized and compared.

Chapter 7 concludes this thesis. It summarizes the results and suggests areas for further research.

Chapter 2

Earth's Magnetic Field

Magnetic control of spacecraft is dependent upon the local magnetic field. A discussion on the geomagnetic field is presented in this chapter. First, background information on magnetics is presented, followed by a discussion of the Earth's magnetic field, including its origin, characteristics, and variations. Mathematical models of the geomagnetic field using the International Geomagnetic Reference Field are developed and compared. In addition, the methods used and hardware required for measuring magnetic fields are discussed. Finally, the magnetic fields of other celestial bodies, including the Sun, moon, and planets are described.

2.1 Magnetic Fields

An understanding in basic magnetic field theory is required before examining the Earth's magnetic field. Background information on magnetics can be located in many physics text books, such as Sears, Zemansky, and Young.[34] An explanation of Maxwell's Equations, as well as magnetic field characteristics, follows.

2.1.1 Origin and Equations

Magnetic and electric fields are closely related. This relationship was first determined in 1819 when Hans Christian Oersted discovered that a compass needle could be caused to rotate by passing a current through a nearby wire. About twelve years later, both Michael Faraday and Joseph Henry realized that an electric voltage could be produced at the terminals of a loop of wire by moving a magnet close to it.

Magnetic fields arise from the motion of electrons. Both the orbital rotation of electrons around the nucleus of the atom and the spin of the electron about its own axis give rise to magnetic fields. However, the electron spin is the dominant contribution.

Maxwell's Equations form the foundation of modern electromagnetic theory, and expand upon the laws of Ampere, Faraday, and Gauss.[32] These equations can be represented in both differential and integral forms as follows:

Maxwell's Equations in Differential Form:

$$\nabla \cdot \mathbf{E} = \frac{\rho}{\epsilon_0} \tag{2.1}$$

$$\nabla \cdot \mathbf{B} = 0 \tag{2.2}$$

$$\nabla \times \mathbf{E} = -\frac{\partial}{\partial t}\mathbf{B} \tag{2.3}$$

$$\nabla \times \mathbf{B} = \mu_0\epsilon_0\frac{\partial}{\partial t}\mathbf{E} + \mu_0\mathbf{J} \tag{2.4}$$

Maxwell's Equations in Integral Form:

$$\oint \mathbf{E} \cdot \mathrm{d}\mathbf{A} = \frac{q}{\epsilon_0} \tag{2.5}$$

$$\oint \mathbf{B} \cdot \mathrm{d}\mathbf{A} = 0 \tag{2.6}$$

$$\oint \mathbf{E} \cdot \mathrm{d}\mathbf{s} = -\frac{\mathrm{d}\Phi_B}{\mathrm{d}t} \tag{2.7}$$

$$\oint \mathbf{B} \cdot \mathrm{d}\mathbf{s} = \mu_0\mathbf{I} + \mu_0\epsilon_0\frac{\mathrm{d}\Phi_E}{\mathrm{d}t} \tag{2.8}$$

Equations 2.1 and 2.5 are two forms of Gauss' Law for Electricity. This law states that the electric flux of a closed surface is proportional to the total charge enclosed in the surface. Gauss' Law for Magnetism is shown in Equations 2.2 and 2.6. This law states that the magnetic flux out of any closed surface is zero. Therefore, the magnetic flux directed inward towards the south pole is equal to the flux outward from the north pole in a magnetic dipole of a closed surface. Equations 2.3 and 2.7 are known as Faraday's Law of Induction. This law states that the integral of an electric field around a closed loop is equal to the negative rate of change of the magnetic flux through the area enclosed by the loop. Ampere's Law (Equations 2.4 and 2.8) is the fourth of Maxwell's Equations. It states that the integral of a magnetic field around a closed loop is proportional to the electric current flowing through the loop.

2.1.2 Characteristics

The magnetic field is a vector quantity, which means that it has both a magnitude and a direction. Macintyre[25] discusses the fundamentals of magnetic fields and the relationship between magnetic quantities. A common example of a magnet and a magnetic field is that of a bar magnet (Figure 2.1).

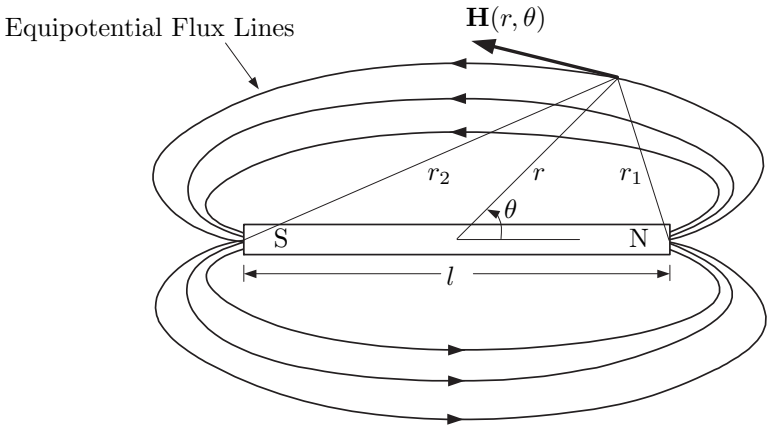

Figure 2.1: Magnetic Field of a Bar Magnet (Adapted from Ref. 25)

The magnetic field of a bar magnet, $\mathbf{H}$, measured at a far distance is

$$\mathbf{H} = \frac{3(\mathbf{M} \times \hat{\mathbf{a}}_\mathbf{r})\hat{\mathbf{a}}_\mathbf{r} - \mathbf{M}}{r^3} \tag{2.9}$$

where r is the distance between the magnetic field source and the measurement point, $\hat{\mathbf{a}}_\mathbf{r}$ is a unit vector from the center of the magnet to the measurement point, and $\mathbf{M}$ is the magnetic dipole moment of the bar magnet.

The magnetization, $\mathcal{M}$, of an object is its magnetic strength or intensity, and depends on the density of its volume-distributed moments.

$$\mathcal{M} = \frac{\mathbf{M}}{\text{volume}} \tag{2.10}$$

Magnetization is a material property, and arises from both internal sources and external sources.

In matter, the relationship between the magnetic field and magnetic induction or flux density, $\mathbf{B}$, is dependent on magnetization and the permeability of free space, μ_0:

$$\mathbf{B} = \mu_0(\mathbf{H} + \mathcal{M}) \tag{2.11}$$

In free space, the magnetic induction is proportional to the magnetic field by the constant factor, μ_0.

$$\mathbf{B} = \mu_0 \mathbf{H} \tag{2.12}$$

The value of μ_0 is equal to 1 in the International System of Units (SI), so the value of the magnetic field and that of the magnetic induction are equal in free space. For the remainder of this document, **B** is used to represent both **H** and **B**.

Different units are used to represent magnetic fields. The relationship between these units is listed in Table 2.1. In this paper, units of Tesla are used to describe magnetic fields.

Table 2.1: Magnetic Field Units

B =	10^4 Gauss (G)
B =	1 Weber/meter^2 (Wb/m^2)
B =	10^9 gamma (γ)
B =	1 Tesla (T)

A comparison of various magnetic field strengths is shown in Table 2.2. The strongest manmade magnetic field sustained in a lab is approximately 400000 Gauss, or 40 T, but stronger fields have been created momentarily by explosive compression. The strongest naturally occurring field is found on a magnetar, which is a type of neutron star.

Table 2.2: Magnetic Field Strengths[21]

Magnetic Field	Strength (Gauss)
Galactic Magnetic Field	0.00001
Solar Wind	0.00005
Interstellar Molecular Cloud	0.001
Earth's Field at Ground Level	1
Solar Surface Field	1-5
Massive Star (pre Supernova)	100
Toy Refrigerator Magnet	100
Sun Spot Field	1000
Jupiter Magnetic Field	1000
Magnetic Stars	11,500
White Dwarf Star Surfaces	1,000,000
Neutron Star Surfaces	1,000,000,000,000
Magnetar Field	1,000,000,000,000,000

2.2 Origin and Effects of the Earth's Magnetic Field

The geomagnetic field is described in detail in NASA Technical Report SP-8017,[1] as well as by Wertz,[46] Campbell,[6] and Thompson.[42] A description of the geomagnetic field, its characteristics, and variations follows.

2.2.1 Geomagnetic Field

The magnetic field around the Earth resembles that of a uniformly magnetized sphere, or a dipole, which is tilted as shown in Figure 2.2. The fact that it approximates a tilted dipole was discovered in 1600 by William Gilbert, and was published in his treatise *De Magnete*.[13] In 1635, Gellibrand was the first to show that the geomagnetic field is both time and position dependent.[42]

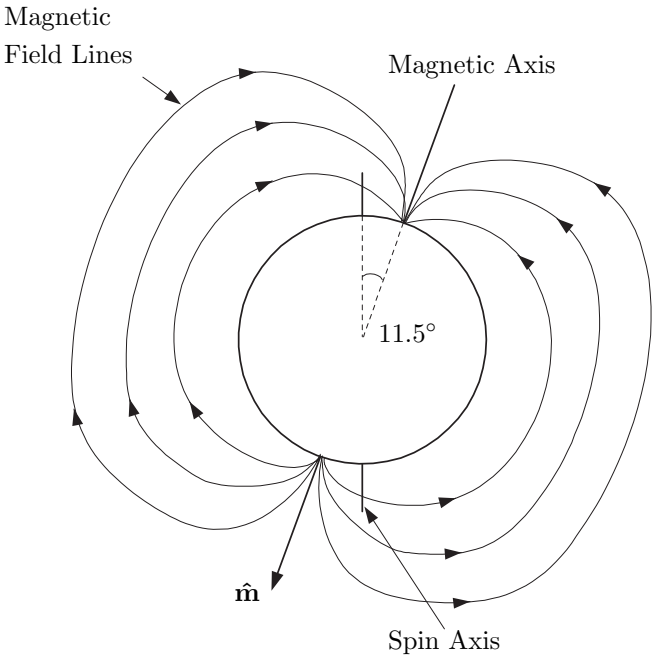

Figure 2.2: Magnetic Field Model

The strength of the magnetic field is approximately 30000 nT at the equator and 60000 nT at the poles on the surface of the Earth, as mentioned in the Geological Survey of Canada.[12] The magnetic dipole axis, designated as $\hat{\mathbf{m}}$ in Figure 2.2, is located at 79.8° N latitude and 107.0° W longitude, in the year 1999. This location is near the Ellef Rignes Island in Canada, and is approximately 700 miles from the geographic North Pole. The magnetic dipole axis is currently at an inclination angle of 11.5° with the equatorial plane. The axis is drifting westward at about 0.2 °/year, and the strength is decreasing by 0.05% per year.

The magnetic field is weakest at the magnetic equator, or the plane perpendicular to the magnetic dipole. The geomagnetic coordinates compared with spin axis coordinates are shown in Figure 2.3.

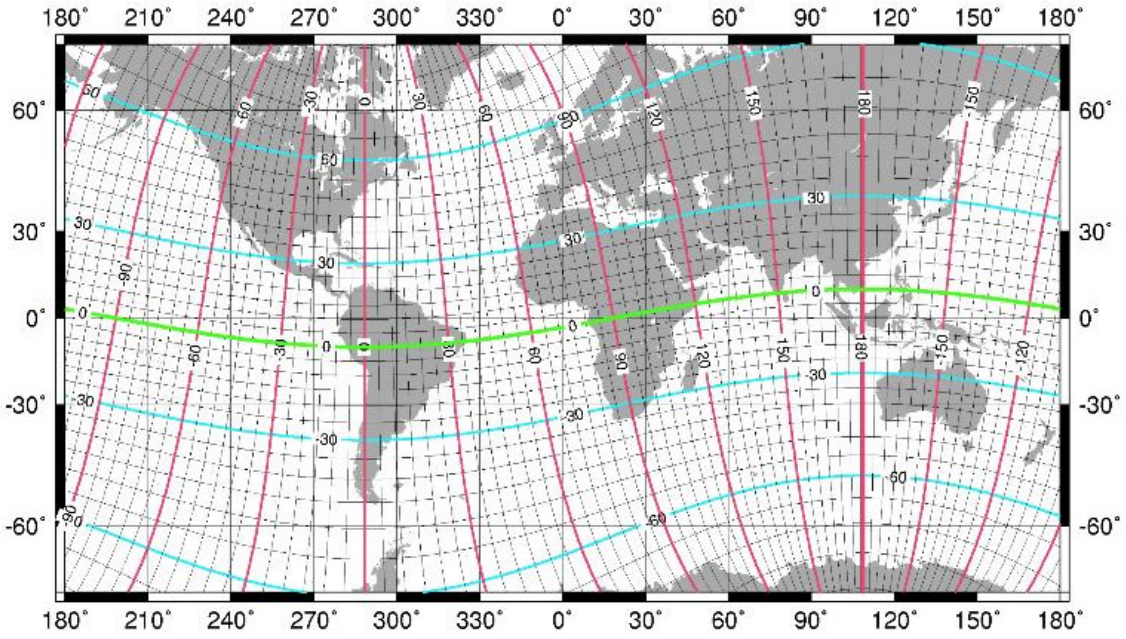

Figure 2.3: Geomagnetic Coordinates[31]

At locations on the Earth's surface, a magnetic dipole model is not closely followed. However, as the altitude increases, the contours of the field strength begin to become regular and resemble a dipole field. There is a low in magnetic intensity at about 25°S, 45°W, called the Brazilian Anomaly, and a high at 10°N, 100°E. Together, these anomalies imply that the center of the dipole is offset from the center of the Earth.[46]

The NASA Technical Report SP-8017[1] and Wertz[46] provide basic information on aspects of the geomagnetic field, including the strength, orientation, and the layout of the magnetosphere. At locations far from the Earth, the effect of a magnetosphere is more dominant than the dipole. This effect is shown in Figure 2.4. The magnetosphere is created from the interaction of the solar plasma flow, or solar wind, and the geomagnetic field. The two areas have a great effect on each other, with the solar wind acting to compress the Earth's magnetic field, while particles of the solar wind are deflected and trapped by the geomagnetic field. This effect causes the structure of the geomagnetic field to be complex and consist of a number of regions.

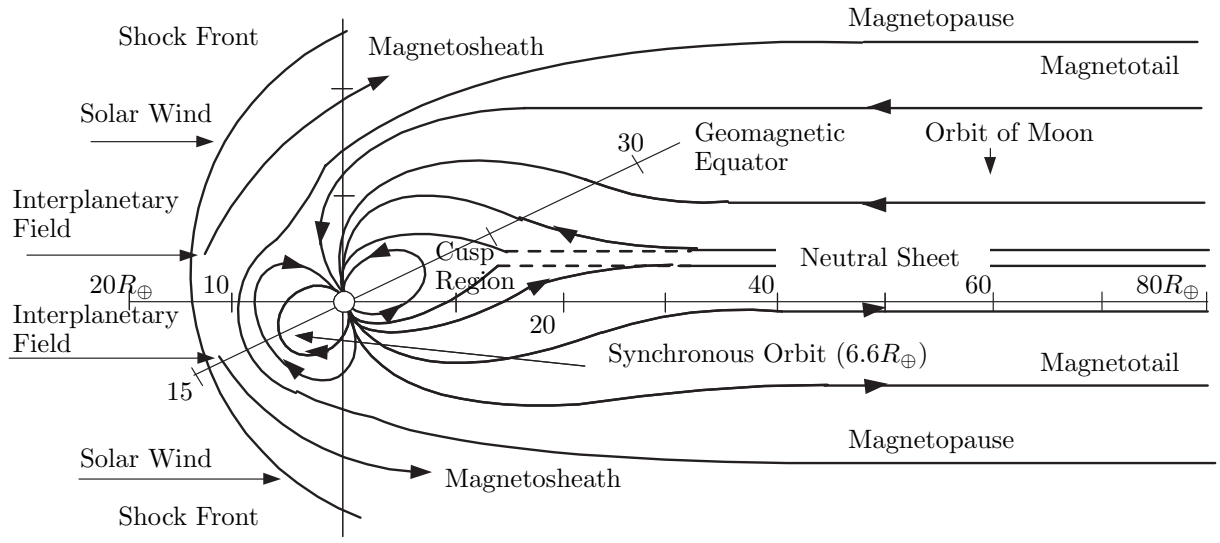

Figure 2.4: The Magnetosphere (Adapted from Ref. 1)

Shock Front

A shock front exists at the boundary between the solar wind and the geomagnetic field. This shock is similar to a sonic boom and occurs because the solar wind is moving faster than the magnetic field can respond. The magnetic field experiences oscillations with large amplitudes at this location. These oscillations can be as large as 10 to 50 nT, whereas on either side of the shock front they usually fall in the range of 2 to 5 nT. Additionally, the oscillations occur at a higher frequency at the shock front.

Magnetosheath

The magnetosheath is a region of turbulence where the solar wind is deflected after passing through the shock front. The field inside the magnetosheath fluctuates rapidly, both in strength and direction. In the direction towards the sun, the magnetosheath is nominally 4 $R_\oplus$, where $R_\oplus$ is the radius of the Earth. However, it can shrink to approximately 2 $R_\oplus$ during a magnetic storm occurring during a year of low solar activity.

Magnetopause

The magnetopause is a boundary layer that separates the magnetic field of the Earth from the magnetosheath. This region is located at approximately 10 $R_\oplus$ on the side close to the sun, and extends to at least 80 $R_\oplus$ on the antisolar side. The location can fluctuate by 1 to

3 $R_\oplus$ and is known to expand or contract at rates larger than 50 km/sec during magnetic storms. The magnetopause is in the range of tens of km in thickness, and acts as a transition zone where the magnetic field direction shifts as much as 180°, and changes strength from more than 40 nT in the magnetosphere to 10 to 30 nT in the magnetosheath.

Magnetotail

The magnetotail is formed by the solar wind dragging the geomagnetic field lines away from the sun. The field lines of the magnetotail in the southern hemisphere are directed away from the Earth in the antisolar direction, while the field lines in the northern hemisphere point towards the sun. The magnetotail extends to a distance of at least 1000 $R_\oplus$ from the Earth, and at 30 $R_\oplus$ from the Earth in the antisolar direction, the radius is approximately 20 $R_\oplus$. At locations from 8 $R_\oplus$ to 10 $R_\oplus$, the magnetic field intensity follows that of the Earth's dipolar field. At further distances, however, the field intensity decreases as the distance from the Earth increases. At 10 $R_\oplus$ the field intensity is 20 nT, and at 80 $R_\oplus$ the strength has decreased to about 7 nT. At 1000 $R_\oplus$, the intensity has been observed to be between 4 and 16 nT.

Neutral Sheet

The neutral sheet separates the incoming and outgoing field lines in the magnetotail. In this region, the magnetic field intensity decreases to about 1 to 4 nT on the dawn meridian side, and to less than 1 nT on the side near the moon-midnight meridian plane. The neutral sheet extends from approximately 10 $R_\oplus$ to the limit of the magnetotail, and is parallel with the solar-magnetospheric equatorial plane. Its position is above the plane during summer months, and below the plane during winter months. During magnetic storms, the neutral plane can be displaced beyond 13 $R_\oplus$. The neutral sheet thickness ranges from 500 km to 5000 km.

Cusp Region

The cusp region is located on the antisolar side of the Earth and is the area where the geomagnetic field lines are first transformed into the magnetotail. This region occurs at a distance of 8 to 16 $R_\oplus$ at geomagnetic latitudes of $\pm$ 25°. This region is part of the Van Allen radiation belts, and the outer boundary experiences sudden large changes in particle density.

2.2.2 Origin of the Magnetic Field

Theories on the origin of the magnetic field are discussed by Thompson.[42] The original thoughts on the origin of the geomagnetic field included ideas that the Earth acted as a large magnet. This idea arose because of the large abundance of iron in the Earth's physical make-up, but in fact, it is impossible for thermodynamic reasons. All materials lose their magnetism at high temperatures, or their Curie temperature. At this point, the magnetic moment of the material becomes randomly oriented, which destroys the magnetization. Since the boundary of the Earth's core may be close to 3000° C and the Curie temperature of iron is not more than 780° C, the Earth can not act as a magnet to produce the magnetic field.

A more generally accepted theory for the origin of the geomagnetic field is one of internal origin, with an approximate 0.1% external contribution. In the 1940's and 1950's, Elsasser and Bullard claimed that the Earth's magnetic field arose from fluid motions in the dense metallic liquid core.[42] This motion is caused by circulation of electric currents, and is able to run for a length of time due to self-induction. In order for this motion to occur, there must be a mechanism that controls and maintains the electric currents. Without this mechanism, all of the energy would be dissipated through Joule heating in 10^5 years. However, all of the energy does not dissipate since the magnetic field has been around for at least 3×10^9 years.

The self-exciting dynamo results from the interactions of the magnetic field with the flow of electric currents arising from fluid motion of the Earth's core. In the core, fluid motions across an existing magnetic field produce their own magnetic field and induced electric currents. The motion of the fluid, therefore, acts to reinforce and maintain the geomagnetic field by the way of a self-exciting dynamo.

The formulation of the self-exciting dynamo theory is simple because it is based on classical mechanics, thermodynamics, and electromagnetism. Solving the problem is much more difficult, however. The mathematical problems are nonlinear, and there are many physical unknowns and only a few observational constraints. Only a few solutions to simple similar problems exist, but scientists believe that any complicated motion in the core of the Earth will give rise to a dynamo.

The energy source for the dynamo is thought to be either radioactive decay of elements in the core, or gravitational energy released by sinking of heavy materials in the outer core. This energy forms the convection currents and drives the dynamo with magnetohydrodynamic actions. There are still objections to the dynamo theory, although it has been generally accepted.

2.2.3 Variations in the Magnetic Field

The magnetic field of the Earth is not a constant over time. Various changes occur in intensity and direction, including daily variations and ones due to the influence of the sun.

The intensity and direction return to their initial states after awhile, and are known as temporal variations. The magnetic field also undergoes drifts over long periods of time, or secular variations, which can eventually result in a reversal of the field. These variations in the magnetic field are discussed by Wertz,[46] Thompson,[42] and Campbell[6] and are mentioned in the NASA Technical Report SP-8017.[1]

Temporal Variations

Temporal variations are described as disturbances in the geomagnetic field which result from the changing positions of the Earth and the Sun. These variations usually only last for a short time, ranging from a few seconds to a few days.

The occurrence of the temporal variations is based on the rotation rates of the Earth and Sun. Every 27 days, the Sun's rotation causes an active solar area to face the Earth. The magnitude of the temporal variations increases during the March-April and September-October times when the Earth is near the equinoxes. The intensity of the variations is linked to the number of sunspots. This number varies through an 11-year cycle. In addition, different types of temporal variations have effects on the intensity.

Diurnal Variations Diurnal variations are one type of temporal variation. These variations occur in the day-to-night magnetic field intensity. The main cause of diurnal variations are changes in ionospheric currents resulting from systems of charged particles moving between 50 and 600 kilometers. These effects are not prevalent in the geomagnetic field more than a few Earth radii away from the Earth's surface since the intensity of the magnetic fields resulting from the currents decreases with increasing distance.

Auroral currents are caused by the polar electrojet, or an intense ionospheric current that flows westward above 67° geomagnetic latitude. The auroral activity is at a maximum in the spring and fall when the Earth is at the equinoxes. Changes in the electrojet can cause intense negative trends which are typically 1000 to 1500 nT at the Earth's surface. These trends can last from 30 to 120 minutes.

An equatorial electrojet is a west-to-east current which occurs in the sunlit portion of the ionosphere at an altitude of 95 to 110 kilometers. This current can produce a 220 nT discontinuity in the total magnetic field between altitudes of 96 to 130 kilometers.

The intensity of the solar current is quantified through the quiet day solar daily variation currents. This quiet day value is determined by taking an average of 5 days each month having the least amount of magnetic variation. Magnetic observatories continuously monitor the amount of magnetic activity, and determine an index, K, which is the deviation of the most disturbed component of the field from the quiet day value. The value of K runs from $K = 0$ for quiet activity, to $K = 9$ for the largest deviations. The values of K from different magnetic observatories are averaged every three hours to determine the planetary index, K_p,

which acts as an indication of the amount of deviation of the magnetic field.

The magnitude of the diurnal variations can be large enough to cause the magnetic pole to be located as much as 80 km away from the average position. The daily wandering of the pole follows an elliptical path, and varies from a magnetically quiet to a magnetically disturbed day.

Magnetic Storms On occasion, plasma bursts emitted from solar flares cause the fairly constant solar wind to behave erratically. When the plasma comes in contact with the geomagnetic field, it causes it to become more compressed, and therefore raises the field intensity on the surface of the Earth. This occurrence is known as a magnetic storm. The initial phase of the magnetic storm lasts about one hour, and during this time, the total field intensity increases by about 50 nT. During very strong storms, the magnetopause can be compressed to below synchronous altitudes at this phase. The main phase of a magnetic storm can last for a few hours. During this time, the total field intensity decreases by more than 400 nT. The initial recovery phase lasts from six hours to two days, with final recovery to pre-storm levels lasting several days after that. During this time, a magnetic bottle is formed, as shown in Figure 2.5.

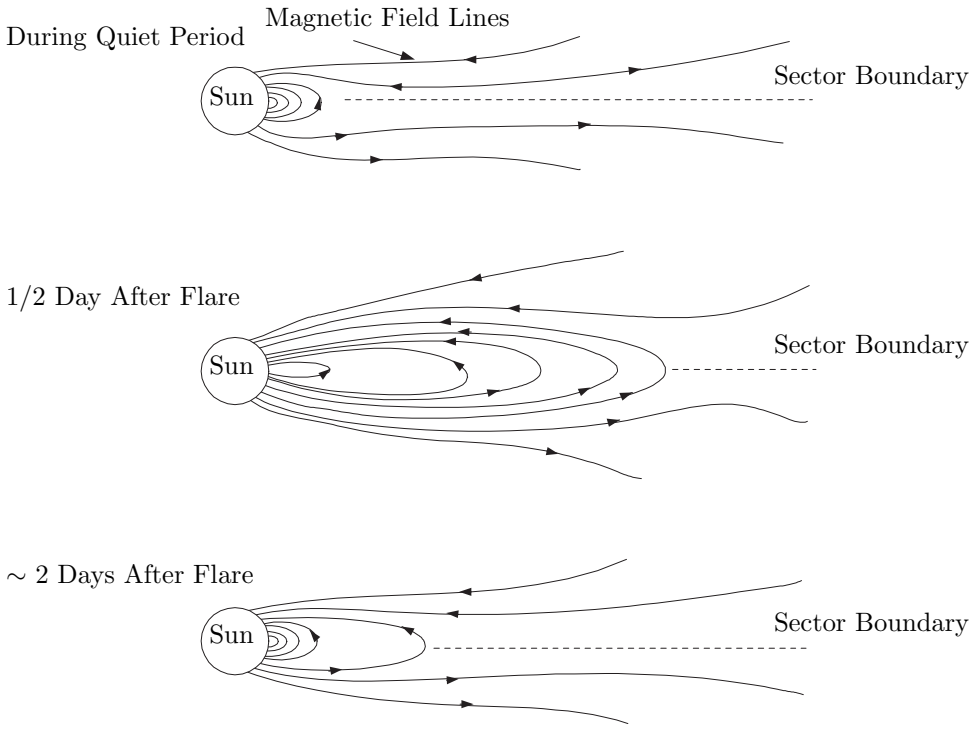

Figure 2.5: Appearance and Evolution of a Magnetic Bottle (Adapted from Ref. 35)

Since solar flares are closely tied to sunspots, the occurrence of magnetic storms is related to

sunspot activity. The rotation rate of the sun is 27 days, which suggests that the frequency of magnetic storms follow a 27-day cycle. In addition, the activity of sunspots follows the 11-year solar cycle, so increases in magnetic storms follow this same trend.

The effects of magnetic storms occur simultaneously in all areas of the world. The intensities vary by latitude, however. The largest effects are noted in the auroral zones, which are located near 67° in geomagnetic latitude. Here, the magnitude of the disturbance can be in excess of 2000 nT. At higher latitudes, the magnetic storm is more irregular than at the lower latitudes.

Secular Variations

Unlike temporal variations, which are short-duration high-intensity variations, secular variations in the magnetic field occur gradually over very long periods of time. The secular variations are very small, but after a few years their accumulation is enough to make the magnetic field models outdated. Secular variation terms are estimated in magnetic field models to propagate data for a few years after the model epoch.

The dipole strength of the magnetic field is decreasing by 0.05% per year. In addition, the portion of the dipole located in the Northern Hemisphere is drifting westward at 0.014 degrees per year. The changes in magnetic pole position in the North and South hemispheres are shown in Figures 2.6 and 2.7 respectively.

This drift implies that the possibility exists for a field reversal after a long period of time.

Field Reversals The existence of field reversals has not been proven without a doubt, but many arguments in its favor exist, including one from Fuller.[11] Over the years, volcanic rocks have been discovered which are magnetized in the opposite direction to the geomagnetic field. Some scientists have argued that this magnetization was caused by a magnetic field reversal, while others insist that the rocks contained an internal mechanism that caused a spontaneous self-reversal. As more rocks were discovered with this property, scientists noted that rocks of the same age at locations all around the world all had the same polarity, while no evidence for self reversal could be located in the rocks. The current theory states that field reversals occur approximately every one or two million years, but this rate has varied over time. During the Cretaceous period, which was between 120 million and 80 million years before the present time, the reversals stopped, leaving the magnetic field in its normal polarity. Conversely, for 50 million years during the Permian period, 300 million years ago, the field remained in a reversed polarity.

Locating evidence for the transition fields that are expected to exist during magnetic field reversals is difficult. Part of the reason for this is that the geomagnetic field has spent the majority of its time in either a stable normal or reversed state, and very little time in a mode of reversal. Therefore, the amount of rocks magnetized during this time is much less than

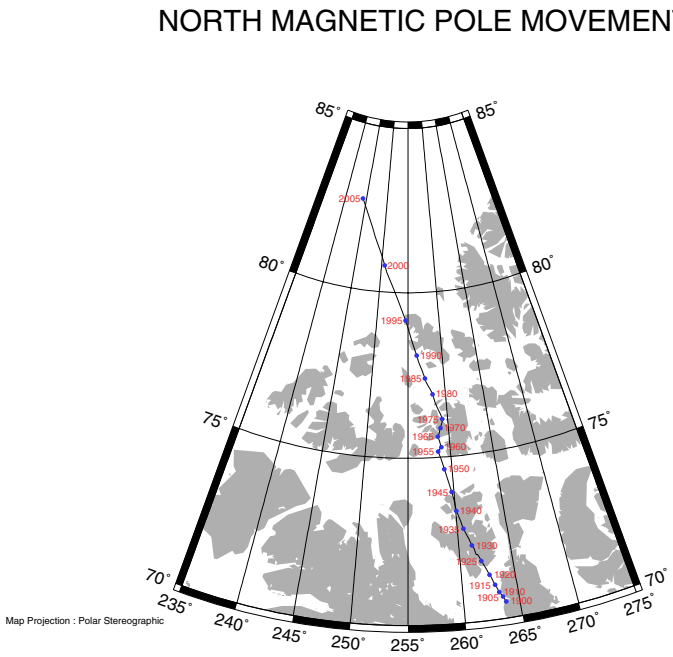

Figure 2.6: Movement of the North Pole over Time[43]

those in the normal or reversed polarities. The currently accepted amount of time for the field to reverse is approximately 10^3 years.

Examples of Secular Variations The occurrence of secular variations in the magnetic field over time can be recognized. In London, the magnetic field was first measured to be 11° east of geographic north in 1580, but almost 100 years later in 1660 the magnetic field pointed due north. In 1820, the field was 24° west of north, and in 1985 it pointed only 5° west of north. It is currently changing at the rate of 9 minutes per year.

Apparent Polar Wander and Magnetic Jerk Paleomagnetic studies of dated sedimentary rocks have suggested that the magnetic pole has circled the geomagnetic pole for the past 10,000 years in a westwardly direction. The path that the pole traces out is referred to as the Apparent Polar Wander Path, because the movement of the pole position from the paleomagnetic analysis is due to continental drift rather than the movement of the geomagnetic pole.

Magnetic field measurements have shown periods of time in which there were sudden worldwide changes in the rate of secular variation. These changes have been globally synchronous, and are called geomagnetic jerks. The most recent geomagnetic jerks occurred in the years

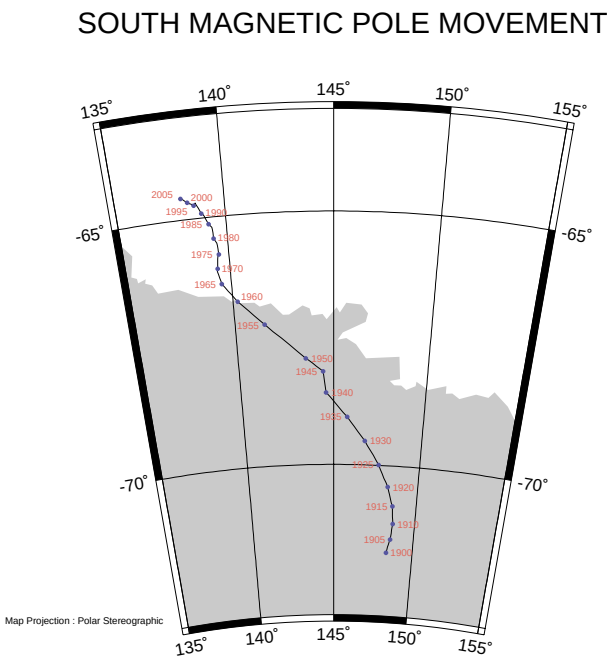

Figure 2.7: Movement of the South Pole over Time[43]

1912-1913 and 1969-1970. These occurances are apparent in Figure 2.6. The duration of both geomagnetic jerks was approximately one year. Many scientists believe that the jerk is caused by a disruptive process at the boundary of the Earth's core and mantle; however, some others believe that it is a solar-terrestrial disturbance.

2.2.4 Effects of the Earth's Magnetic Field on Spacecraft

Examining magnetic fields is extremely important in spacecraft applications. In some cases, the magnetic field can negatively affect the performance of the satellite. The lifetime of spacecraft on-board computers is based on the amount of radiation damage to their circuitry. During solar storms, it is possible for the solar wind to push the boundary of the magnetosphere such that the distribution of particles that harm spacecraft computers is greater. The possibility for single event upsets (SEUs), or bit flips, becomes increased. A SEU has the ability to change critical data in a computer program.[6]

The magnetic field can be used to the advantage of the spacecraft, however. The magnetic field has the ability to change the orientation of a body. While this may act to complicate the dynamics of the spacecraft, when used correctly the magnetic field may be used for satellite control.

2.3 Theory and Mathematical Models

The Earth's magnetic field can be analytically calculated at any point around the Earth, and it is possible to describe the magnetic field in a variety of coordinate systems, depending on computation requirements. Information on the mathematical models of the geomagnetic field is provided by Wertz.[46]

2.3.1 Coordinate Systems

The magnetic field can be described in a variety of ways, each requiring 3 numbers and detailed in Figure 2.8. One way is with an angular relationship. This relationship uses the intensity of the field, F, the inclination, or angle of dip of the field below the horizontal plane, I, and the declination, or angle between the horizontal component of the field and true geographic north, D. Another way to define the magnetic field at any point is to examine component directions. This definition has X northward, Y eastward, and Z downward. Another component, the horizontal field intensity, H, is often used. These components are related by the following equations:

$$\begin{aligned} H &= F\cos I && (2.13)\\ Z &= F\sin I && (2.14)\\ \tan I &= Z/H && (2.15)\\ X &= H\cos D && (2.16)\\ Y &= H\sin D && (2.17)\\ \tan D &= Y/X && (2.18) \end{aligned}$$

$$F^2 = H^2 + Z^2 = X^2 + Y^2 + Z^2 \quad (2.19)$$

In literature, the magnetic field is often presented in X, Y, Z form. The transformation from local tangential coordinates to X, Y, Z is:

$$\begin{aligned} X &= -B_\theta\cos\epsilon - B_r\sin\epsilon && (2.20)\\ Y &= B_\phi && (2.21)\\ Z &= B_\theta\sin\epsilon - B_r\cos\epsilon && (2.22) \end{aligned}$$

where B_r is the radial component measured outward positive, B_θ is the coelevation measured south positive, and B_ϕ is the azimuthal component measured east positive. The correction term for the oblateness of the Earth, ϵ, is

$$\epsilon \equiv \lambda - \delta < 0.2^\circ \quad (2.23)$$

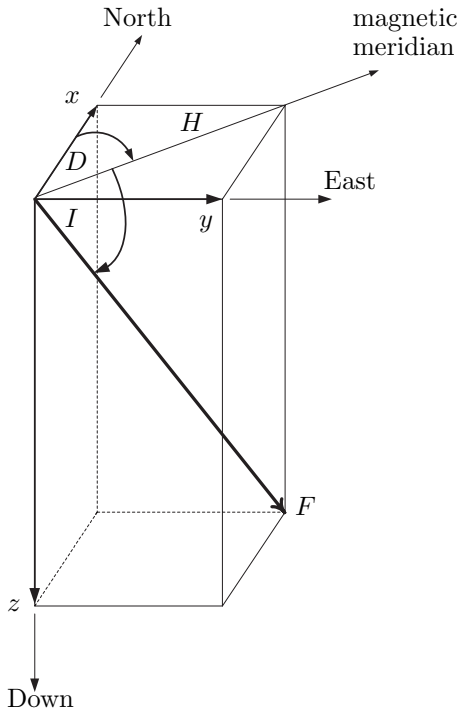

Figure 2.8: Magnetic Field Coordinates (Adapted from Ref. 42)

where the geodetic latitude is defined by λ, and δ is the declination, where

$$\delta = 90^\circ - \theta \tag{2.24}$$

and θ is the co-elevation.

In satellite applications, the geocentric inertial components are often used. The transformation from local tangential to geocentric inertial is:

$$B_x = (B_r \cos\delta + B_\theta \sin\delta)\cos\alpha - B_\phi \sin\alpha \tag{2.25}$$
$$B_y = (B_r \cos\delta + B_\theta \sin\delta)\sin\alpha + B_\phi \cos\alpha \tag{2.26}$$
$$B_x = (B_r \sin\delta - B_\theta \cos\delta) \tag{2.27}$$

The magnetic field is a function of both declination and right ascension, α, defined by $\phi = \alpha - \theta_g$. Here, ϕ is the longitude and θ_g is the sidereal time at Greenwich.

2.3.2 Analytic Models

Analytic models have been created to describe the characteristics of the geomagnetic field. These models provide the local magnetic field at any location around the Earth, assuming

an undistorted, steady state field that has no external sources or localized Earth anomalies. The most commonly used models are the spherical harmonic model and the tilted dipole model.

The Earth's magnetic field, $\mathbf{B}$, can be described as the negative gradient of a scalar potential function, V, or

$$\mathbf{B} = -\nabla V \tag{2.28}$$

V is described by a series of spherical harmonics,

$$V(r,\theta,\phi) = R_\oplus \sum_{n=1}^{k} \left(\frac{R_\oplus}{r}\right)^{n+1} \sum_{m=0}^{n} (g_n^m \cos m\phi + h_n^m \sin m\phi) P_n^m(\theta) \tag{2.29}$$

where $R_\oplus$ is the equatorial radius of the Earth, g_n^m and h_n^m are Gaussian coefficients, r, θ, and ϕ are the geocentric distance, coelevation, and East longitude from Greenwich, and P_n^m is the associated Legendre function of degree n and order m.

International Geomagnetic Reference Field

The set of Gaussian coefficients for use in the analytical models describing the Earth's magnetic field are called the International Geomagnetic Reference Field (IGRF). Every five years, a group from the International Association of Geomagnetism and Aeronomy examines the measured geomagnetic field representations and produces the coefficients for that particular year in nT. In addition, previous IGRFs are occasionally updated using new data, and named a Definitive Geomagnetic Reference Field (DGRF). A specific field model is referred to by including the year of epoch in the name, *i.e.* IGRF2000 or DGRF1990. Two sets of coefficients are linearly interpolated to calculate the magnetic field for years in between IGRF epochs. The most recent publication is the IGRF2000.[8]

The IGRF models also include a set of secular variation terms that are valid for five years after the model epoch. These values are listed in nT/year, and can be used to extrapolate the coefficients for five years past the IGRF data. The IGRF and DGRF data for the 20th century is listed in Appendix B.

Spherical Harmonic Model

Gauss first proposed the idea that the geomagnetic field follows spherical harmonics in the 1830's.[42] This expansion model of the magnetic field satisfies both LaPlace's and Maxwell's equations. The spherical harmonic analysis creates a mathematic representation of the entire main field using only a small table of numbers. The resulting field is equivalent to that of a bumpy sphere, similar to that in Figure 2.9.

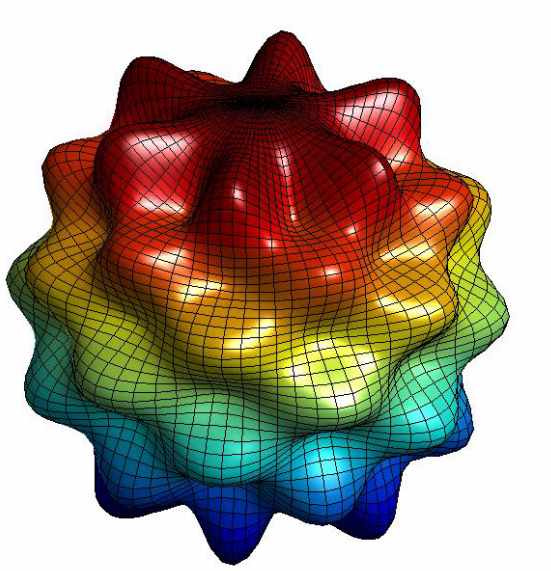

Figure 2.9: Spherical Harmonic Model of Degree 6, Order 1

The **B** field in tangential coordinates is calculated as

$$\begin{aligned}
B_r &= \frac{-\partial V}{\partial r} = \sum_{n=1}^{k} \left(\frac{R_\oplus}{r}\right)^{n+2} (n+1) \sum_{m=0}^{n} (g^{n,m} \cos m\phi + h^{n,m} \sin m\phi) P^{n,m}(\theta) \\
B_\theta &= \frac{-1}{r} \frac{\partial V}{\partial \theta} = -\sum_{n=1}^{k} \left(\frac{R_\oplus}{r}\right)^{n+2} \sum_{m=0}^{n} (g^{n,m} \cos m\phi + h^{n,m} \sin m\phi) \frac{\partial P^{n,m}(\theta)}{\partial \theta} \\
B_\phi &= \frac{-1}{r \sin\theta} \frac{\partial V}{\partial \phi} \\
&= \frac{-1}{\sin\theta} \sum_{n=1}^{k} \left(\frac{R_\oplus}{r}\right)^{n+2} \sum_{m=0}^{n} m(-g^{n,m} \sin m\phi + h^{n,m} \cos m\phi) P^{n,m}(\theta)
\end{aligned} \tag{2.30}$$

where

$$g^{n,m} \equiv S_{n,m} g_n^m \tag{2.31}$$

$$h^{n,m} \equiv S_{n,m} h_n^m \tag{2.32}$$

and

$$S_{n,m} = \left[\frac{(2-\delta_m^0)(n-m)!}{(n+m)!}\right]^{1/2} \frac{(2n-1)!!}{(n-m)!} \tag{2.33}$$

The Kronecker delta, $\delta^i_j = 1$ if $i = j$ and 0 otherwise. In addition $P^{n,m}$ is defined by

$$\begin{aligned} P^{0,0} &= 1 && (2.34)\\ P^{n,n} &= \sin\theta P^{n-1,n-1} && (2.35)\\ P^{n,m} &= \cos\theta P^{n-1,m} - K^{n,m} P^{n-2,m} && (2.36) \end{aligned}$$

where

$$K^{n,m} = \begin{cases} \frac{(n-1)^2 - m^2}{(2n-1)(2n-3)} & n > 1 \\ 0 & n = 1 \end{cases} \quad (2.37)$$

The magnetic field values can be rotated into other reference frames depending on the required use.

Tilted Dipole Model

For analytic purposes, a tilted dipole model of the geomagnetic field can be obtained by calculating the spherical harmonic model to the first degree ($n = 1$) and all orders ($m = 0, 1$). The scalar potential, V, becomes

$$\begin{aligned} V(r,\theta,\phi) &= \frac{{R_\oplus}^3}{r^2}\Big[g_1^0 P_1^0(\theta) + (g_1^1\cos\phi + h_1^1\sin\phi)P_1^1(\theta)\Big] \\ &= \frac{1}{r^2}\big(g_1^0 {R_\oplus}^3\cos\theta + g_1^1 {R_\oplus}^3\cos\phi\sin\theta + h_1^1 {R_\oplus}^3\sin\phi\sin\theta\big) \end{aligned} \quad (2.38)$$

The first degree Gaussian coefficients in the year 2000 are

$$\begin{aligned} g_1^0 &= -29615 \text{ nT} \\ g_1^1 &= -1728 \text{ nT} \\ h_1^1 &= 5186 \text{ nT} \end{aligned} \quad (2.39)$$

The total dipole strength is given by

$${R_\oplus}^3 H_0 = {R_\oplus}^3\Big(g_1^{0^2} + g_1^{1^2} + h_1^{1^2}\Big)^{1/2} \quad (2.40)$$

which leads to a value of $H_0 = 30115$ nT.

The coelevation of the dipole in the year 2000 is

$$\theta'_m = \cos^{-1}\left(\frac{g_1^0}{H_0}\right) = 196.54^\circ \quad (2.41)$$

and the East longitude of the dipole is

$$\phi'_m = \tan^{-1}\left(\frac{h_1^1}{g_1^1}\right) = 108.43^\circ \tag{2.42}$$

This equation shows that the geomagnetic field is caused by a dipole that has its northern magnetization pointing towards the Southern hemisphere. Magnetic dipoles located in this region, which are free to rotate, will point towards the North Pole. The end of the Earth's magnetic dipole that is located in the Northern hemisphere is thus located at 79.54°N, 288.43°E, and is referred to as the magnetic North Pole. This value differs from the values listed in section 2.2.1 because this calculation assumes a tilted dipole that is centered in the Earth.

The magnetic field in local tangential coordinates with a tilted dipole model is

$$B_r = 2\left(\frac{R_\oplus}{r}\right)^3\Big[g_1^0\cos\theta + (g_1^1\cos\phi + h_1^1\sin\phi)\sin\theta\Big] \tag{2.43}$$

$$B_\theta = \left(\frac{R_\oplus}{r}\right)^3\Big[g_1^0\sin\theta - (g_1^1\cos\phi + h_1^1\sin\phi)\cos\theta\Big] \tag{2.44}$$

$$B_\phi = \left(\frac{R_\oplus}{r}\right)^3\Big[g_1^1\sin\phi - h_1^1\cos\phi\Big] \tag{2.45}$$

By assuming that the magnetic field of the Earth is due to a vector dipole with strength and pole direction given above, the magnetic field can be calculated in vector form:

$$\mathbf{B}(\mathbf{R}) = \frac{{R_\oplus}^3 H_0}{R^3}\Big[3(\hat{\mathbf{m}}\cdot\hat{\mathbf{R}})\hat{\mathbf{R}} - \hat{\mathbf{m}}\Big] \tag{2.46}$$

where $\mathbf{R}$ is the position vector of the desired point in the magnetic field, and $\hat{\mathbf{m}}$ is the dipole direction. $\hat{\mathbf{R}}$ and $\hat{\mathbf{m}}$ designate unit vectors. This vector can be calculated in any coordinate system, and this value in the geocentric inertial frame is shown below.

$$\hat{\mathbf{m}} = \begin{bmatrix} \sin\theta'_m\cos\alpha_m \\ \sin\theta'_m\sin\alpha_m \\ \cos\theta'_m \end{bmatrix} \tag{2.47}$$

where

$$\alpha_m = \theta_{g0} + \omega_\oplus t + \phi'_m \tag{2.48}$$

where θ_{g0} is the Greenwich sidereal time at some reference time, $\omega_\oplus$ is the average rotation rate of the Earth equal to 7.2921152×10^{-5} rad/sec, t is the time since reference, and θ'_m and ϕ'_m are defined in Equations 2.41 and 2.42.

This calculation leads to magnetic field components in geocentric inertial components of

$$\begin{aligned} B_x &= \frac{{R_\oplus}^3 H_0}{R^3}\Big[3(\hat{\mathbf{m}}\cdot\hat{\mathbf{R}})R_x - \sin\theta'_m\cos\alpha_m\Big] \\ B_y &= \frac{{R_\oplus}^3 H_0}{R^3}\Big[3(\hat{\mathbf{m}}\cdot\hat{\mathbf{R}})R_y - \sin\theta'_m\sin\alpha_m\Big] \\ B_z &= \frac{{R_\oplus}^3 H_0}{R^3}\Big[3(\hat{\mathbf{m}}\cdot\hat{\mathbf{R}})R_z - \cos\theta'_m\Big] \end{aligned} \tag{2.49}$$

for a tilted dipole model.

Other Models

The most popular methods of describing the magnetic field are the spherical harmonic model and the tilted dipole model, but a few other models are occasionally used. These models include the quadrupole and centered dipole models.[1]

Quadrupole The quadrupole model is another way to represent the geomagnetic field using spherical harmonics. With this model, the first eight terms of the spherical harmonic model are expanded, and includes both dipolar and quadrupolar effects.

Centered Dipole A centered dipole model is obtained by using the first term in the spherical harmonic expansion model. This expansion models the magnetic field with the magnetic dipole coincident with the spin-axis of the Earth. This model of the geomagnetic field is the least accurate.

2.3.3 Accuracy of Models

When using the spherical harmonic expansions to describe the geomagnetic field, it usually follows that the more coefficients there are, the more accurate the results. However, using too many coefficients can be unfavorable because of an increase in computation time that does not correspond with an increase in accuracy, as described in the IGRF guide.[8]

The terms in the IGRF are truncated at degree 10, which contains 120 coefficients. This accuracy provides a well-determined main field model and avoids contamination from surface effects. At the Earth's surface, the accuracy is within a few tens of nT's in intensity. When the distance from the center of the Earth is increased to $4R_\oplus$, the error is reduced by a factor of 3 or 4. As the distance is increased, the spherical harmonic model becomes less representative of the magnetic field. This result is due to the higher effects of the solar wind, and these effects cause this model to not be valid past $6.6R_\oplus$, or synchronous orbit.

The quadrupole model is the next most accurate model, after the spherical harmonic expansion. At a distance greater than $1.2R_{\oplus}$, the maximum error is 20% in magnitude, and 10° in direction. As the distance to the surface of the Earth decreases, the error increases, until it reaches 40% in magnitude and 20° in direction at the surface.

The dipole models are less accurate than the quadrupole model. At distances greater than $3R_{\oplus}$, the errors for the tilted dipole model are approximately 9% in magnitude and 7° in direction. This inaccuracy increases as the distance to the surface of the Earth decreases. When the dipole axis is coincident with the spin axis, the centered dipole model gives results that are too low.

The coefficients in the IGRF are rounded to the nT and carried out to $n = 10$, which represents the limits of the resolution of the measured data. The secular variation terms are carried out to $n = 8$, which includes 80 coefficients, and is rounded to 0.1 nT to reduce rounding error.

The less accurate dipole models have some advantages over the more complex spherical harmonic ones since they take less computation time. Dipole models are valid for preliminary designs, when the magnitude of the spacecraft dipole moment is an estimated value, if average value results are required, or if the orbit radius is greater than $3R_{\oplus}$. When the spacecraft dipole moment is known and the instantaneous attitude is required, the spherical harmonic models are used.

2.4 Measuring Magnetic Fields

The simplest way to determine the direction and strength of magnetic fields is through the use of a magnetic needle. If allowed to freely pivot, the needle moves to a position parallel to the local lines of force of the magnetic field pointing north. If the magnetic needle is able to tilt, it will also become aligned with the inclined position. Additionally, the field intensity can be determined with a magnetic needle. If the needle is turned through an angle of 90° from its rest position, the torque required to keep the needle from returning to equilibrium is a measure of the field intensity.[42]

2.4.1 Measurement Hardware

Many different devices are currently utilized in order to obtain measurements of the magnetic field, as described by Macintyre.[25] The separate techniques that are used have different technologies that make each one suitable for particular applications, ranging from sensing the presence of a magnetic field to obtaining accurate measurements of the magnitude and direction of a field.

Magnetic field sensors can be grouped into two categories. The first collection of devices

are those that measure low field strengths, or magnetometers. These sensors are capable of making measurements of fields that are < 1 mT. Magnetometers can further be separated into ones that measure vector components, and ones that measure scalar magnitudes. The second group of devices are those that measure high field strengths that are >1 mT. These are known as gaussmeters. A comparison of the characteristics of various field strength instruments is shown in Table 2.3.

Table 2.3: Field Strength Instrument Characteristics (Adapted from Ref. 25)

Instrument	Range (mT)	Resolution (nT)	Comment
Induction Coil	10^{-10} to 10^{6}	Variable	Cannot measure static fields
Fluxgate	10^{-4} to 0.5	0.1	General-purpose vector magnetometer
SQUID	10^{-9} to 0.1	10^{-4}	Highest sensitivity magnetometer
Hall Effect	0.1 to 3×10^{4}	100	Best for fields above 0.1T
Magnetoresistance	10^{-3} to 5	10	Good for mid-range applications
Proton precession	0.02 to 0.1	0.05	General-purpose scalar magnetometer
Optically pumped	0.01 to 0.1	0.005	Highest resolution scalar magnetometer

Vector Magnetometers

Types of low field vector magnetometers include induction air coil magnetometers, fluxgate magnetometers, and Superconducting Quantum Interference Device (SQUID) magnetometers.

Induction Coil Magnetometer The induction coil is one of the most widely used vector measurements, as well as one of the simplest. It is based on Faraday's law, which states that a changing magnetic flux, ϕ, through the area enclosed by a loop of wire causes a voltage to be induced which is proportional to the rate of change of the flux, or

$$e(t) = -\frac{\mathrm{d}\phi}{\mathrm{d}t} \tag{2.50}$$

Two types of induction coil configurations for measuring field strength are air core loop antennas and rod antennas. These both operate using the same assumptions and techniques.

The air core loop antenna (Figure 2.10) is made of a loop consisting of one or more turns of wire, and no magnetic core. The diameter of the loop is much greater than that of the winding cross section. The air core loop antenna is most useful for measuring magnetic

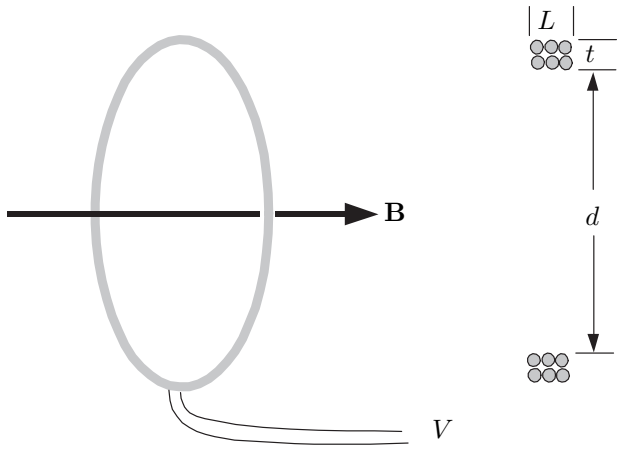

Figure 2.10: Air Core Loop Antenna (Adapted from Ref. 25)

fields whose frequencies range from 100 Hz to several megahertz. This type of antenna has no intermodulation distortion because it has a linear response to the magnetic field strength. However, when high sensitivities at low frequencies are required, the sensor is required to be very large.

A rod antenna (Figure 2.11) consists of a solenoid with a magnetic core. The core is made from a material that has a high relative permeability, such as a ferrite, a nickel-iron alloy, or an amorphous metal glass alloy. The rod antenna has advantages over the air core loop antenna since it can be smaller with the same sensitivity, and also can be designed to operate at lower frequencies. However, the response to the magnetic field strength can be nonlinear, and the core can add noise to the system.

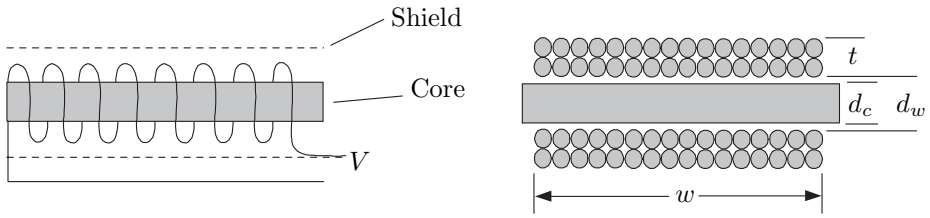

Figure 2.11: Rod Antenna (Adapted from Ref. 25)

Fluxgate Magnetometer A fluxgate magnetometer is extremely popular for use in many applications. Characteristically, it is small, reliable, and does not require much power to operate. It is able to measure the vector components of a magnetic field in a 0.1 nT to 1 mT range. These are the magnetometers of choice for satellite attitude systems.

The fluxgate magnetometer is a transducer which converts a magnetic field into an electric voltage. Fluxgates are configured with windings through which a current is applied. If there is no component of the magnetic field along the axis of the winding, the flux change detected by the winding is zero. If there is a field component present, the flux in the core changes from a low level to a high level when the material goes from one saturation level to another. From Faraday's law, a changing flux produces a voltage at the terminals of the winding proportional to the rate of change of the flux.

SQUID Magnetometer The SQUID (Superconducting Quantum Interference Device) magnetometer works on the principle that the magnitude of a superconducting current flowing between two superconductors separated by a thin insulating layer is affected by the presence of a magnetic field. These magnetometers are the most sensitive devices available to measure the magnetic field strength. However, one disadvantage is that only the change in the magnetic field can be measured, instead of the absolute value of the field.

Vector Gaussmeters

Two types of high-field vector gaussmeters are Hall effect gaussmeters and magnetoresistive gaussmeters.

Hall Effect Gaussmeter The Hall effect gaussmeter is the most widely used sensor for measuring strong magnetic fields. It is based on the Hall effect, which states that under the influence of a magnetic induction field, a moving charge experiences a force that is at a right angle to the field vector and the velocity vector of the charge.

$$\mathbf{F} = -q\big(\mathbf{E} + \mathbf{v} \times \mathbf{B}\big) \tag{2.51}$$

Hall effect devices can be made out of conductors such as copper, but using semiconducting materials such as gallium arsenide, indium antimonide, or indium arsenide produces the most stable Hall coefficients. The most favored material is indium arsenide because it has a low temperature coefficient of sensitivity, low resistance, and a relatively good sensitivity.

Magnetoresistive Gaussmeter Magnetoresistive gaussmeters work because the resistivity of a ferromagnetic material changes under the influence of a magnetic field. The amount of changed is based on the magnitude of the magnitization, as well as the direction of flow of the current to measure resistivity.

Scalar Magnetometers

Scalar magnetometers measure the magnitude of the magnetic field. This measurement is accomplished by using the atomic and nuclear properties of matter. Scalar magnetometers have very high resolution and accuracy, and are almost independent of orientation to the magnetic field. A few limitations exist with scalar magnetometers, however. They require the magnetic field to be constant throughout the sensing element area, and have a limited measurement range, which is typically 20 μT to 100 μT. In addition, while the orientation of the magnetic field does not affect the reading of the sensor, there are a few limitations of the direction of the magnetic field vector relative to the sensor in order for a measurement to be taken.

Proton Precession Magnetometer A proton precession magnetometer works under the principle that a spinning nucleus precesses around a magnetic field like a gyroscope. The frequency of the precession is proportional to the magnitude of the magnetic field present.

The proton precession magnetometer is the most popular device for measuring the scalar magnetic field strength. It is primarily used to calibrate magnetometers and systems which are used to generate magnetic fields.

Optically Pumped Magnetometer The optically pumped magnetometer is based on the Zeeman effect. When a field is applied to an atom emitting or absorbing light, the spectral lines of the atoms split into sets of new spectral lines which are closer together than the normal lines. The energy-related frequency interval is proportional to the magnitude of the applied field.

The sampling rate of the optically pumped magnetometer is greater than the rate of the proton precession magnetometer. It has a greater sensitivity, but the drawbacks include a higher cost and decreased reliability.

2.4.2 Magnetic Field Measurement of Celestial Bodies

Physically measuring the magnetic field of celestial bodies proves to be very difficult. Through much experimentation, different techniques have been discovered to perform these measurements.[35] Some particles in space can be captured and the magnetic fields can be measured directly. Pieces of meteorites, moonrock, and solar wind particles can be tested in a terrestrial laboratory. For some celestial bodies, it is possible to take actual measurements. This is accomplished through the use of space probes traveling through the areas of interest. For other inaccessible bodies in space, it is necessary to rely on indirect measurements of the magnetic field. These measurements are based on the influence of the celestial bodies on the electromagnetic radiation.

2.4.3 Data Collection for the IGRF

The spherical harmonic expansion model uses the Gaussian coefficients. Attempts have been made to calculate these coefficients theoretically, but better results have been obtained by measuring the magnetic field at points around the Earth and using a fitting technique.

The magnetic field measurements are made at magnetic observatories on the Earth, as well as by orbiting satellites. There are approximately 250 permanent observatories located around the world. These are not evenly spaced, however, so some field estimation in required in areas with sparse magnetic observatories. In recent years, a switch has been made from relying on Earth-based magnetic observatories, to utilizing satellites to do a large portion of the modelling of the main magnetic field. The IGRF 2000 model was strongly based on data from the Ørsted satellite.

Whereas satellite measurements offer many advantages to ground magnetic measurements, they also provide a few difficulties. Ionospheric dynamos and equatorial electrojet currents are internal to the satellite orbit, along with high-latitude electrojet and field-aligned currents, which contaminate the measured data. Also, satellite lifetimes are often not long enough to measure a long-term secular change. In order to compensate for this, satellites used for magnetic measurements are put in near circular orbits at altitudes above 500 km, which is as low as possible for field sensitivity, but high enough to avoid the majority of the atmospheric drag. The best magnetic field models are obtained when the ground and space data are combined.

2.5 Magnetic Fields of Other Bodies

The study of celestial magnetic fields has grown a great deal in the past century. While an abundance of information is still unknown, much advancement has been made in the understanding of magnetic fields other than Earth. Many instruments have been built, and observational data has been examined with specially formulated methods of analysis. The magnetic fields of a few celestial bodies have been discovered, and their strengths and fields have been modeled. An understanding of the role that the magnetic field plays in activities such as the birth of sunspot, flare outbursts, and solar cycles has been acquired. In addition, there has been a beginning into the investigation of the theory behind the origin of cosmic magnetism and its effect on stars, galaxies, and other bodies. Unfortunately, even with these advancements, much is still unknown about the magnetic fields of celestial bodies.

While the information in the NASA Technical Report SP-8018 from 1969[1] is informative for the geomagnetic field, it is outdated when dealing with the magnetic fields of other celestial bodies. Current information is discussed by Shi-hui,[35] Campbell,[6] and Hindmarsh.[18]

2.5.1 Reasons for Examination

The geomagnetic field is well known and modeled, and therefore can be used for attitude determination and control of Earth orbiting spacecraft. However, these same techniques cannot be used when the spacecraft is more than a few Earth radii from the surface. For satellites travelling to other planets, knowledge of the interplanetary magnetic field must be understood. In addition, if a satellite is to orbit other bodies, a complete and accurate model of the individual planetary magnetic model is required. The knowledge of planetary magnetic fields is limited at this time, so using magnetic determination and control is currently only feasible in Earth orbits.

2.5.2 Interstellar Magnetic Field

The interstellar magnetic field, or magnetic field in between celestial objects, varies greatly from the magnetic field of planets and starts. The Sun, stars, and planets have relatively strong magnetic fields concentrated in small volumes, whereas intergalactic space possesses a faint field over a large area.

The Galactic magnetic field of the Milky Way is complex, but a few things are known about it. The angle of deviation of the magnetic field from the spiral arms is small, and the field in the center of the Galaxy is perpendicular to the Galactic plane. These trends are most likely common in other galaxies as well.

2.5.3 Celestial Bodies

Current data show that all planets possess a magnetosphere, but these are often dissimilar. The main causes of these differences are due to the variations in distance from the sun, as well as the angle between the rotation axis of the planet and the axis of the magnetic field. Direct experiments to measure the magnetic field have only been carried out on the Moon and a few planets.

The Sun and Other Stars

The Sun has a complicated magnetic field because it is made up of inhomogeneous magnetic elements that differ greatly in field strength. Elements located next to each other may have opposite polarities. For this reason, obtaining an average magnetic field strength for the sun is difficult. Mean values of 10^{-4}T have been calculated, but individual elements may possess strengths of up to 10^{-2}T.

Sunspots The strongest sources of magnetism on the surface of the Sun are sunspots. The sunspots usually appear in groups, with two large spots apparent in each group. The large spot in the western part of the group, or on the front side of the direction of solar rotation, is called the preceding spot, and the large spot at the opposite position is the following spot. These spots have different magnetic polarities, with the same type of spots in the same hemisphere having the same polarity. Magnetic field lines originate in one member of a sunspot pair and enter the Sun through the other.[29]

Solar activity cycles last approximately 11 years, and at the end of this period, the polarity arrangements of the sunspots reverse. This reversal causes the sunspots to have a 22-year magnetic cycle. The mechanism behind the reversals is complex and not yet fully understood, but is monitored at the Sunspot Index Data Center in Brussels.[41] The reversals do not necessarily occur simultaneously at both poles, as was discovered in the reversal of 1957-1958. During a portion of this time, the polarity of both poles was the same. The geographic South Pole switched from south to north slowly from March to July in 1957, but the geographic North Pole switched from north to south abruptly in November of 1958. The most recent increase in sunspot activity began in 1996, with a maximum occurring around April 2000. This increase corresponds to the solar cycle 23. The number of sunspots over a 45 year range is shown in Figure 2.12.

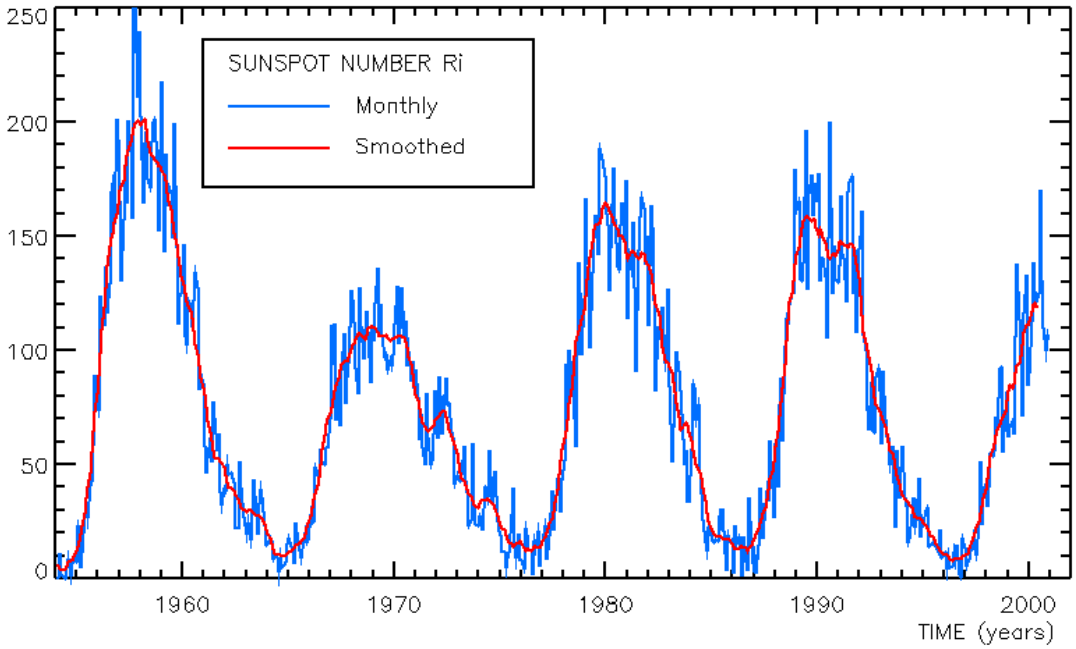

Figure 2.12: Sunspot Activity[41]

Heliosphere The magnetosphere of the Sun is called the heliosphere, and is the area created by the solar wind in interstellar space. The heliosphere has two boundaries. The inner one is the shock which terminates the region of supersonic solar wind. The outer boundary equilibrates the pressure between the solar wind and the interstellar plasma. Outside of the outer boundary in front of the heliosphere is a possible interstellar bow shock.

An Archimedes spiral (Figure 2.13) exists in the direction of the solar wind in the heliosphere. The individual solar wind particles move radially outward from the surface of the Sun, but the effect of the rotating solar surface causes a spiral pattern to occur. At the distance of 1 AU, the average spiral angle is close to 45°.[6]

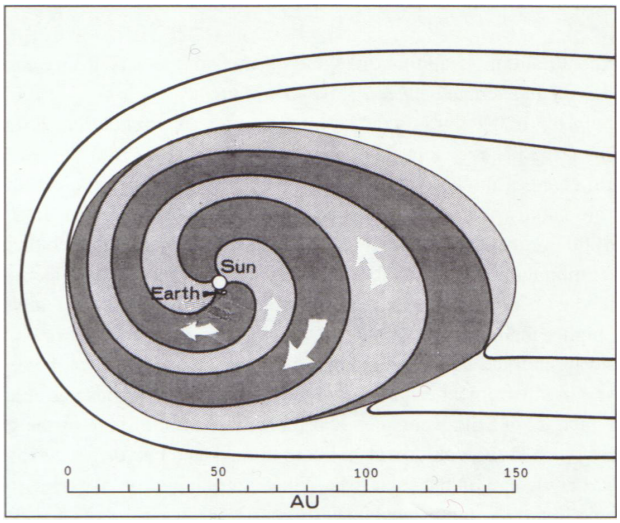

Figure 2.13: Archimedes Spiral[6]

Other Stars Not much is known about the magnetic fields of other stars besides the Sun because their great distance makes observation and measurement difficult. Only a few hundred magnetic stars have been discovered, and this information does not offer an adequate representation of the trend of the magnetic fields of stars. In addition, the observations that have been gathered only include the mean magnetic strength and do not offer any information about the structure of the field.

Some stars, known as magnetic stars, have magnetic fields of up to 3 T. White dwarfs have magnetic fields that are in the range of 10 to 10^3 T.

Moon

The first attempts to measure the magnetic field of the Moon occurred during the Lunik 2 mission in 1959. No magnetic field was detected at this point. Later missions of Lunik 10

and Explorer 35 also resulted in negative magnetic field detection. However, during Apollo 11 and 12, lunar rock was collected and brought to Earth for studying. Upon inspection, the lunar rock was discovered to contain alloys of iron along with some of nickel and cobalt, and possessed a small magnetic field. This magnitude of the lunar magnetic field is on the order of 10×10^2nT. There is no lunar shock, so the Moon absorbs the majority of the solar wind plasma.

There is much debate over the origin of the lunar magnetic field. The theories can be broken into two categories: external origins and inherent origins. The external theories suggest that an outside field magnetized the lunar material. Such outside fields include the field of the solar wind, was well as the geomagnetic field. As the Moon orbits the Earth, it moves in and out of the Earth's magnetosphere, which could act to magnetize it. The current most popular theory for the origin of the Lunar magnetic field is the inherent origin dynamo effect, which is similar to the dynamo theory for the Earth's magnetic field. In this, the Moon contains a core of liquid metal, and this motion produces the magnetic field. Another inherent origin theory is the battery theory, where the lunar magnetism is produced by a temperature gradient in the inner region of the Moon. A third inherent origin theory suggests that the Moon began as a dust cluster with a weak magnetic field. As the Moon was created, the field gradually became stronger.[29]

Mercury

The strength of the magnetic moment of Mercury is more than 2000 times smaller than that of the Earth. Since Mercury is the closest planet to the Sun, the solar wind density is high. This high density causes the magnetosphere of Mercury to be small. In fact, it is nearly $1/20^{\text{th}}$ the size of the Earth's magnetosphere. The magnetic field of Mercury resembles that of the Earth, and is inclined 11.5° from the rotational axis.

Venus

No magnetic field has been detected for Venus. The planet does, however, possess an ionosphere which deflects the solar wind and can also exclude the magnetic field from this outside source. Venus also possesses a magnetosphere, but unlike the Earth, it is not caused by its own magnetic field. Instead, it is formed by the solar wind being compressed by the ionosphere. The initial compression causes a long magnetic tail to be formed by the solar wind, but when the pressure of compression becomes high enough, the solar wind can penetrate the ionosphere and magnetize it.

Mars

Whether or not Mars has an intrinsic magnetic field is unknown. It does have a magnetosphere, however. Like the magnetosphere of Venus, it is formed by the interaction of the ionosphere with the solar wind.

Jupiter

Jupiter possesses the strongest magnetic field of any of the planets. Its magnetic moment is approximately 2×10^4 times larger than that of the Earth. Since Jupiter is located far from the sun, the planet's magnetosphere is very large. In fact, the subsolar point of the magnetopause is 100 times further than the corresponding Earth magnetopause point. Four of Jupiter's moons are located inside the magnetosphere.

The magnetic field of Jupiter is dipolar, and its axis is inclined 11° from the rotational axis. The center of the field is displaced from the center of the planet by a distance of one tenth of Jupiter's radius in the direction of the rotational axis. This displacement causes an inequality in the magnetic field strength at each of the poles.

Saturn

The magnetic field of Saturn is approximately 600 times stronger than the geomagnetic field. It has a large magnetosphere, and like Jupiter, a few of Saturn's moons are contained in this area. The magnetic axis is inclined only 1° from the rotational axis. In addition, the displacement of the magnetic center is located only 0.01 times the Saturn radius away from the geometric center of the planet. This displacement causes the magnetic field to be nearly axial symmetric. The magnetic field of Saturn is in the reversed position compared to that of the Earth.

Uranus

A magnetic field of approximately 0.3×10^{-4} T has been detected around Uranus. The rotational axis of Uranus lies near the ecliptic plane, and the magnetic axis is inclined approximately 55° to the rotational axis. This large inclination causes the magnetosphere of Uranus to undergo complicated changes over the course of one planetary day.

Neptune

The magnetic field of Neptune is at approximately the same inclination as that of Uranus. The field strength is very asymmetric, with the northern hemisphere at 0.06×10^{-4} T and

the southern hemisphere at 1.2^{-4} T.

Pluto

No magnetic field has been detected for Pluto as of the present time.

2.6 Summary

In this chapter, the basics of the geomagnetic field are presented, along with information on measuring magnetic fields, and magnetic fields of other celestial bodies. The geomagnetic field models are used in following chapters in magnetic control applications. Chapter 3 discusses spacecraft dynamics, including orbit dynamics, attitude dynamics, and attitude determination and control.

Chapter 3

Spacecraft Dynamics

The way that a spacecraft moves is described using orbit dynamics, which determines the position of the body, as well as attitude dynamics, which determines the orientation. This chapter develops equations describing both orbit and attitude dynamics. In addition, frames of reference and attitude rotations are discussed, along with environmental disturbance torques. This chapter concludes with information on attitude determination and control methods.

3.1 Orbit Dynamics

Orbit dynamics determine the position of a body orbiting another body. It is applicable for spacecraft orbiting planets, as well as for planets, such as the Earth, orbiting the Sun. Orbit dynamics are described by Bate, Mueller, and White.[4]

3.1.1 Keplerian Orbits

In 1609, Johann Kepler discovered that heavenly bodies orbit in elliptical paths. He determined three laws which describe all planetary motion.

Kepler's Laws

1. The orbit of each planet is an ellipse, with the Sun at a focus.
2. The line joining the planet to the Sun sweeps out equal areas in equal times.
3. The square of the period of a planet is proportional to the cube of its mean distance from the Sun.

All bodies are under the influence of Newton's Laws. In particular, Newton's Second Law states that the rate of change of momentum is proportional to the force impressed and is in the same direction as that force, or

$$\sum \mathbf{F} = m\ddot{\mathbf{r}} \tag{3.1}$$

where $\sum \mathbf{F}$ is the vector sum of the forces acting on mass m, and $\ddot{\mathbf{r}}$ is the vector acceleration of m relative to an inertial reference frame.

In addition, Newton formulated his Law of Universal Gravitation. This law states that any two bodies attract one another with a force proportional to their masses and inversely proportional to the square of the distance between them, or

$$\mathbf{F} = -\frac{GMm}{r^2}\frac{\mathbf{r}}{r} \tag{3.2}$$

where $\mathbf{F}$ is the force on mass m due to mass M, $\mathbf{r}$ is the vector from M to m, and G is the universal gravitational constant with a value of 6.670×10^{-11} $\mathrm{m}^3/(\mathrm{kg}{\cdot}\mathrm{s}^2)$.

When examining the relative motion of two bodies, such as the orbit of a planet around the Sun, or a satellite around a planet, it is convenient to consider the two-body problem. Two assumptions are made to simplify the problem. One is that the bodies are spherically symmetric, and can be modeled with the masses concentrated at the center of the body. The second assumption declares that there are no external or internal forces acting on the system other than the force of the gravitational attractions.

The relative motion of two bodies is shown in Figure 3.1. The vector $\mathbf{r}$ is defined as

$$\mathbf{r} = \mathbf{r}_m - \mathbf{r}_M \tag{3.3}$$

Applying Newton's laws to the system gives

$$m\ddot{\mathbf{r}}_m = -\frac{GMm}{r^2}\frac{\mathbf{r}}{r} \tag{3.4}$$

$$M\ddot{\mathbf{r}}_M = \frac{GMm}{r^2}\frac{\mathbf{r}}{r} \tag{3.5}$$

which leads to

$$\ddot{\mathbf{r}}_m = -\frac{GM}{r^3}\mathbf{r} \tag{3.6}$$

$$\ddot{\mathbf{r}}_M = \frac{Gm}{r^3}\mathbf{r} \tag{3.7}$$

By subtracting Equation 3.7 from Equation 3.6 and implementing a twice differentiated form of Equation 3.3, the following relation is obtained.

$$\ddot{\mathbf{r}} = -\frac{G(M+m)}{r^3}\mathbf{r} \tag{3.8}$$

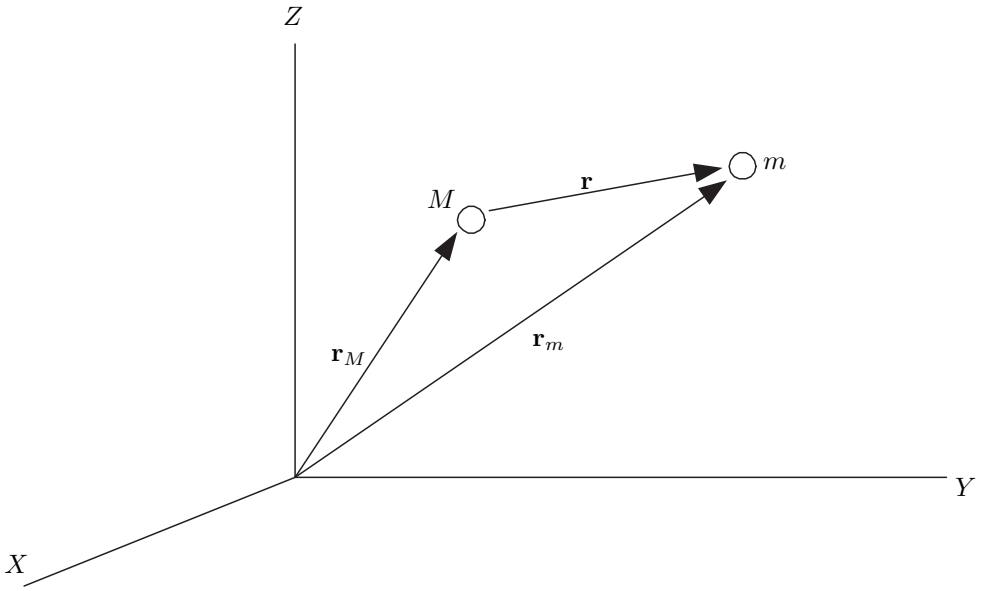

Figure 3.1: Relative Motion of Two Bodies

This is the vector differential equation of the relative motion for a two body problem.

For the application of the interaction of a satellite and a planet, the mass of the satellite, m, is much less than the mass of the planet, M. Therefore,

$$G(M+m) \approx GM \tag{3.9}$$

The gravitational parameter, μ, is defined as

$$\mu \equiv GM \tag{3.10}$$

For the Earth, this value is equal to

$$\mu_{\oplus} = 3.986032 \times 10^5 \quad \text{km}^3/\text{sec}^2 \tag{3.11}$$

With the approximation in Equation 3.9, the two-body equation of motion becomes

$$\ddot{\mathbf{r}} + \frac{\mu}{r^3}\mathbf{r} = 0 \tag{3.12}$$

where $\mathbf{r}$ is the position vector of the second body with respect to the first.

Angular Momentum

Angular momentum, $\mathbf{h}$, is a constant of motion because it is a central force . A force tangential to the center of rotation must be applied to change the angular momentum of a

rotational motion system. Since the gravitational force is always directed inward towards the center of mass, the angular momentum of the spacecraft around the center of mass does not change. The specific angular momentum is defined as

$$\mathbf{h} = \mathbf{r} \times \mathbf{v} \tag{3.13}$$

The directions of $\mathbf{r}$ and $\mathbf{v}$ must remain in the plane of the orbit in order for the angular velocity to be constant.

The magnitude of the angular velocity is

$$h = rv \cos \phi_f \tag{3.14}$$

where ϕ_f is the flight path angle, or the angle between the local horizontal and the velocity vector direction.

Orbit Equations

Although the majority of satellites follow elliptical or circular orbits, these are not the only paths satisfied by Equation 3.12. Any curve defined by a conic section is a valid orbit. The type of curve is determined by examining the polar equation of a conic section

$$r = \frac{p}{1 + e \cos \nu} \tag{3.15}$$

where ν is the polar angle between $\mathbf{r}$ and the point on the orbit closest to the focus, and p is the semi-latus parameter. These values are shown in Figure 3.2. The value of the eccentricity, e, determines the shape of the orbit as detailed below:

$e = 0$	circle
$0 < e < 1$	ellipse
$e = 1$	parabola
$e > 1$	hyperbola

The orbits discussed in this report are elliptical, and therefore the eccentricity is constrained as $0 \leq e < 1$.

The period of the orbit is equal to

$$\mathcal{T} = \frac{2\pi}{\sqrt{\mu}} a^{3/2} \tag{3.16}$$

where a is the semi-major axis. This agrees with Kepler's third law which states that the square of the period is proportional to the cube of the mean distance.

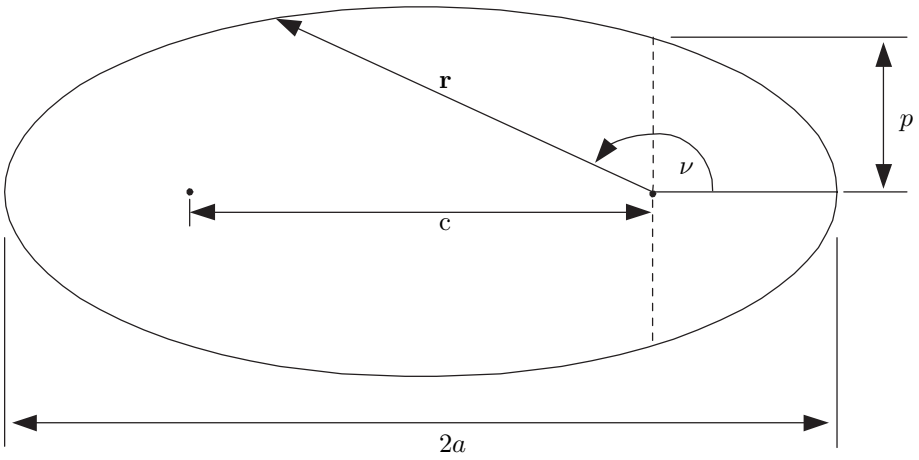

Figure 3.2: Elliptical Orbit

Orbital Elements

The orbit of a satellite can be described by five numbers, known as orbital elements. A sixth orbital element is added to determine the location of the satellite along the orbit. The orbital elements are shown in Figure 3.3.

The first two elements describe the shape of the orbit.

1. a, semi-major axis - a constant defining the size of the orbit
2. e, eccentricity - a constant defining the shape of the orbit

The next two elements describe the position of the plane of the orbit.

3. i, inclination - angle between the **K** axis and the angular momentum vector, **h**
4. Ω, right ascension of the ascending node - the angle in the fundamental plane, between the **I** axis and the point where the satellite crosses the fundamental plane in an ascending direction measured counterclockwise when viewed from North of the fundamental plane

The fifth element describes the rotation of the elliptical orbit in its plane.

5. ω, argument of periapsis - the angle, in the plane of the satellite's orbit, between the ascending node and the periapsis point, measured in the direction of the satellite's motion

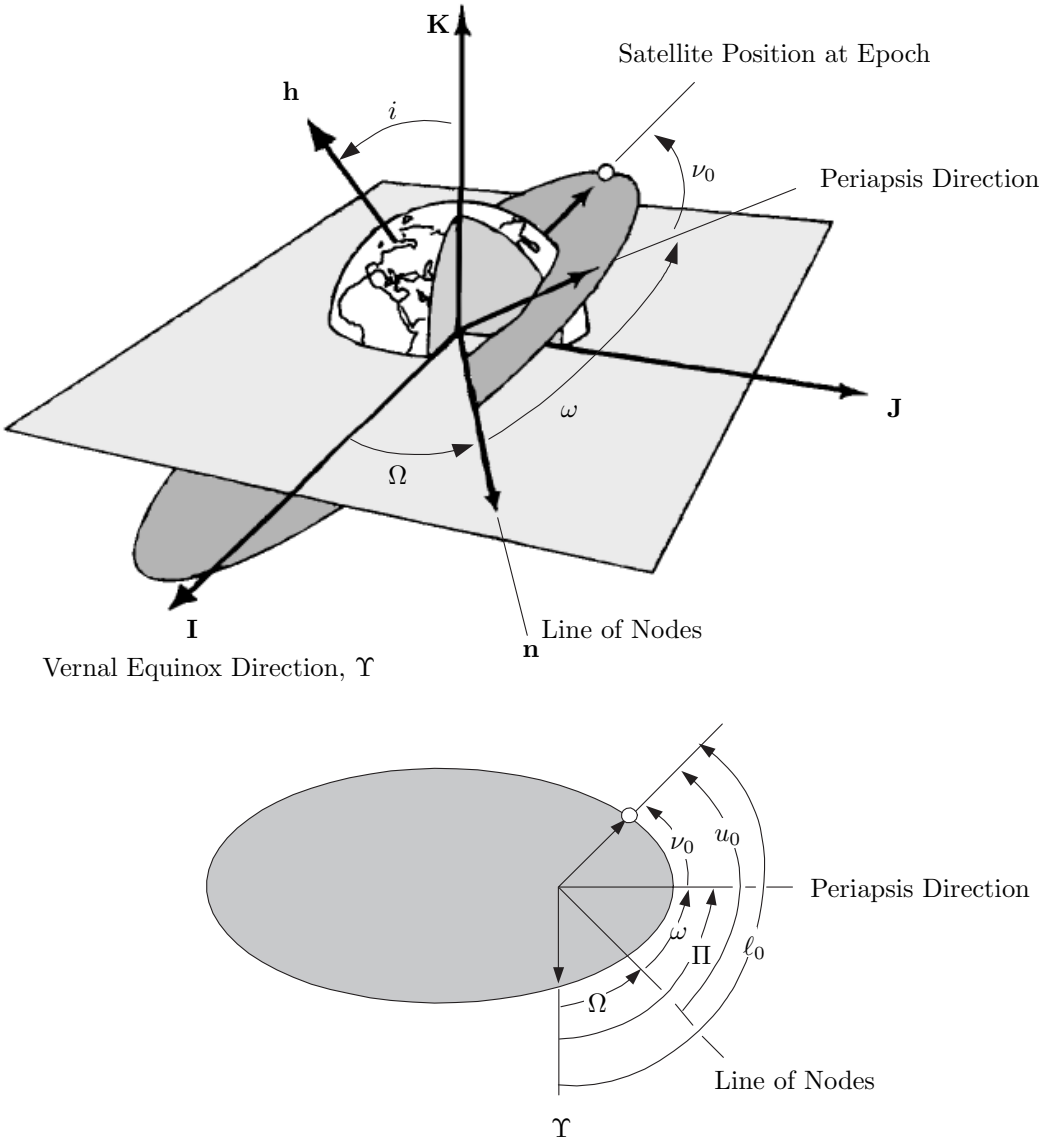

Figure 3.3: Orbital Elements (Adapted from Ref. 4)

The sixth element describes the position of the satellite in the orbit.

6. T, time of periapsis passage - time when the satellite was at periapsis

While the above six orbital elements are classically used to describe the position of a satellite, they are not exclusive. Instead of the argument of periapsis, the longitude of periapsis, Π, is occasionally used. This is the angle from the **I** direction to periapsis measured eastward.

The time of periapsis passage, T, can be replaced with the true anomaly at epoch, ν_0, which is the angle in the plane of the satellite's orbit between periapsis and the position of the satellite at a particular epoch, t_0. Additionally, the argument of latitude at epoch, u_0 can be used. This is the angle in the plane of the orbit between the ascending node and the radius vector of the satellite at epoch. These values are related by

$$u_0 = \omega + \nu_0 \tag{3.17}$$

The true longitude at epoch, ℓ_0, may also be used to describe the position of the satellite. This angle is measured eastward from the **I** axis to the ascending node, and then in the orbital plane to the radius direction at epoch. This relation is defined as

$$\ell_0 = \Omega + \omega + \nu_0 = \Pi + \nu_0 = \Omega + u_0 \tag{3.18}$$

Certain orbits cause some of the orbital elements to be undefined. When the orbit is circular, there is no periapsis, and ω, Π, and ν_0 are undefined. When the orbit is equatorial, there is no ascending node and therefore ω and u_0 are undefined. In these cases, using ℓ_0 instead of ω is useful.

3.1.2 Coordinate Systems

When describing orbital motion, it is necessary to reveal which coordinate system is used. The coordinate systems must be inertial such that the frame is fixed to an outside observer. A fixed coordinate system may also be used to describe satellite motion, but a rotation between the inertial and Earth-fixed coordinate systems must be incorporated into the definition.

Heliocentric-Ecliptic

Bodies that orbit around the Sun, such as the Earth and other planets as well as interplanetary space vehicles, are typically described in the Heliocentric-ecliptic frame of reference shown in Figure 3.4 . This reference frame is inertial, with the **Z** direction perpendicular to the plane of the ecliptic, which is the plane of the Earth's revolution around the Sun. The direction of the **X** axis is in the vernal equinox direction, and the **Y** direction is orthogonal.

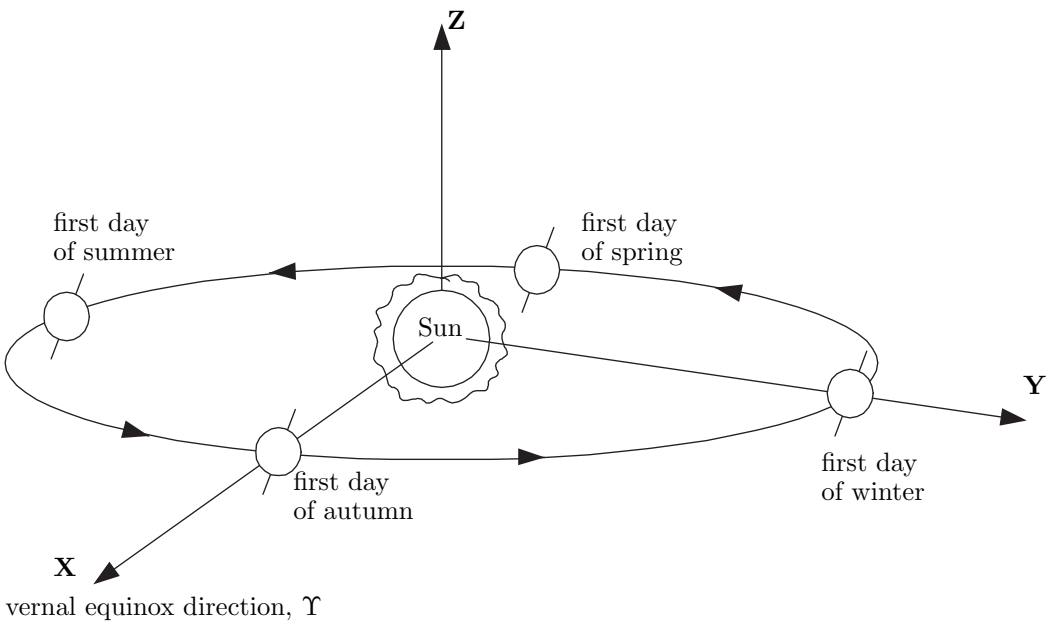

Figure 3.4: Heliocentric-Ecliptic Coordinate System (Adapted from Ref. 4)

Earth-Centered Inertial

The Earth-Centered Inertial (ECI) coordinate system is centered in the middle of the Earth, as shown in Figure 3.5. The **Z** axis points through the geographic North Pole, or the axis of rotation. The **X** axis is in the direction of the vernal equinox, and the **Y** direction is orthogonal. The Earth rotates with respect to the ECI coordinate frame.

Earth-Centered Earth-Fixed

The Earth-centered Earth-fixed (ECEF) reference frame also has its origin at the center of the Earth, but it rotates relative to inertial space, shown in Figure 3.6. The **K** axis is through the North Pole, and the **I** axis points to the Greenwich Meridian. The angle between the vernal equinox direction and the Greenwich Meridian must be defined. This is known as the Greenwich sidereal time, θ_g. Greenwich sidereal time is documented at various epochs and can be extracted from data tables as θ_{g0}. At any time after epoch, θ_g can be determined from θ_{g0} by

$$\theta_g = \theta_{g0} + \omega_\oplus (t - t_0) \tag{3.19}$$

where $\omega_\oplus$ is the angular velocity of the Earth. On January 1, 2000 at midnight, the value of θ_{g0} was equal to $6^{\text{h}}39^{\text{m}}52.2707^{\text{s}}$, or 99.96779° according to the Multiyear Interactive Computer Almanac from the U.S. Naval Observatory.[44] This value changes slightly from year to year, and on January 1, 2001 was equal to $6^{\text{h}}42^{\text{m}}51.5354^{\text{s}}$, or 100.71473°.

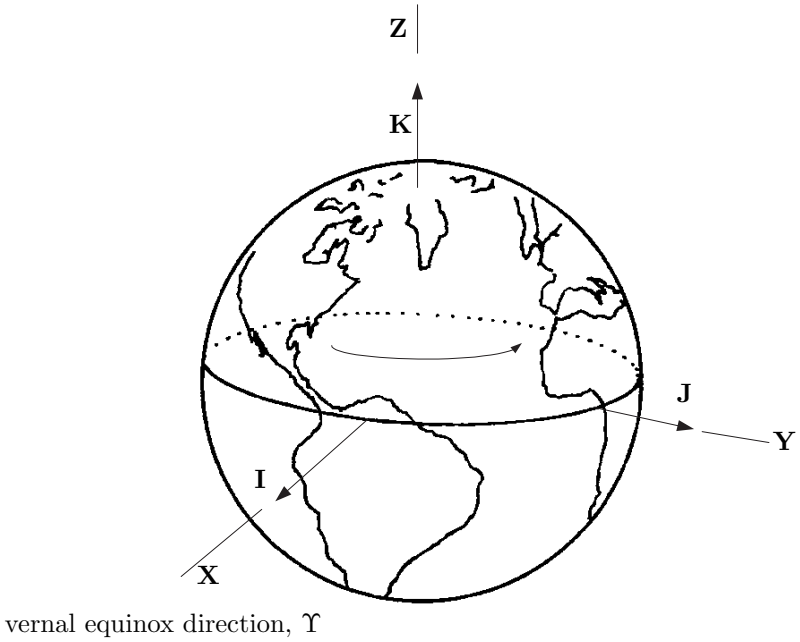

Figure 3.5: Earth-Centered Inertial Reference Frame (Adapted from Ref. 4)

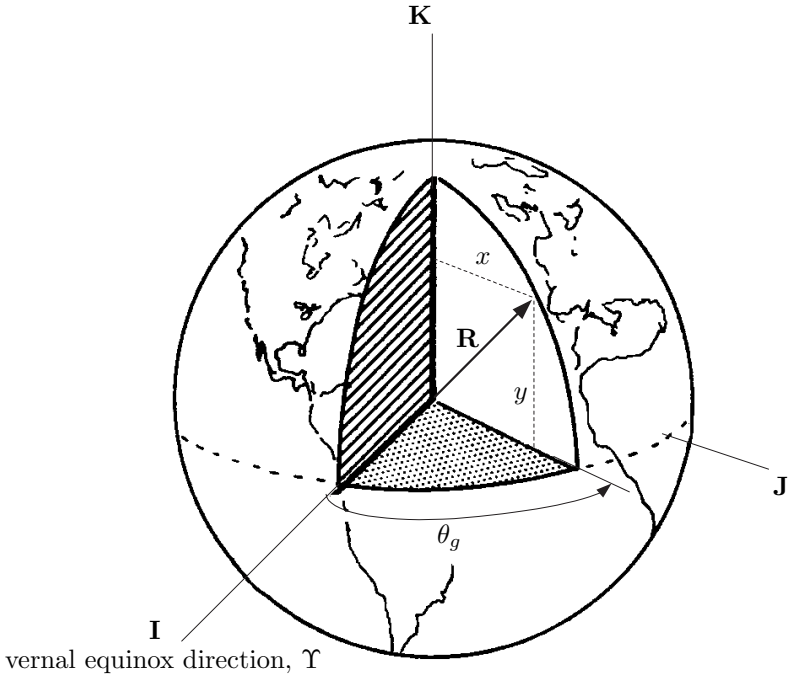

Figure 3.6: Earth-Centered Earth-Fixed Reference Frame (Adapted from Ref. 4)

3.2 Attitude Dynamics

Attitude dynamics describe the orientation of a body in an orbit and can be explained using rotations. When examining attitude dynamics, it is important to describe the reference frames being used to give a basis for the rotations.

3.2.1 Reference Frames

Three main reference frames are used to describe the orientation, or attitude, of a spacecraft in orbit. These are the inertial, orbital, and body frames.

Inertial Frame

An inertial frame is used for attitude applications. The **X** direction points from the focus of the orbit to the vernal equinox, Υ, the **Z** direction is in the orbital angular velocity direction, and **Y** is perpendicular to **X** and **Z**.

Orbital Frame

The orbital frame is located at the mass center of the spacecraft, and the motion of the frame depends on the orbit. This frame is non inertial because of orbital acceleration and the rotation of the frame. The $\hat{\mathbf{o}}_3$ axis is in the direction from the spacecraft to the Earth, $\hat{\mathbf{o}}_2$ is the direction opposite to the orbit normal, and $\hat{\mathbf{o}}_1$ is perpendicular to $\hat{\mathbf{o}}_2$ and $\hat{\mathbf{o}}_3$. In circular orbits, $\hat{\mathbf{o}}_1$ is the direction of the spacecraft velocity. The three directions $\hat{\mathbf{o}}_1$, $\hat{\mathbf{o}}_2$, and $\hat{\mathbf{o}}_3$ are also known as the roll, pitch, and yaw axes, respectively. Figure 3.7 shows a comparison of the inertial and orbital frames in an equatorial orbit.

Body Frame

Like the orbital frame, the body frame has its origin at the spacecraft's mass center. This frame is fixed in the body, and therefore is non-inertial. The relative orientation between the orbital and body frames is the basis of attitude dynamics and control.

Principal Axis

Principal axes are a specific body-fixed reference frame. This axis system has its origin at the mass center, and is oriented such that the moment of inertia matrix is diagonal and known as the principal moments of inertia.

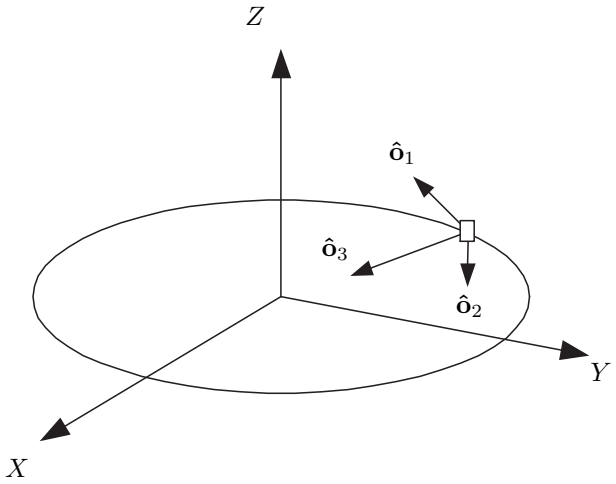

Figure 3.7: Earth-Centered Inertial and Orbital Reference Frames

3.2.2 Rotations

Rotations and transformations are performed to obtain the desired vector in alternate reference frames. Two notations commonly used to describe this rotation are Euler angles and quaternions. Rotations are discussed by Hall.[17]

Rotation Matrix

The relationship between vectors expressed in different reference frames is described as

$$\mathbf{v}_i = \mathbf{R}^{ib}\mathbf{v}_b \tag{3.20}$$

where $\mathbf{R}^{ib}$ is the rotation from $\mathcal{F}_b$ to $\mathcal{F}_i$, $\mathbf{v}_i$ is a vector in $\mathcal{F}_i$, and $\mathbf{v}_b$ is the same vector in $\mathcal{F}_b$.

The components of a rotation matrix are the direction cosines of the two sets of reference axes. In general,

$$\mathbf{R}^{21} = \begin{bmatrix} \cos\theta_{x_2x_1} & \cos\theta_{x_2y_1} & \cos\theta_{x_2z_1} \\ \cos\theta_{y_2x_1} & \cos\theta_{y_2y_1} & \cos\theta_{y_2z_1} \\ \cos\theta_{z_2x_1} & \cos\theta_{z_2y_1} & \cos\theta_{z_2z_1} \end{bmatrix} \tag{3.21}$$

where $\cos\theta_{x_2x_1}$ is the cosine of the angle between the x axis of the first frame and the x axis of the second frame.

The rotation matrix from the inertial reference frame to the orbital reference frame is defined

as

$$\mathbf{R}^{oi} = \begin{bmatrix} -\sin u\cos\Omega - \cos u\cos i\sin\Omega & -\sin u\sin\Omega + \cos u\cos i\cos\Omega & \cos u\sin i \\ -\sin i\sin\Omega & \sin i\cos\Omega & -\cos i \\ -\cos u\cos\Omega + \sin u\cos i\sin\Omega & -\cos u\sin\Omega - \sin u\cos i\cos\Omega & -\sin u\sin i \end{bmatrix} \tag{3.22}$$

which is a rotation based on the orbital elements.

Quaternions

A second way to express a rotation is through the use of quaternions. The quaternion set, $\bar{\mathbf{q}}$, is a 4×1 matrix consisting of a vector portion, $\mathbf{q}$ and a scalar portion, q_4.

$$\bar{\mathbf{q}} = \begin{bmatrix} \mathbf{q}^T & q_4 \end{bmatrix}^T \tag{3.23}$$

The rotation matrix in terms of the quaternion is

$$\mathbf{R} = \left({q_4}^2 - \mathbf{q}^T\mathbf{q}\right)\mathbf{1} + 2\mathbf{q}\mathbf{q}^T - 2q_4\mathbf{q}^\times \tag{3.24}$$

where $\mathbf{q}^\times$ is the skew symmetric of $\mathbf{q}$ defined as:

$$\mathbf{q}^\times = \begin{bmatrix} 0 & -q_3 & q_2 \\ q_3 & 0 & -q_1 \\ -q_2 & q_1 & 0 \end{bmatrix} \tag{3.25}$$

In addition, $\bar{\mathbf{q}}$ can be expressed in terms of $\mathbf{R}$ as

$$q_4 = \pm\frac{1}{2}\sqrt{1 + \text{trace}\,\mathbf{R}} \tag{3.26}$$

$$\mathbf{q} = \frac{1}{4q_4}\begin{bmatrix} R_{23} - R_{32} \\ R_{31} - R_{13} \\ R_{12} - R_{21} \end{bmatrix} \tag{3.27}$$

Quaternions have advantages and disadvantages over rotation matrix notation. The singularities that exist when certain Euler angles are small are eliminated with the use of quaternions. However, the physical meaning of quaternions is obscure and not as intuitive as rotation angles.

3.2.3 Angular Velocity

The angular velocity, $\boldsymbol{\omega}$, is used to examine the angular displacements that occur over time. Angular velocities are dependent on the frame of reference, and are designated by $\boldsymbol{\omega}_b^{ca}$, which is a rotation of $\mathcal{F}_c$ with respect to $\mathcal{F}_a$ as seen by $\mathcal{F}_b$.

Angular velocities add, but only when they are in the same reference frame. For example, the following relation is valid

$$\boldsymbol{\omega}_b^{bi} = \boldsymbol{\omega}_b^{bo} + \boldsymbol{\omega}_b^{oi} \tag{3.28}$$

When the angular velocities are in different reference frames, however, it is necessary to perform rotations. This is evident in

$$\boldsymbol{\omega}_b^{bi} = \mathbf{R}^{bo}\boldsymbol{\omega}_o^{bo} + \mathbf{R}^{bi}\boldsymbol{\omega}_i^{oi} \tag{3.29}$$

where the angular velocity is seen by the body frame.

3.3 Equations of Motion

The following is a derivation of equations of motion for a satellite system.

3.3.1 Dynamic Equations of Motion

The rotational equations for a rigid body are derived by beginning with the rotational equivalent of $m\vec{\mathbf{a}} = \vec{\mathbf{f}}$, or

$$\dot{\vec{\mathbf{h}}} = \vec{\mathbf{g}} \tag{3.30}$$

where $\vec{\mathbf{h}}$ is the angular momentum about the mass center, and $\vec{\mathbf{g}}$ is the torque. This relationship is represented in matrix form by

$$\dot{\mathbf{h}} + \boldsymbol{\omega}_b^{bi\times}\mathbf{h} = \mathbf{g} \tag{3.31}$$

Assuming that the body frame is fixed to the body at the mass center, the angular momentum can be represented by

$$\mathbf{h} = \mathbf{I}\boldsymbol{\omega}_b^{bi} \tag{3.32}$$

which leads to

$$\mathbf{I}\dot{\boldsymbol{\omega}}_b^{bi} + \boldsymbol{\omega}_b^{bi\times}\mathbf{I}\boldsymbol{\omega}_b^{bi} = \mathbf{g} \tag{3.33}$$

Solving for $\dot{\boldsymbol{\omega}}_b^{bi}$ leads to

$$\dot{\boldsymbol{\omega}}_b^{bi} = -\mathbf{I}^{-1}\boldsymbol{\omega}_b^{bi\times}\mathbf{I}\omega_b^{bi} + \mathbf{I}^{-1}\mathbf{g} \tag{3.34}$$

In this study, the only torques, $\mathbf{g}$, are gravity-gradient and magnetic.

Equation 3.34 is expanded into

$$\dot{\boldsymbol{\omega}}_b^{bi} = \begin{bmatrix} \frac{I_2-I_3}{I_1}\omega_2\omega_3 & + & \frac{g_1}{I_1} \\ \frac{I_3-I_1}{I_2}\omega_3\omega_1 & + & \frac{g_2}{I_2} \\ \frac{I_1-I_2}{I_3}\omega_1\omega_2 & + & \frac{g_3}{I_3} \end{bmatrix} \tag{3.35}$$

if principle axes ares used. These equations are known as Euler's Equations.

3.3.2 Kinematic Equations of Motion

The kinematic equations of motion are obtained by beginning with the definition of a quaternion. The quaternion is in the form

$$\bar{\mathbf{q}} = \begin{bmatrix} \mathbf{a} \sin \frac{\Phi}{2} \\ \cos \frac{\Phi}{2} \end{bmatrix} \tag{3.36}$$

where $\mathbf{a}$ is the Euler axis vector and Φ is the angle of rotation.

At time $t + \Delta t$, the quaternion is equal to

$$\bar{\mathbf{q}}(t + \Delta t) = \left(\cos \frac{\Delta\Phi}{2} \mathbf{1} + \sin \frac{\Delta\Phi}{2} \begin{bmatrix} 0 & a_3 & -a_2 & a_1 \\ -a_3 & 0 & a_1 & a_2 \\ a_2 & -a_1 & 0 & a_3 \\ -a_1 & -a_2 & -a_3 & 0 \end{bmatrix} \right) \bar{\mathbf{q}}(t) \tag{3.37}$$

Since Δt is infinitesimal and $\Delta\Phi = \omega\Delta t$, where ω is the magnitude of the instantaneous angular velocity of the body, the following small angle assumptions are used:

$$\cos \frac{\Delta\Phi}{2} \approx 1 \qquad \sin \frac{\Delta\Phi}{2} \approx \frac{1}{2}\omega\Delta t \tag{3.38}$$

This leads to

$$\bar{\mathbf{q}}(t + \Delta t) = \left[1 + \frac{1}{2}\mathbf{\Omega}\Delta t \right] \bar{\mathbf{q}}(t) \tag{3.39}$$

where $\mathbf{\Omega}$ is the skew symmetric matrix

$$\mathbf{\Omega} = \begin{bmatrix} 0 & \omega_3 & -\omega_2 & \omega_1 \\ -\omega_3 & 0 & \omega_1 & \omega_2 \\ \omega_2 & -\omega_1 & 0 & \omega_3 \\ -\omega_1 & -\omega_2 & -\omega_3 & 0 \end{bmatrix} \tag{3.40}$$

The derivative of the quaternion is

$$\dot{\bar{\mathbf{q}}} = \lim_{\Delta t \to 0} \frac{\bar{\mathbf{q}}(t + \Delta t) - \bar{\mathbf{q}}(t)}{\Delta t} = \frac{1}{2}\mathbf{\Omega}\bar{\mathbf{q}} \tag{3.41}$$

This is rearranged as

$$\dot{\bar{\mathbf{q}}} = \frac{1}{2} \begin{bmatrix} q_4 & -q_3 & q_2 \\ q_3 & q_4 & -q_1 \\ -q_2 & q_1 & q_4 \\ -q_1 & -q_2 & -q_3 \end{bmatrix} \begin{bmatrix} \omega_1 \\ \omega_2 \\ \omega_3 \end{bmatrix} = \frac{1}{2} \begin{bmatrix} \mathbf{q}^{\times} + q_4 \mathbf{1} \\ -\mathbf{q}^T \end{bmatrix} \boldsymbol{\omega} \tag{3.42}$$

This equation represents the kinematic equation of motion of the spacecraft.

3.4 Environmental Disturbance Torques

Spacecraft in orbit encounter small disturbance torques from various environmental sources. These torques are either secular, which accumulate over time, or cyclic, which vary sinusoidally over an orbit. Both types are discussed by Hughes.[20]

Different environmental torques are more prevalent at different altitudes. The relationship between altitude and disturbance torque strength is shown in Figure 3.8.

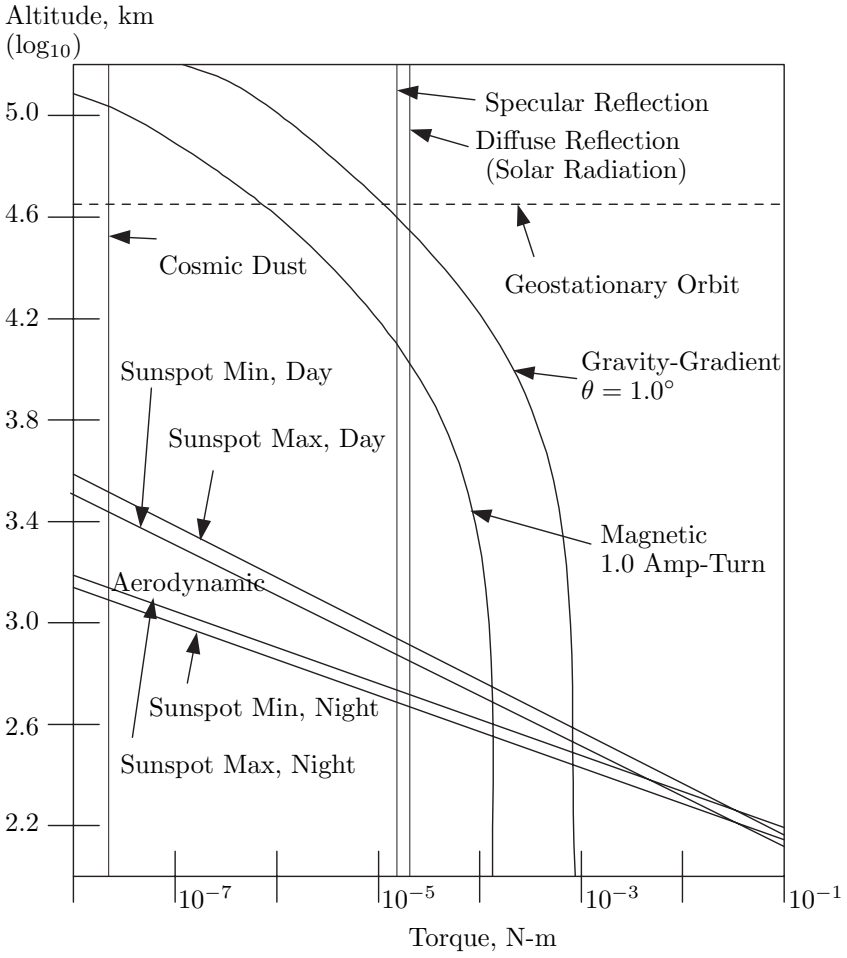

Figure 3.8: Comparison of Environmental Torques (Adapted from Ref. 20)

In low Earth orbits (LEO) the largest environmental torques are gravity-gradient, magnetic, and aerodynamic. In this analysis, only gravity-gradient and magnetic torques are considered.

3.4.1 Gravity-Gradient Torque

A gravity-gradient torque exists because of the variation in the gravitational field. Since the gravitational force field varies with the inverse square of the distance from the Earth, there is a greater force on the portion of the spacecraft closer to the Earth.

The gravity-gradient torque is constant for Earth-oriented spacecraft and cyclic for inertially oriented vehicles. It is mainly influenced by the moment of inertia of the spacecraft and the altitude of the orbit. The gravity-gradient torque, $\mathbf{g}_g$, is calculated from

$$\mathbf{g}_g = 3{\omega_c}^2 \hat{\mathbf{o}}_\mathbf{3}^\times \mathbf{I} \cdot \hat{\mathbf{o}}_\mathbf{3} \tag{3.43}$$

where $\mathbf{I}$ is the moment of inertia of the spacecraft, ω_c is the orbital angular velocity, and $\hat{\mathbf{o}}_\mathbf{3}$ is the third column in the rotation matrix from the orbital to body frame. The orbital angular veolcity is defined by

$$\omega_c = \sqrt{\frac{\mu}{a^3}} \tag{3.44}$$

if the orbit is circular.

3.4.2 Magnetic Torque

A magnetic torque is caused by the interaction between the spacecraft residual magnetic field and the the geomagnetic field. The primary sources of this torque are the spacecraft magnetic moment, eddy currents, and hysteresis, with the magnetic moment being dominant.

The magnetic torque is cyclic throughout an orbit. This torque is influenced the most by orbit altitude and the residual spacecraft magnetic field and geomagnetic field. This value, $\mathbf{g}_m$, is represented by

$$\mathbf{g}_m = \mathbf{M}^\times \mathbf{B} \tag{3.45}$$

where $\mathbf{M}$ is the sum of the individual magnetic moments caused by permanent and induced magnetism and spacecraft generated current loops, and $\mathbf{B}$ is the magnetic field.

The magnetic disturbance torque is further discussed in Section 4.1.2.

3.5 Attitude Determination

The orientation of a spacecraft can be determined by describing the rotation between a spacecraft-fixed reference frame and a known reference frame. This description is accomplished by finding rotations between measured attitude vectors and known quantities. For example, a Sun sensor determines the vector from the spacecraft to the Sun in the body

frame, $\mathbf{s}_b$. Since the vector in the inertial frame, $\mathbf{s}_i$, can be calculated from ephemeris data, the following relation is useful

$$\mathbf{s}_b = \mathbf{R}^{bi}\mathbf{s}_i \tag{3.46}$$

The attitude is determined by solving for $\mathbf{R}^{bi}$. This equation does not have a unique solution, however, so it is necessary to obtain a second attitude measurement to fully describe the attitude of a spacecraft. This second measurement results in an overdetermined problem, and an attitude determination algorithm, such as the triad algorithm or QUEST, must be utilized to reconcile the data. The QUEST algorithm is discussed by Shuster and Oh.[37]

Common attitude sensors include Sun sensors, Earth sensors, magnetometers, star trackers, and gyroscopes, and are described by Wertz and Larson.[47] A comparison of the ranges of these attitude sensors is shown in Table 3.1

Table 3.1: Ranges of Sensor Accuracy[47]

Sensor	Accuracy	Characteristics and Applicability
Magnetometers	1.0° (5,000 km alt) 5° (200 km alt)	Attitude measured relative to Earth's local magnetic field. Magnetic field uncertainties and variability dominate accuracy. Usable only below ∼6,000 km.
Earth Sensors	0.05° (GEO) 0.1° (low altitude)	Horizon Uncertainties dominate accuracy. Highly accurate units use scanning.
Sun Sensors	0.01°	Typical field of view ±130°
Star Sensors	2 arc sec	Typical field of view ±16°
Gyroscopes	0.001°/hour	Normal use involves periodically resetting the reference position.

3.5.1 Magnetometers

Magnetometers measure the strength and direction of the Earth's magnetic field to determine the orientation of a spacecraft with respect to the local magnetic field. Magnetometers are often inexpensive and have low power requirements. In addition, the magnetic field can always be measured in low Earth orbits. Magnetometers have some disadvantages, too. They often have poor resolution and do not give good results if they are far from the Earth. The measurements are limited by the strength of the local field strength, as well as the accuracy of the magnetic field model. Magnetometers were discussed previously in Section 2.4.1.

3.5.2 Earth Sensors

The Earth can be detected for attitude determination by examining the location of the horizon. Most Earth sensors use a spinning motion that can scan for the horizon line. Detecting the Earth has advantages because it is bright and not easily confused with other bodies. It has disadvantages including a resolution of only 0.1° due to an uncertainty in the horizon. Also, if a scanning motion is required, the sensors can be complicated.

3.5.3 Sun Sensors

Sun sensors are one of the most common attitude determination sensors because the Sun is easy to detect. It is bright and not easily confused with other bodies. Sun sensors have low power requirements. However, the Sun is not always visible. In addition, the accuracy is limited since the angular diameter of the Sun as seen from the Earth is approximately 1/2°.

3.5.4 Star Trackers

Star trackers work by examining constellations of stars and comparing with a library of constellations to determine the attitude of a spacecraft. These are accurate and work at any point in an orbit. However, star trackers are often massive, complex, and expensive. Searching the library of constellations is time-consuming, so for high accuracy and rapid response, star trackers are used along with gyroscopes.

3.5.5 Gyroscopes

Gyroscopes determine the attitude by measuring the rate of rotation of the spacecraft. They are located internal to the spacecraft and work at all points in an orbit. Gyroscopes have a high accuracy for limited time intervals. Some disadvantages exist with gyroscopes. Since they measure a change instead of absolute attitude, gyroscopes must be used along with other attitude hardware to obtain full measurements. They also are subject to drift, and since they have moving parts, there is more complexity.

3.6 Attitude Control

Some form of attitude control is required to change the attitude of a spacecraft or keep it in a stable position. Three main types of control are often used. These types of control include spin stabilization, three-axis control techniques, and passive control. Wertz and Larson,[47] Chobotov,[7] and Sidi[38] discuss attitude control.

3.6.1 Spin Stabilization

Spin-stabilized satellites spin about their major or minor axes, with the spin axis, or angular momentum vector, fixed with respect to inertial space. When energy dissipation is considered, only spin about a spacecraft's major axis is stable.

Single Spin

In single spin satellites, the entire spacecraft spins about the angular momentum vector. This method of stabilization is simple and has a high reliability. The cost is generally low, and it has a long system life. One disadvantage to this technique is that systems that need to be Earth pointing, such as communications antennas, are spinning. In addition, power obtained from solar cells is not efficient due to spin.

Spin-stabilized spacecraft are subject to nutation and precession, but have a gyroscopic resistance which provides stability about the transverse axis. Since spin-stabilized satellites have a high angular momentum, they have poor maneuverability.

Dual Spin

In spacecraft with dual spin, a major portion of the spacecraft is spun, while the payload section is despun at a different rate about the same axis. This technique is favorable because fixed inertial orientation is possible on the despun portion. This method of stabilization has a few disadvantages, however. This system is much more complex, which leads to an increase in cost and a decrease in reliability. In addition, the stability is sensitive to mass imbalances.

3.6.2 Three-axis Stabilization

Some spacecraft require autonomous control of all three axes during their missions. Three-axis control systems include wheels, magnetic control devices, and thrusters. Advantages to these systems include good pointing accuracy, and a non-inertial pointing accuracy. However, the hardware is often expensive, and complicated, leading to a higher weight and power.

Wheels

Three-axis stabilization wheels include reaction wheels, momentum wheels, and control moment gyros. Reactions wheels have a variable speed and a continuous and smooth control. Momentum wheels have a nonzero speed and provide angular momentum to the spacecraft.

Control moment gyros are fixed-speed gimballed wheels, but are not often used on small satellites because of their large weight.

Magnetic Control

Magnetic control devices use the interaction of the spacecraft magnetic dipole moment and the Earth's magnetic field to provide a control torque. Magnetic control torques work better in low Earth orbits than higher orbits, such as geostationary, because as the distance from the Earth increases, the geomagnetic strength decreases. Magnetic control torques are discussed in detail in Section 4.1.3.

Thrusters

Mass propulsive devices, such as thrusters, can be used for three-axis stabilization. These often consist of six or more thrusters located on the satellite body. The strength of the obtainable torque is dependent on the thrust level as well as the torque-arm length about the axis of rotation. Some disadvantages to thrusters exist because the location of the thrusters on the external surface of the spacecraft must take into account other components such as solar cells. In addition, the mass properties of the spacecraft change over time as propellent is used, which leads to a more complicated system.

3.6.3 Passive Control

Passive control techniques can be used for attitude control. These can be advantageous because they do not require moving parts, and therefore there is a savings on mass, power, and cost. In addition, they have the possibility for long lifetimes. However, there is a poor pointing accuracy that can be obtained. The most common passive control is gravity gradient, but a passive magnetic system is also possible.

Gravity-Gradient

Gravity-gradient stability uses the inertial properties of a vehicle to keep it pointed towards the Earth, but the magnitude of torque decreases with the cube of the orbit radius. The equation for gravity-gradient torque, $\mathbf{g}_g$, was given in Equation 3.43.

The following relation must be satisfied for a spacecraft to be have gravity-gradient stability:

$$I_y > I_x > I_z \tag{3.47}$$

such that I_y is the moment of inertia about the major axis, I_x is about the intermediate axis, and I_z is about the minor axis.

An elongated object in a gravity field aligns its longitudinal axis through the Earth's center. A spacecraft can be treated as gravity-gradient by having deployable booms or tethers with tip masses, causing the elongated shape. Gravity-gradient booms and tethers are sensitive to thermal shocks when entering and leaving eclipse.

Gravity-gradient torques stabilize spacecraft such that an amplitude-bounded harmonic angular motion about an average bias value remains. However, passive dampers can damp out these oscillations. One type of passive damper is a point-mass damper, where mass-spring or dashpot dissipates energy to damp the oscillatory motion. Another type is a wheel damper, where a wheel immersed in a container of viscous fluid damps the angular motion of the spacecraft.

Passive Magnetic

Another type of passive stabilization uses permanent magnets. The magnets force alignment along along the Earth's magnetic field lines. This stabilization is most effective in near equatorial orbits since the magnetic field orientation is almost constant. This method can only be used in orbits close to the Earth, and only when the mission allows the orientation of the spacecraft to vary with the magnetic field.

3.7 Summary

This chapter discussed orbit and attitude dynamics, and presented equations describing the dynamic motion of each. Options for attitude determination and control were discussed. In Chapter 4, the specifics of using magnetic control and the effect on the spacecraft are presented.

Chapter 4

Spacecraft Magnetic Field Interactions

The examination of the interaction between spacecraft and magnetic fields is important because magnetic fields cause magnetic torques to act on spacecraft. These torques can be favorable control torques, or non-desired disturbance torques. This chapter discusses the effects of these magnetic torques, and looks at types of hardware for magnetic control. In addition, the dependence of the local magnetic field strength and orientation on the orbit position is examined.

4.1 Magnetic Torques

Magnetic torques are prevalent in spacecraft. These torques can be in the form of magnetic disturbance torques which can alter the nominal motion of the spacecraft, or magnetic control torques which act to counteract the effects of the disturbance torques and change the orientation. Disturbance torques are discussed in the NASA Technical Report SP-8018.[2] Control torques are discussed by Arduini and Baiocco[3] and Chobotov.[7]

4.1.1 Magnetic Torque Origins

The origin of magnetic torque can be examined by looking at the forces in a current carrying conductor. Current carrying loops produce magnetic torques, and a description of these torques follows.

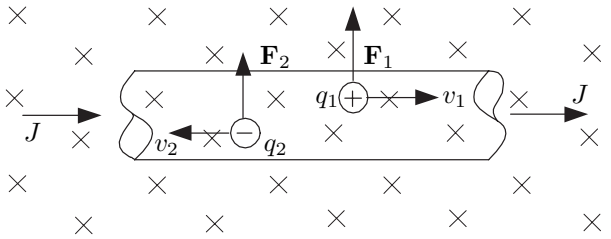

Figure 4.1: Forces on the Moving Charges in a Current-Carrying Conductor (Adapted from Ref. 34)

Forces along a straight wire

The force, F, on a current carrying conductor, such as a length of wire (Figure 4.1), is a summation of the forces on the moving charges:

$$\begin{aligned} F &= (n_1 A_w \ell_w)(q_1 v_1 B) + (n_2 A_w \ell_w)(q_2 v_2 B) \\ &= (n_1 q_1 v_1 + n_2 q_2 v_1) A_w \ell_w B \end{aligned} \tag{4.1}$$

where a charge is represented by q_i, the drift velocity of the positive charge is v_i, and the number of positive charges is n_i, where $i = 1$ for a positive charge, and $i = 2$ for a negative charge. The cross-sectional area of the wire is A_w, and ℓ_w is the length. Since $(n_1 q_1 v_1 + n_2 q_2 v_1)$ is equal to the current density, J, and JA_w is equal to the current, I, the force is

$$F = I \ell_w B \tag{4.2}$$

This equation is only valid when the magnetic field is perpendicular to the wire. The component of the **B** field which is parallel to the wire, $B_\parallel$, exerts no force because it is in the same direction as the drift velocities. This relation leads to a general case force of

$$F = I \ell_w B_\perp = I \ell_w B \sin\phi \tag{4.3}$$

where ϕ is the angle between the **B** field and the wire. In vector form this equation is written as

$$\mathbf{F} = \mathbf{I} \ell_w \times \mathbf{B} \tag{4.4}$$

for the general case.

Current Loops

When a current-carrying wire is arranged in a rectangular loop with sides a and b, and rotated an angle α with respect to the magnetic field as shown in Figure 4.2, the resultant

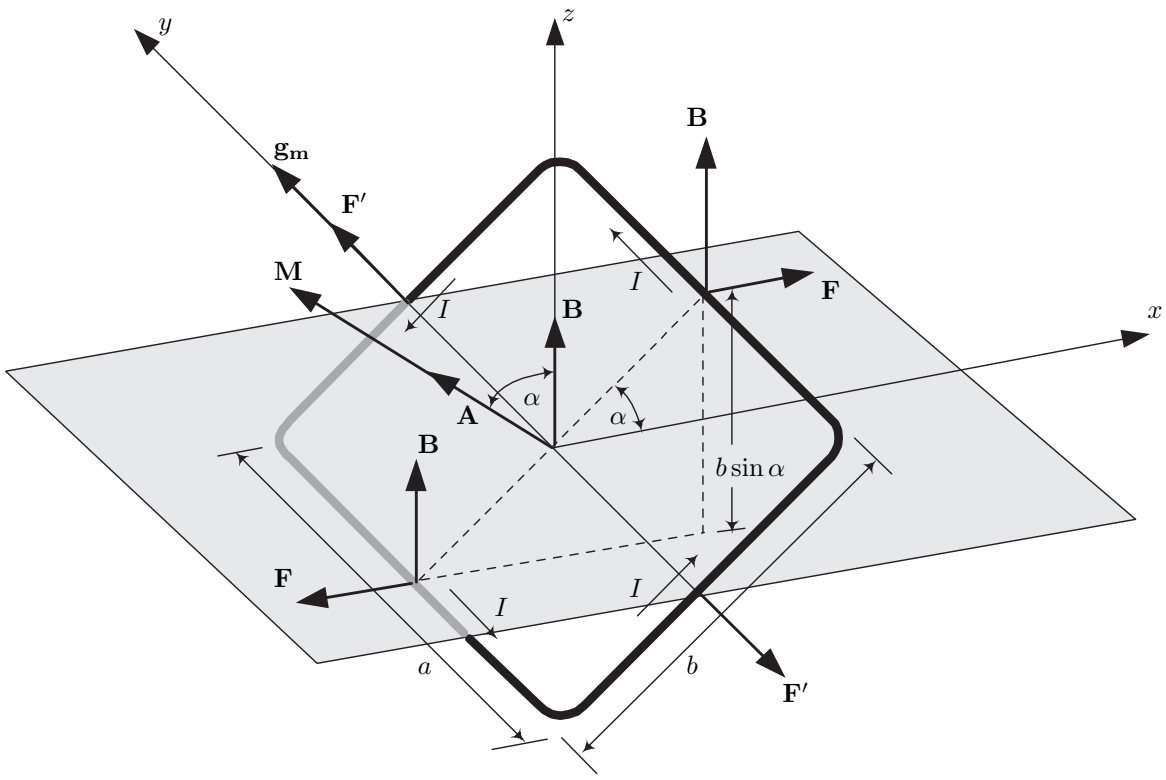

Figure 4.2: Forces on a Current-Carrying Loop in a Magnetic Field (Adapted from Ref. 34)

force on the loop is zero. This resultant occurs because the forces on opposite sides of the loop are equal and opposite, and therefore cancel. A nonzero torque exists, however, arising from the fact that a moment couple is formed on sides a due to the angle α between the coil and magnetic field. This torque is equal to

$$g_m = IBA\sin\alpha \tag{4.5}$$

where A is the area of the coil, ab. From this equation, it is evident that the magnetic torque is a maximum when $\alpha = 90°$, and the plane of the coil is parallel to the magnetic field. When $\alpha = 0°$, the magnetic torque is equal to zero. In vector form, the torque is equal to

$$\mathbf{g}_m = I\mathbf{A} \times \mathbf{B} \tag{4.6}$$

Here, $\mathbf{A}$ is the area vector of the loop, or

$$\mathbf{A} = NA\mu\hat{\mathbf{n}} \tag{4.7}$$

where N is the number of turns of wire, μ is the permeability of the core material, and $\hat{\mathbf{n}}$ is a unit vector normal to plane of the coil.

The product $I\mathbf{A}$ is also known as the magnetic moment, or $\mathbf{M}$. The magnetic torque can therefore be described as

$$\mathbf{g}_m = \mathbf{M}^{\times}\mathbf{B} \tag{4.8}$$

The magnetic torque tends to rotate the loop towards an equilibrium position with $\mathbf{M}$ in the same direction as $\mathbf{B}$.

Equation 4.8 holds true for planar current loops of any shape. This relationship exists because any shape can be approximated by a large number of rectangular coils. Currents that are in the same sense in each of the rectangular loops will cancel, and only the currents along the boundary will be left.

Magnetic torques are further discussed by Sears, Zemansky, and Young.[34]

4.1.2 Magnetic Disturbance Torques

The NASA Technical Report SP-8018[2] discusses the disturbance torques caused by magnetic fields. A spacecraft magnetic disturbance torque can be determined if characteristics of the spacecraft and local magnetic field are known. A knowledge of the strength and direction of the ambient magnetic field, the magnetic dipole of the spacecraft, and the orientation of the dipole relative to the local magnetic field vector is required.

The main sources of magnetic disturbance torques arise from both internal and external magnetic activity. The spacecraft provides magnetic torques through permanent magnetism and spacecraft-generated current loops, while magnetism and currents induced by external

fields also have an effect. Magnetic torques may also be a result of spacecraft assemblies that rotate relative to each other, such as rapidly spinning parts, or movable solar panels.

Magnetic disturbance torques must be given consideration in spacecraft and satellite design. The main areas that need to be examined are attitude motion, control actuator sizing, expendable fuel requirements, and spin decay effects. Minimizing magnetic disturbance torques is important when the control torques are small, such as with gravity-gradient stabilization, or if long term small disturbances cause non-negligible effects, such as the precession of a spin stabilized spacecraft. These disturbance torques do not cause a significant problem for attitude control, however, if the ambient field is negligibly small or if the spacecraft needs to be magnetically clean solely for the presence of magnetically sensitive equipment.

Examples of Magnetic Disturbance Torques on Satellites

The magnetic disturbance torque effect was observed on a few early satellites, such as Vanguard I and Tiros I.[2] The Vanguard I satellite was despun by an interaction between the magnetic field of the Earth and eddy currents generated in the rotating outer shell of the satellite. This interaction caused the spin rate of Vanguard I to be reduced from its initial rate of 2.7 rps at launch to less than 0.2 rps 2 years later. Tiros I displayed a different effect of magnetic disturbance torques. On this satellite, a large magnetic dipole moment in the satellite interacted with the geomagnetic field causing the spin axis to precess.

Once the effects of magnetic disturbance torques were better understood, some satellites were built taking advantage of this property. The Transit IB and Transit 2A satellites were rapidly despun in orbit by using the same type of magnetic torque that decreased the Vanguard I satellite. In addition, Transit IB used a permanent magnetic dipole in order to stabilize the symmetry axis of the satellite along the Earth's magnetic field lines.

Effects

Different sources of magnetic disturbance torques affect non-spinning and spinning spacecraft in various ways. In non-spinning spacecraft, permanent magnetism and spacecraft-generated current loops are a major source of torque. Magnetism induced by external fields causes the magnetic moment to vary depending on the intensity of the external field and characteristics of the magnetic material. There is no significant effect on non-spinning spacecraft by currents induced by a magnetic field.

In spinning spacecraft, only a portion of the torque from permanent magnetism and spacecraft-generated current loops are affected. In these current loops, the component of torque normal to the spin axis has a zero average value, and only the portion of dipole moment along the spin axis is considered. The magnetism induced by external fields causes the magnetic moment to vary depending on the external field as with the non-spinning spacecraft. It also

causes spin decay due to magnetic hysteresis. Currents induced by external fields cause spin decay and precession by altering the spin-axis dipole moment.

Control of Magnetic Disturbances

If a satellite is gravity-gradient stabilized, or if accurate control of the spin-axis of a spin-stabilized spacecraft is required, the spacecraft magnetic dipole moment must be minimized such that it does not disturb the satellite orientation. Magnetic cleanliness for instruments onboard a spacecraft is obtained by reducing the magnetic field at a specific location on the spacecraft.

The dipole moment of a spacecraft can be determined by exposing the satellite to a known, uniform magnetic field and determining the resulting torque. Once the dipole moment is known, curative procedures can be utilized to remove any necessary magnetization. One method of cancelling the effects of the spacecraft dipole moment is deperming, where residual magnetization is removed from major components and the entire spacecraft. Another method is compensation, in which small permanent magnets are attached to the spacecraft in order to minimize the dipole moment or magnetic field at a certain location.

Shielding components which produce large magnetic dipole moments by enclosing them in a container made from a highly permeable material is not a favorable action. The shielded product may have problems operating correctly, and therefore other means of reducing the dipole moment are preferred.

Minimization and Avoidance

In addition to controlling the effects of a spacecraft dipole moment, it is possible to avoid or reduce the dipole moment and other magnetic torque sources in the design of the spacecraft.

One way to minimize and avoid magnetic effects on a spacecraft is by carefully examining the magnetic properties of materials used. Nonmagnetic materials include aluminum, magnesium, titanium, beryllium, copper, and some brasses and bronzes. Since nickel is often used in the process of creating electroplated materials, these materials must be examined carefully to check for magnetization before use. Stainless steel often proves to be a difficult material to use because even nonmagnetic stainless steel becomes magnetic when machined through a processing effect. "Mysterious Substitution"[1] is frequently observed, in which a batch of nonmagnetic screws contain a small number that are magnetic.

Some components on a spacecraft unavoidably produce magnetic dipole moments. Substantial dipole moments may be produced by latching relays, batteries, motors, gyros, or other equipment. When possible, the components with large dipole moments should be paired such that their effects cancel. If pairing is not possible, other techniques, such as individual compensation, should be utilized.

The spacecraft dipole moment can be greatly affected by current flowing in the solar array because of the effect of current loops on magnetic torque. This problem can be avoided by routing current return wires behind the solar cells with a technique called backwiring. This technique succeeds in minimizing the loop area. Another recommended method of reducing the magnetic dipole moment is to twist the leads in wiring harnesses.

4.1.3 Magnetic Control Torques

Magnetic control torques can be applied to spacecraft to counteract disturbance torques or change the attitude. This counteraction is accomplished by applying a magnetic moment to the spacecraft by using current loops. The magnetic moment is in the form

$$\mathbf{M} = INA\mu\hat{\mathbf{n}} \tag{4.9}$$

where $\mathbf{M}$ is the magnetic moment, I is the current, N is the number of coils, A is the cross-sectional area of the loop, μ is the permeability of the core material, and $\hat{\mathbf{n}}$ is a unit vector in the direction of the magnetic coil dipole.

As discussed previously, the magnetic torque acts in a direction orthogonal to both the magnetic field and the dipole moment. This interaction is illustrated in Figure 4.3.

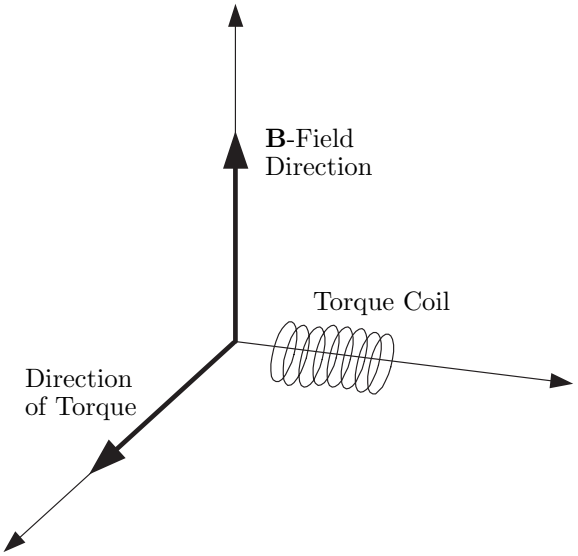

Figure 4.3: Magnetic Torque Direction

Often, the desired direction of torque is not perpendicular to the magnetic field. In this case, only the component of the desired torque in the direction perpendicular to the magnetic field

is possible and can be developed. This relationship is demonstrated graphically in Figure 4.4 where $\mathbf{g}_{m_i}$ is the desired, or ideal, torque, $\mathbf{\Delta g}_m$ is the undesired component of torque, and $\mathbf{g}_m$ is an attainable magnetic torque, as described by Arduini.[3]

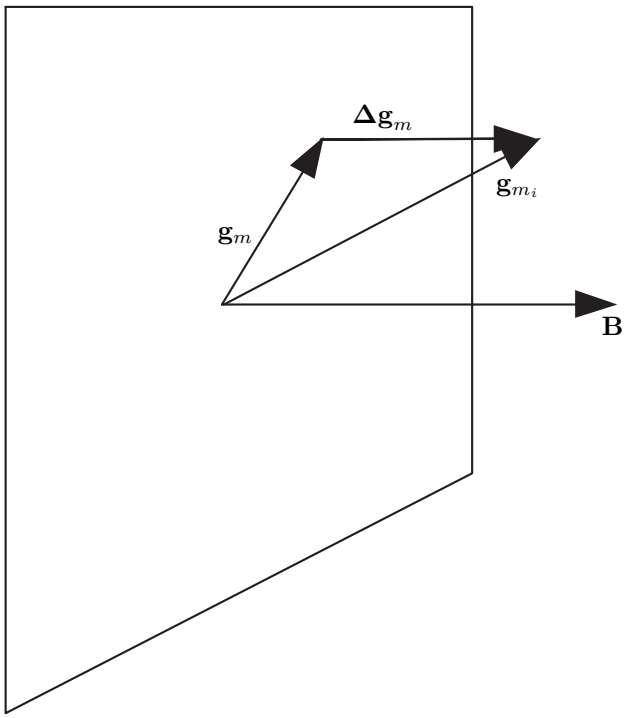

Figure 4.4: Magnetic Control Torques (Adapted from Ref. 3)

The moment developed in a coil is determined by attempting to minimize the magnitude of the undesired magnetic torque, $\mathbf{\Delta g}_m$, such that

$$\| \mathbf{g}_m - \mathbf{g}_{m_i} \| = \text{minimum} \tag{4.10}$$

which leads to

$$\mathbf{\Delta g}_m = \big(\mathbf{g}_{m_i} \cdot \hat{\mathbf{B}}\big)\hat{\mathbf{B}} \tag{4.11}$$

where $\hat{\mathbf{B}}$ is a unit vector in the direction of the magnetic field. From vector addition,

$$\mathbf{g}_m = \mathbf{g}_{m_i} - \mathbf{\Delta g}_m \tag{4.12}$$

Once the actual applicable torque is known, the magnetic moment that should be developed can be calculated with Equation 4.8 and the knowledge that $\mathbf{M} \cdot \mathbf{B} = 0$ as

$$\mathbf{M} = (\mathbf{B} \times \mathbf{g}_m)/B^2 \tag{4.13}$$

where $\mathbf{B}$ is the local magnetic field.

4.2 Magnetic Control Hardware

As discussed by Sidi,[38] the main types of hardware used for magnetic control are torque coils, torque rods, and permanent magnets.

4.2.1 Torque Coils

Torque Coils consist of loops of a conducting wire, such as copper, around an air core. They work by providing a magnetic moment, which interacts with the magnetic field to produce a torque, as in the current loops of Section 4.1.1. The magnetic moment of the coil is defined from Equation 4.9. For an air core loop, the value for the permeability of the core material, μ, is equal to 1.

4.2.2 Torque Rods

Torque rods work under the same principal as torque coils. The main difference between torque coils and torque rods is the core material and thus the values of μ are different. Whereas torque coils have air in their core, torque rods have cores of metal.

The core material choice is important for the torque rods. Ferromagnetic materials are often used because they have high permeabilities which can lead to a reduction in power consumption. However, ferromagnetic materials saturate at low values of magnetic field intensity. In addition, their permeability is a function of the magnitude of the magnetic field intensity, and therefore the dipole moment is difficult to predict.

4.2.3 Permanent Magnets

Florin[10] describes a technique of using a system of gimballed permanent magnets for magnetic control. A gimbal is used to position two permanent magnets so a magnetic moment can be induced in any direction. The strength of the magnetic moment created ranges from zero to twice that of one magnet.

4.3 Magnetic Field and Orbit Interaction

Since the magnetic control torque on a spacecraft can only act perpendicular to the magnetic field, the direction of the magnetic field over the duration of an orbit is important to determine.

4.3.1 Equatorial Orbits

If it is assumed that the magnetic field axis is coincident with the spin axis, the magnetic field direction around the equator is nearly parallel with the angular momentum direction of the Earth, as shown in Figure 4.5. In an equatorial orbit, therefore, the pitch direction, or $\hat{\mathbf{o}}_2$, is always in the same direction as the magnetic field. For this reason, no magnetic control in the pitch direction is possible in equatorial orbits.

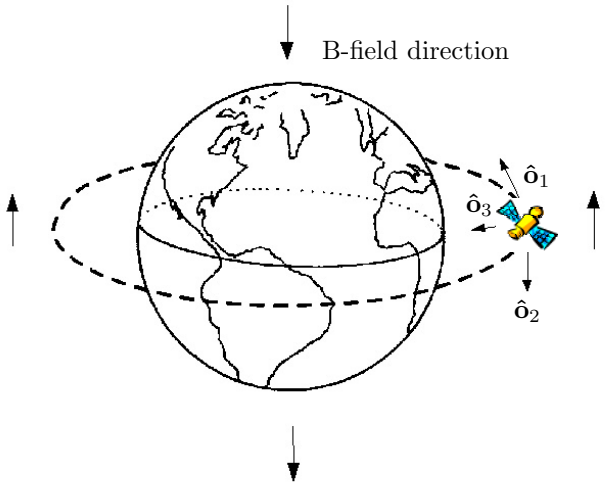

Figure 4.5: Equatorial Orbit in Magnetic Field

4.3.2 Polar Orbits

Once again assuming that the magnetic field axis is coincident with the spin axis, the controllability of a polar orbit can be examined. As the spacecraft passes over the equator, the magnetic field is aligned with the roll direction, or $\hat{\mathbf{o}}_1$, as shown in Figure 4.6, and no roll control is possible. As the distance from the equator increases, the amount of roll control possible increases but the amount of yaw control decreases. When the spacecraft is over the poles, the magnetic field is in the same direction as the yaw vector, $\hat{\mathbf{o}}_3$. Therefore no magnetic yaw control is possible in these locations.

4.3.3 Circular Orbits

For circular orbits that are neither equatorial or polar, the controllability varies depending on the position in the orbit. One thing that does remain nearly constant is the magnitude of the magnetic field component in the $\hat{\mathbf{o}}_\mathbf{2}$ direction.

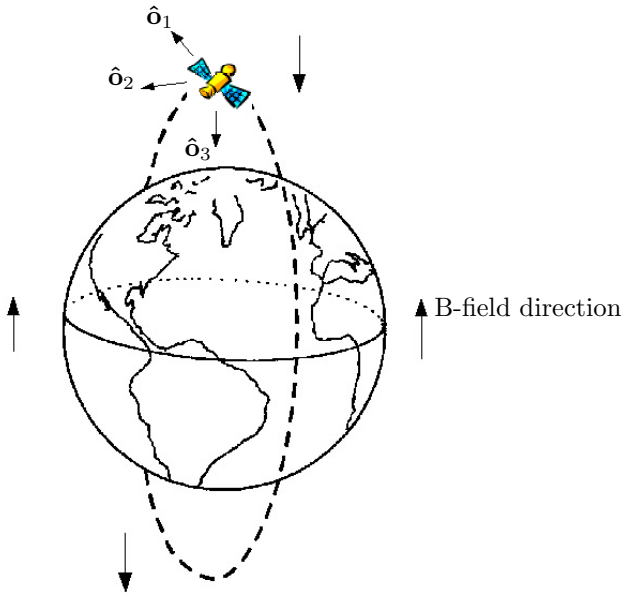

Figure 4.6: Polar Orbit in Magnetic Field

In order to prove that B_{o_2} is nearly constant, $\mathbf{B} \cdot \hat{\mathbf{o}}_2$ must be shown to be a constant, where

$$\mathbf{B} = \frac{{R_\oplus}^3 H_0}{r^3}\Big(3\big(\hat{\mathbf{m}} \cdot \hat{\mathbf{r}}\big)\hat{\mathbf{r}} - \hat{\mathbf{m}}\Big) \tag{4.14}$$

and

$$\hat{\mathbf{o}}_2 = -\frac{(\mathbf{r} \times \mathbf{v})}{rv} \tag{4.15}$$

As defined previously, $R_\oplus$, H_0, r, and v are constants, $\hat{\mathbf{m}}$ is a unit vector in the direction of the magnetic pole, and $\hat{\mathbf{r}}$ is a unit vector in the direction of the satellite in geocentric inertial coordinates.

If the constants in Equation 4.14 are designated by c_1, and the constants in Equation 4.15 are replaced with c_2, the relationship $\mathbf{B} \cdot \hat{\mathbf{o}}_2$ can be written as

$$\begin{aligned}
\mathbf{B} \cdot \hat{\mathbf{o}}_2 &= c_1\Big(3\big(\hat{\mathbf{m}} \cdot \hat{\mathbf{r}}\big)\hat{\mathbf{r}} - \hat{\mathbf{m}}\Big) \cdot c_2\big(\mathbf{r} \times \mathbf{v}\big) && (4.16)\\
&= 3c_1\big(\hat{\mathbf{m}} \cdot \hat{\mathbf{r}}\big)\hat{\mathbf{r}} \cdot \big(c_2(\mathbf{r} \times \mathbf{v})\big) - c_1\hat{\mathbf{m}} \cdot \big(c_2(\mathbf{r} \times \mathbf{v})\big) && (4.17)\\
&= 3c_1c_2\big(\hat{\mathbf{m}} \cdot \hat{\mathbf{r}}\big)\big(\hat{\mathbf{r}} \cdot (\mathbf{r} \times \mathbf{v})\big) - c_1c_2\big(\hat{\mathbf{m}} \cdot (\mathbf{r} \times \mathbf{v})\big) && (4.18)
\end{aligned}$$

since $\hat{\mathbf{r}} \cdot (\mathbf{r} \times \mathbf{v}) = 0$, this equation can be further reduced to

$$\mathbf{B} \cdot \hat{\mathbf{o}}_2 = -c_1c_2\big(\hat{\mathbf{m}} \cdot (\mathbf{r} \times \mathbf{v})\big) \tag{4.19}$$

Since the angular momentum $\mathbf{r} \times \mathbf{v}$ is constant, and the direction of the magnetic pole vector, $\hat{\mathbf{m}}$, is nearly constant, B_{o_2} is nearly constant.

This relation is consistent with Sections 4.3.1 and 4.3.2. In an equatorial orbit, almost all of the magnetic field is in the pitch direction, and therefore B_{o_2} has a constant value equal to the magnitude of the magnetic field. In a polar orbit, almost none of the magnetic field is in the pitch direction, so B_{o_2} has a constant value of zero. These relationships assume that the magnetic field axis is not tilted with respect to the Earth's spin axis.

4.4 Time to Slew

The time to perform a slew maneuver depends on the spacecraft's orbital location, as well as its attitude position and the direction of slew. The fastest maneuver takes place when the direction of slew is perpendicular to the magnetic field, and the full amount of magnetic moment can be productively used, *i.e.* the direction of slew, magnetic moment, and the magnetic field are orthogonal. If the direction of magnetic moment application is parallel to the magnetic field, the time to slew approaches infinity since no useful torque can be obtained. At points in between, calculation is more difficult, especially if the relation between the torque direction and magnetic field is not constant.

An example of a time-to-slew calculation is possible by looking at a simple case. The best case scenario for the time it takes to perform a slew maneuver can be calculated by examining a yaw maneuver while in an equatorial orbit, where the slew direction is always perpendicular to the magnetic field direction. For this case, the torque equation as a function of yaw acceleration can be written as

$$I_3 \ddot{\theta}_y = g_y \tag{4.20}$$

or

$$I_3 \frac{\mathrm{d}}{\mathrm{d}t} \dot{\theta}_y = g_y \tag{4.21}$$

where I_3 is the z-component of the moment of inertia, θ_y is the yaw angle, and g_y is the amount of torque in the yaw direction. This equation can be reduced to

$$\int_{\dot{\theta}_{y_0}}^{\dot{\theta}_y} I_3 \mathrm{d}\dot{\theta}_y = \int_{t_0}^{t} g_y \mathrm{d}t \tag{4.22}$$

$$I_3 \frac{\mathrm{d}}{\mathrm{d}t} \theta_y - I_3 \dot{\theta}_{y_0} = g_y (t - t_0) \tag{4.23}$$

where t is the time to complete the slew maneuver. This equation can be further reduced to

$$\int_{\theta_{y_0}}^{\theta_y} I_3 \mathrm{d}\theta_y - \int_{t_0}^{t} I_3 \dot{\theta}_{y_0} \mathrm{d}t = \int_{t_0}^{t} g_y (t - t_0) \mathrm{d}t \tag{4.24}$$

$$I_3(\theta_y - \theta_{y_0}) - I_3\dot{\theta}_{y_0}(t - t_0) = \frac{1}{2}g_y(t - t_0)^2 \tag{4.25}$$

The following initial conditions are applied

$$\theta_{y_0} = \theta_y(0) = 0 \tag{4.26}$$
$$\dot{\theta_{y_0}} = \dot{\theta_y}(0) = 0 \tag{4.27}$$
$$t_0 = 0 \tag{4.28}$$

Rearranging, the following is obtained

$$I_3\theta_y = \frac{1}{2}g_y t^2 \Rightarrow t = \sqrt{\frac{2I_3\theta_y}{g_y}} \tag{4.29}$$

The total time-to-slew is obtained by assuming that half of the total time-to-slew is used to speed up, and half is used to slow down:

$$t = 2\sqrt{\frac{I_3\theta_y}{g_y}} \tag{4.30}$$

This value is the minimum time-to-slew, assuming that the direction of slew is perpendicular to both the magnetic field and the applied magnetic moment.

4.5 Summary

This chapter discussed the interaction of magnetic fields and spacecraft. Details of magnetic disturbance and control torques were presented. Chapter 5 develops control laws for magnetic control for both linear and nonlinear systems.

Chapter 5

Control Laws

Chapters 3 and 4 discussed dynamic equations of a spacecraft. In this chapter, those equations are arranged as linear and nonlinear time variant equations of motion of the system. The periodic nature of the equations is discussed and implemented to obtain linear time invariant equations.

Magnetic control laws are derived in the form of proportional-derivative controllers and constant coefficient linear quadratic regulator controllers. Floquet Theory is implemented to determine if the linear time variant system is stable using the periodic characteristics. An optimization technique is introduced which is used to damp the system in the least time.

5.1 Equations of Motion

Nonlinear and linear equations of motion are derived for the system. These equations begin with the nonlinear attitude equations of motion, and are then linearized about the desired equilibrium point. The linearization is performed with both Euler angles and quaternions. Because the equations are periodic, the average value of the periodic coefficients is used to obtain linear time invariant equations.

5.1.1 Nonlinear Equations of Motion

A nonlinear model is used to calculate the motion of a spacecraft with magnetic control applied. As stated in Section 3.3, the nonlinear dynamic equations of motion are

$$\dot{\bar{\mathbf{q}}} = \frac{1}{2}\begin{bmatrix} \mathbf{q}^{\times} + q_4\mathbf{1} \\ -\mathbf{q}^T \end{bmatrix}\boldsymbol{\omega} \tag{5.1}$$

and

$$\dot{\boldsymbol{\omega}} = -\mathbf{I}^{-1}\boldsymbol{\omega}^{\times}\mathbf{I}\boldsymbol{\omega} + 3{\omega_c}^2\mathbf{I}^{-1}\hat{\mathbf{o}}_3^{\times}\mathbf{I}\hat{\mathbf{o}}_3 + \mathbf{I}^{-1}\mathbf{g}_m \tag{5.2}$$

The magnetic torque, $\mathbf{g}_m$, is equal to

$$\mathbf{g}_m = \mathbf{M}^{\times}\mathbf{B} \tag{5.3}$$

Since the magnetic torque must be perpendicular to the magnetic field, the following mapping function is used for $\mathbf{M}$ as suggested by Wiśniewski:[50,51]

$$\tilde{\mathbf{M}} \mapsto \mathbf{M} : \mathbf{M} = \frac{\tilde{\mathbf{M}}^{\times}\mathbf{B}}{\|\mathbf{B}\|} \tag{5.4}$$

This relation ensures that $\mathbf{M}$ is perpendicular to the magnetic field by determining a mapped magnetic moment, $\tilde{\mathbf{M}}$, of the same magnitude. When crossed into the magnetic field, the mapped magnetic moment provides a feasible control magnetic moment, $\boldsymbol{M}$, which is the possible component of $\tilde{\mathbf{M}}$.

The magnetic control is then represented by

$$\mathbf{I}^{-1}\mathbf{g}_m = \frac{\mathbf{I}^{-1}}{\|\mathbf{B}\|}\big(\tilde{\mathbf{M}}^{\times}\mathbf{B}\big)^{\times}\mathbf{B} = \frac{-\mathbf{I}^{-1}}{\|\mathbf{B}\|}\mathbf{B}^{\times}\mathbf{B}^{\times}\tilde{\mathbf{M}} \tag{5.5}$$

in terms of the mapped magnetic moment.

5.1.2 Desired Equilibrium Attitude

For three-axis stability, the body frame should be aligned with the orbital frame, or

$$\boldsymbol{\omega}^{bo} = \mathbf{0} \tag{5.6}$$

$$\bar{\mathbf{q}}^{bo} = \begin{bmatrix} \mathbf{0} \\ 1 \end{bmatrix} \tag{5.7}$$

This relation implies that the spacecraft nadir vector always points to the center of the Earth.

5.1.3 Linearized Equations of Motion Using Euler Angles

The equations of motion are linearized in terms of Euler angles so that they are in the form

$$\dot{\mathbf{x}} = \mathbf{F}\mathbf{x} + \mathbf{G}(t)\mathbf{u} \tag{5.8}$$

where $\mathbf{F}$ is the system matrix of linearized equations, $\mathbf{G}(t)$ is the input matrix for control, and $\mathbf{u}$, is the amount of applied control. The control applied to this system is in the form

of magnetic moment, or $\mathbf{M}(t)$. Therefore, the state equation for magnetic control can be rewritten as

$$\dot{\mathbf{x}} = \mathbf{F}\mathbf{x} + \mathbf{G}(t)\mathbf{M}(t) \tag{5.9}$$

This method was used by Wisniewski[50,51] and Musser and Ebert.[30]

The state vector, $\mathbf{x}$, contains the Euler angles and their rates of change, or

$$\mathbf{x} = \begin{bmatrix} \boldsymbol{\theta} \\ \dot{\boldsymbol{\theta}} \end{bmatrix} \tag{5.10}$$

The $\mathbf{F}$ matrix can be calculated by beginning with the change in angular velocity as seen by the body frame from Equation 5.2.

The equations of motion are linearized about the equilibrium attitude. If the angles of rotation are small, the rotation matrix, $\mathbf{R}^{bo}$, in a 1-2-3 rotation sequence can be linearly approximated as

$$\mathbf{R}^{bo} \approx \mathbf{1} - \boldsymbol{\theta}^{\times} = \begin{bmatrix} 1 & \theta_3 & -\theta_2 \\ -\theta_3 & 1 & \theta_1 \\ \theta_2 & -\theta_1 & 1 \end{bmatrix} \tag{5.11}$$

so that

$$\hat{\mathbf{o}}_2 = \begin{bmatrix} \theta_3 \\ 1 \\ -\theta_1 \end{bmatrix} \qquad \hat{\mathbf{o}}_3 = \begin{bmatrix} -\theta_2 \\ \theta_1 \\ 1 \end{bmatrix} \tag{5.12}$$

The angular velocity is written as

$$\boldsymbol{\omega}^{bi} = \boldsymbol{\omega}^{bo} + \boldsymbol{\omega}^{oi} \tag{5.13}$$

For a small angle assumption,

$$\boldsymbol{\omega}^{bo} \approx \dot{\boldsymbol{\theta}} \tag{5.14}$$

Also,

$$\boldsymbol{\omega}^{oi} = -\omega_c \hat{\mathbf{o}}_2 \tag{5.15}$$

Therefore,

$$\boldsymbol{\omega}^{bi} = \begin{bmatrix} \dot{\theta}_1 - \theta_3\omega_c \\ \dot{\theta}_2 - \omega_c \\ \dot{\theta}_3 + \theta_1\omega_c \end{bmatrix} \tag{5.16}$$

Substituting the above relations into Equation 5.2 yields a dynamic model in terms of $\boldsymbol{\theta}$.

By assumption, $\boldsymbol{\theta}$ is small, so terms of $\theta \cdot \theta$, $\theta \cdot \dot{\theta}$, and $\dot{\theta} \cdot \dot{\theta}$ are neglected. This simplification leads to a linear dynamic model of

$$\begin{bmatrix} \dot{\theta}_1 \\ \dot{\theta}_2 \\ \dot{\theta}_3 \\ \ddot{\theta}_1 \\ \ddot{\theta}_2 \\ \ddot{\theta}_3 \end{bmatrix} = \mathbf{F} \begin{bmatrix} \theta_1 \\ \theta_2 \\ \theta_3 \\ \dot{\theta}_1 \\ \dot{\theta}_2 \\ \dot{\theta}_3 \end{bmatrix} + \mathbf{I}^{-1}\mathbf{g}_m \tag{5.17}$$

where

$$\mathbf{F} = \begin{bmatrix} 0 & 0 & 0 & 1 & 0 & 0 \\ 0 & 0 & 0 & 0 & 1 & 0 \\ 0 & 0 & 0 & 0 & 0 & 1 \\ -4{\omega_c}^2\sigma_1 & 0 & 0 & 0 & 0 & \omega_c - \omega_c\sigma_1 \\ 0 & 3{\omega_c}^2\sigma_2 & 0 & 0 & 0 & 0 \\ 0 & 0 & {\omega_c}^2\sigma_3 & -\omega_c - \omega_c\sigma_3 & 0 & 0 \end{bmatrix} \tag{5.18}$$

and

$$\sigma_1 = \frac{I_2 - I_3}{I_1} \qquad \sigma_2 = \frac{I_3 - I_1}{I_2} \qquad \sigma_3 = \frac{I_1 - I_2}{I_3} \tag{5.19}$$

Here, $\mathbf{G}(t)\mathbf{M}(t)$ is equal to $\mathbf{I}^{-1}\mathbf{g}_m$.

5.1.4 Linearized Equations of Motion Using Quaternions

Linearized equations are also obtained in quaternion form. Once again, the equations of motion follow the linear state equation

$$\dot{\mathbf{x}} = \mathbf{F}\mathbf{x} + \mathbf{G}(t)\mathbf{M}(t) \tag{5.20}$$

In this case, the state vector $\mathbf{x}$ contains the vector portion of the quaternions and their rates of change, or

$$\mathbf{x} = \begin{bmatrix} \mathbf{q} \\ \dot{\mathbf{q}} \end{bmatrix} \tag{5.21}$$

The $\mathbf{F}$ matrix can be calculated by beginning with the change in angular velocity as seen by the body frame from Equation 5.2.

Using Equations 5.6 and 5.7, the linearized rotation from the orbit to the body frame is

$$\mathbf{R}^{bo} = \begin{bmatrix} 1 & 2q_3^{bo} & -2q_2^{bo} \\ -2q_3^{bo} & 1 & 2q_1^{bo} \\ 2q_2^{bo} & -2q_1^{bo} & 1 \end{bmatrix} \tag{5.22}$$

and therefore

$$\hat{\mathbf{o}}_2 = \begin{bmatrix} 2q_3^{bo} \\ 1 \\ -2q_1^{bo} \end{bmatrix} \qquad \hat{\mathbf{o}}_3 = \begin{bmatrix} -2q_2^{bo} \\ 2q_1^{bo} \\ 1 \end{bmatrix} \tag{5.23}$$

The angular rotation rate of the orbital frame with respect to the inertial frame is

$$\boldsymbol{\omega}^{oi} = -\omega_c \hat{\mathbf{o}}_2 = \begin{bmatrix} -2q_3^{bo}\omega_c \\ -w_c \\ 2q_1^{bo}\omega_c \end{bmatrix} \tag{5.24}$$

Recalling the relation

$$\boldsymbol{\omega}^{bi} = \boldsymbol{\omega}^{bo} + \boldsymbol{\omega}^{oi} \tag{5.25}$$

$\dot{\boldsymbol{\omega}}^{bi}$ can be expressed as

$$\dot{\boldsymbol{\omega}}^{bi} = \dot{\boldsymbol{\omega}}^{bo} + \begin{bmatrix} -2\dot{q}_3^{bo}\omega_c \\ 0 \\ 2\dot{q}_1^{bo}\omega_c \end{bmatrix} \tag{5.26}$$

In addition, $\boldsymbol{\omega}^{bi}$ can be expressed as

$$\boldsymbol{\omega}^{bi} = \boldsymbol{\Omega}(\bar{\mathbf{q}}^{bi})\dot{\bar{\mathbf{q}}}^{bi} = 2\big(q_4^{bi}\dot{\mathbf{q}}^{bi} - \dot{q}_4^{bi}\mathbf{q}^{bi}\big) - 2\mathbf{q}^{bi\times}\dot{\mathbf{q}}^{bi} \tag{5.27}$$

Assuming small angles, $q_4^{bi} \approx 1$ and $\dot{q}_4^{bi} \approx 0$. Therefore,

$$\boldsymbol{\omega}^{bi} \approx 2\dot{\mathbf{q}}^{bi} \tag{5.28}$$

Through substitution, the first portion of Equation 5.2 is determined to be

$$-\mathbf{I}^{-1}\boldsymbol{\omega}^{bi\times}\mathbf{I}\boldsymbol{\omega}^{bi} = \begin{bmatrix} \frac{I_2-I_3}{I_1}\omega_2^{bi}\omega_3^{bi} \\ \frac{I_3-I_1}{I_2}\omega_3^{bi}\omega_1^{bi} \\ \frac{I_1-I_2}{I_3}\omega_1^{bi}\omega_2^{bi} \end{bmatrix} \tag{5.29}$$

$$= \begin{bmatrix} \frac{I_2-I_3}{I_1}\big(-2\dot{q}_3\omega_c - 2q_1{\omega_c}^2\big) \\ 0 \\ \frac{I_1-I_2}{I_3}\big(-2\dot{q}_1\omega_c - 2q_3{\omega_c}^2\big) \end{bmatrix} \tag{5.30}$$

Similarly, the gravity gradient torque is calculated as

$$3{\omega_c}^2\mathbf{I}^{-1}\mathbf{o}_3^{\times}\mathbf{I}\mathbf{o}_3 = -3{\omega_c}^2 \begin{bmatrix} \frac{I_2-I_3}{I_1}o_{3_2}o_{3_3} \\ \frac{I_3-I_1}{I_2}o_{3_3}o_{3_1} \\ \frac{I_1-I_2}{I_3}o_{3_1}o_{3_2} \end{bmatrix} \tag{5.31}$$

$$= -3{\omega_c}^2 \begin{bmatrix} \frac{I_2-I_3}{I_1}(2q_1^{bo}) \\ \frac{I_3-I_1}{I_2}(-2q_2^{bo}) \\ 0 \end{bmatrix} \tag{5.32}$$

Substituting Equations 5.26, 5.28, 5.30, and 5.32 into Equation 5.2 provides the following relation

$$\begin{bmatrix} \dot{q}_1 \\ \dot{q}_2 \\ \dot{q}_3 \\ \ddot{q}_1 \\ \ddot{q}_2 \\ \ddot{q}_3 \end{bmatrix} = \mathbf{F} \begin{bmatrix} q_1 \\ q_2 \\ q_3 \\ \dot{q}_1 \\ \dot{q}_2 \\ \dot{q}_3 \end{bmatrix} + \mathbf{I}^{-1}\mathbf{g}_m \tag{5.33}$$

where

$$\mathbf{F} = \begin{bmatrix} 0 & 0 & 0 & 1 & 0 & 0 \\ 0 & 0 & 0 & 0 & 1 & 0 \\ 0 & 0 & 0 & 0 & 0 & 1 \\ -4{\omega_c}^2\sigma_1 & 0 & 0 & 0 & 0 & \omega_c - \omega_c\sigma_1 \\ 0 & 3{\omega_c}^2\sigma_2 & 0 & 0 & 0 & 0 \\ 0 & 0 & {\omega_c}^2\sigma_3 & -\omega_c - \omega_c\sigma_3 & 0 & 0 \end{bmatrix} \tag{5.34}$$

Here, $\mathbf{q} = \mathbf{q}^{bo}$ and the values of σ_i are defined in Equation 5.19.

This relation is identical to the Euler angle relation in Equations 5.17 and 5.18.

The magnetic control portion of the equations of motion is

$$\mathbf{I}^{-1}\mathbf{g}_m = \mathbf{G}(t)\mathbf{M}(t) \tag{5.35}$$

where

$$\mathbf{g}_m = \mathbf{M}^{\times}\mathbf{B} \tag{5.36}$$

Using the mapping function of Equation 5.4, the input control matrix, $\mathbf{G}(t)$, is

$$\mathbf{G}(t) = \frac{-\mathbf{I}^{-1}}{\|\mathbf{B}\|}\mathbf{B}^{\times}\mathbf{B}^{\times} = \frac{-\mathbf{I}^{-1}}{\|\mathbf{B}\|} \begin{bmatrix} -{B_2}^2 - {B_3}^2 & B_1B_2 & B_1B_3 \\ B_1B_2 & -{B_1}^2 - {B_3}^2 & B_2B_3 \\ B_1B_3 & B_2B_3 & -{B_1}^2 - {B_2}^2 \end{bmatrix} \tag{5.37}$$

where the magnetic field, $\mathbf{B}$, is in the body frame.

5.1.5 Quasi-Periodic Nature of Equations of Motion

The value of the magnetic torque portion of the equations depends on the value of $\mathbf{G}(t)$, which is time varying. The $\mathbf{G}(t)$ matrix, as shown in Equation 5.37, is dependent only upon the moments of inertia of the spacecraft, which are constant in the body frame, and the magnetic field. The magnetic field is roughly periodic with orbital period, leading to a roughly periodic $\mathbf{G}(t)$.

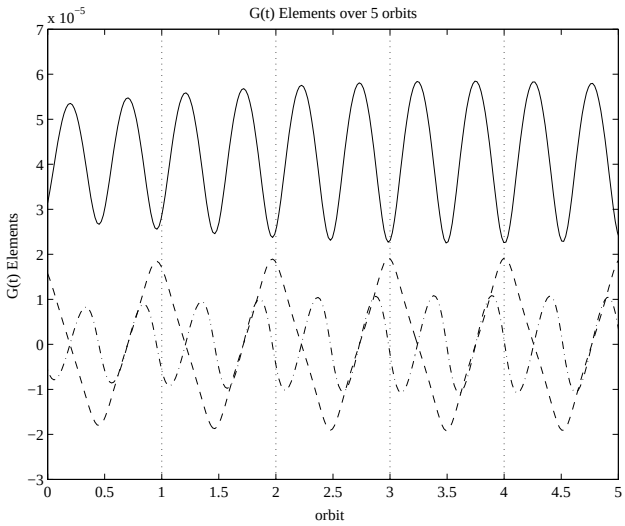

Figure 5.1: $\mathbf{G}(t)$ Elements

The first three elements of the $\mathbf{G}(t)$ matrix are plotted over time for several orbits in Figure 5.1 to show this periodic nature. These values are for an orbit with an inclination of 30°, semi-major axis of 6758.145 km, and an eccentricity of 0°.

After a few orbits, the magnitude of $\mathbf{G}(t)$ changes slightly, and there is a small periodic drift. This change occurs because of the daily rotation of the Earth, as well as the tilt of the magnetic axis. However, the changes are small, and the relation

$$\mathbf{G}(t + \mathcal{T}) = \mathbf{G}(t) \tag{5.38}$$

can be used over several orbits.

5.1.6 Average Value Linearized Equations of Motion

The input control matrix, $\mathbf{G}(t)$, can be further simplified into time invariant equations by replacing the time varying parameters with their average values. As mentioned in Section 5.1.5, $\mathbf{G}(t)$ is only dependent on the moment of inertia matrix, which is constant, and the magnetic field, which is periodic. The average value of $\mathbf{G}(t)$ is equal to $\bar{\mathbf{G}}$ where

$$\bar{\mathbf{G}} = \frac{1}{\mathcal{T}} \int_0^{\mathcal{T}} \mathbf{G}(t) \mathrm{d}t \tag{5.39}$$

and $\mathcal{T}$ is the period of the orbit.

5.1.7 Summary

In this section, equations of motion describing the attitude of spacecraft are derived. The nonlinear equations are linearized to a time varying form, and then reduced to linear time invariant by replacing periodic variables with their average values.

5.2 Control Laws

Magnetic control laws are derived to stabilize a spacecraft. Both a proportional-derivative controller and a linear quadratic regulator are implemented in the equations of motion. Floquet Theory is used to check the stability of the control laws, and an optimization method further optimizes the results.

5.2.1 Proportional-Derivative Controller

In a proportional-derivative, or P-D, Controller, the magnetic torque, $\mathbf{g}_m$, is written as

$$\mathbf{g}_m = -(\mathbf{K}_p\boldsymbol{\theta} + \mathbf{K}_d\dot{\boldsymbol{\theta}}) \tag{5.40}$$

where $\mathbf{K}_p$ and $\mathbf{K}_d$ are gain matrices. The proportional gain matrix, $\mathbf{K}_p$, and the derivative gain matrix, $\mathbf{K}_d$, can be represented by

$$\mathbf{K}_p = \begin{bmatrix} K_{p11} & K_{p12} & K_{p13} \\ K_{p21} & K_{p22} & K_{p23} \\ K_{p31} & K_{p32} & K_{p33} \end{bmatrix} \qquad \mathbf{K}_d = \begin{bmatrix} K_{d11} & K_{d12} & K_{d13} \\ K_{d21} & K_{d22} & K_{d23} \\ K_{d31} & K_{d32} & K_{d33} \end{bmatrix} \tag{5.41}$$

For this controller, the attitude and angular velocity error are fed back into the system. The challenge of a P-D controller is determining gain matrices that damp the system. After the 18 elements in the two gain matrices are chosen, the resulting system is examined the check for damping. The elements are altered to obtain desired results.

In this application, the gain matrices are constrained to be diagonal to reduce the number of elements that can be altered from 18 to six.

5.2.2 Constant Coefficient Linear Quadratic Regulator

A constant coefficient linear quadratic regulator can be used instead of a P-D controller.

To provide the desired response, the controller is set equal to

$$\tilde{\mathbf{M}}(t) = -\mathbf{K}\mathbf{x}(t) \tag{5.42}$$

where $\mathbf{K}$ is the gain feedback matrix. The controller gain, $\mathbf{K}$, can be calculated using the steady-state solution to the Ricatti equation

$$-\dot{\mathbf{S}} = \mathbf{SF} + \mathbf{F}^T\mathbf{S} - \mathbf{S}\bar{\mathbf{G}}\mathbf{B}^{-1}\bar{\mathbf{G}}^T\mathbf{S} + \mathbf{Q} \tag{5.43}$$

where $\mathbf{Q}$ is defined as a diagonal matrix. A linear quadratic regulator is used to calculate the optimal gain matrix for the time invariant system where $\mathbf{Q}$ is the weight matrix. The gain matrix is equal to

$$\mathbf{K} = -\mathbf{B}^{-1}\bar{\mathbf{G}}^T\mathbf{S} \tag{5.44}$$

and thus

$$\tilde{\mathbf{M}}(t) = -\mathbf{B}^{-1}\bar{\mathbf{G}}^T\mathbf{S}\mathbf{x}(t) \tag{5.45}$$

This controller is implemented in Equation 5.35.

5.2.3 Application of Floquet Theory

Floquet's theory describes dynamic systems in which the coefficients are periodic.[27] This theory has applications that are directly applicable to the magnetic control problem. After the controller gain is calculated for the time invariant linear equations, the stability of the gains in the linear time variant equations is examined using Floquet's theory.

For stability, $\mathbf{Q}$ must be chosen such that the eigenvalue of $\mathcal{X}(\mathcal{T})$, or the monodromy matrix, is located inside the unit circle, where

$$\mathcal{X}(\mathcal{T}) = \begin{bmatrix} \mathbf{x}_1(\mathcal{T}) & \mathbf{x}_2(\mathcal{T}) & \cdots & \mathbf{x}_6(\mathcal{T}) \end{bmatrix} \tag{5.46}$$

using initial values

$$\mathcal{X}(0) = \begin{bmatrix} \mathbf{x}_1(0) & \mathbf{x}_2(0) & \cdots & \mathbf{x}_6(0) \end{bmatrix} = \begin{bmatrix} 1 & 0 & \cdots & 0 \\ 0 & 1 & \cdots & 0 \\ \vdots & \vdots & \ddots & \vdots \\ 0 & 0 & \cdots & 1 \end{bmatrix} \tag{5.47}$$

With the control gain matrix known, the linear system

$$\dot{\mathbf{x}} = \mathbf{Fx} - \mathbf{G}(t)\mathbf{Kx} \tag{5.48}$$

is solved.

The mapped magnetic moment is then equal to

$$\tilde{\mathbf{M}}(t) = -\mathbf{Kx} \tag{5.49}$$

and the applied magnetic moment is equal to

$$\mathbf{M}(t) = \frac{\tilde{\mathbf{M}}(t)^{\times}\mathbf{B}(t)}{\|\mathbf{B}(t)\|} \tag{5.50}$$

This is implemented in the linear time varying system of equations for control.

5.2.4 Optimization of Q

As **Q** is varied, different values of **K** are obtained. An optimum **Q** exists which leads to a set of gains that damp the system in the least time. This optimum **Q** occurs for the linear time varying case when the eigenvalues of the matrix, $\mathcal{X}(\mathcal{T})$, are closest to the origin.

A Nelder-Mead Simplex, or direct search, method is used as the minimizer.[24] This method has a few disadvantages because it can not consider constraints in the system and is not the most efficient minimizer. However, the Nelder-Mead simplex method is useful in this application because it can deal with multidimensional problems and does not require derivatives, so it takes less computation time. The eigenvalues of $\mathcal{X}(\mathcal{T})$ are minimized to determine the values of **Q** leading to the optimal gain matrix for the linear time varying system. The cost function used in the optimization is equal to the sum of the squares of the eigenvalues of $\mathcal{X}(t)$.

A secondary method of optimization can be used to optimize the results of the control laws. This method involves examining the eigenvalues of the $\mathcal{X}(t)$ matrix. The largest eigenvalue of $\mathcal{X}(t)$ is identified and the corresponding eigenvector is isolated. The **Q** value corresponding to the largest value in the isolated eigenvector is altered. This method is used with trial and error to obtain favorable results.

5.2.5 Implementation of Gains in Nonlinear System

The constant gain matrix determined from the linear quadratic regulator can be implemented in the nonlinear system. However, since these gains were formed using the linear time invariant system and optimized for use in the linear time varying system, there is no guarantee that the nonlinear system will be stable. The results from each nonlinear simulation must be individually examined to check for stability.

The linear quadratic regulator method of control is summarized in Figure 5.2.

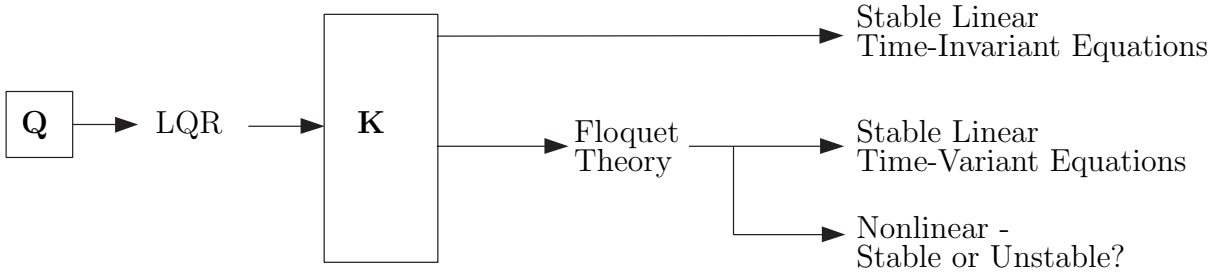

Figure 5.2: Summary of LQR Method

5.3 Summary

In this chapter, linear and nonlinear equations of motion were derived for the motion of a spacecraft. Control laws were developed to stabilize the spacecraft around a desired equilibrium using two methods. The control laws are implemented in Chapter 6 with various spacecraft configurations and initial conditions.

Chapter 6

Simulation Results

The control laws for magnetic control are tested in this chapter though computer simulations. Simulations are performed using Matlab and examine the stability of the system for both linear and nonlinear equations using a proportional-derivative controller and a constant coefficient linear quadratic regulator. The difference in magnetic control stability between gravity-gradient stable and non gravity-gradient spacecraft is examined. The results obtained using an optimizer are compared with non-optimized results.

6.1 Simulation Parameters

The control laws are implemented using computer code written in Matlab. By altering the input values, different cases can be simulated. The outputs are plotted and compared.

6.1.1 Inputs

The inputs to the simulation include the geometry of the spacecraft, its initial orbit and attitude, and the gain characteristics.

The initial orbital position is:

- $a = 6764.44$ km
- $e = 9.877 \times 10^{-4}$
- $i = 51.6^{\circ}$
- $\Omega = 356.9^{\circ}$

- $\omega = 143.5°$
- $\nu = 216.6°$
- epoch = July 27, 1999, 2:51:34.6

which is a nearly circular orbit at an altitude of approximately 380 km that is similar to the initial orbit of HokieSat. The initial attitude characteristics are:

$$\bar{\mathbf{q}}^{bo} = \begin{bmatrix} 0.04963 \\ 0.11436 \\ 0.00138 \\ 0.99220 \end{bmatrix} \qquad \boldsymbol{\omega}^{bo} = \begin{bmatrix} 3.1540 \times 10^{-3} \\ 6.9167 \times 10^{-3} \\ 1.2041 \times 10^{-3} \end{bmatrix} \tag{6.1}$$

which is approximately 14° out of plane from the desired nadir pointing orientation.

The moment of inertia matrix, $\mathbf{I}$, is different for gravity-gradient and non gravity-gradient stabilized spacecraft. For nominal gravity-gradient stable simulations, the following matrix is used:

$$\mathbf{I} = \begin{bmatrix} 1 & 0 & 0 \\ 0 & 1.4 & 0 \\ 0 & 0 & 0.6 \end{bmatrix} \tag{6.2}$$

For non gravity-gradient stable spacecraft, the moment of inertia matrix is

$$\mathbf{I} = \begin{bmatrix} 1.1 & 0 & 0 \\ 0 & 1 & 0 \\ 0 & 0 & 1.2 \end{bmatrix} \tag{6.3}$$

The gain inputs are in the form of $\mathbf{K}_p$ and $\mathbf{K}_d$, which are 3×3 matrices, when the $P - D$ controller is used, and $\mathbf{Q}$, which is a 6×6 diagonal matrix, for the linear quadratic regulator technique.

6.1.2 Outputs

The Matlab simulation determines the time varying spacecraft attitude and angular velocity in the form $\bar{\mathbf{q}}^{bo}$ and $\boldsymbol{\omega}_b^{bo}$. In addition, the simulation outputs the time varying magnetic moment. This value represents the amounts of moment the magnetic torque system is required to produce.

6.2 System With No Magnetic Control

The equations of motion for the linear and nonlinear systems are compared when no magnetic control is applied to determine how well the two relate. Only the gravity-gradient spacecraft was examined because it is inherently stable, while the non gravity-gradient is not.

Lack of magnetic control was simulated by setting the gains, $\mathbf{K}$, equal to zero. A simulation was performed for the linear system with Euler angles, the linear system with quaternions, and the nonlinear system. The two linear systems yield identical results, and the comparison between the resulting quaternion from the linear and nonlinear simulations are shown in Figure 6.1.

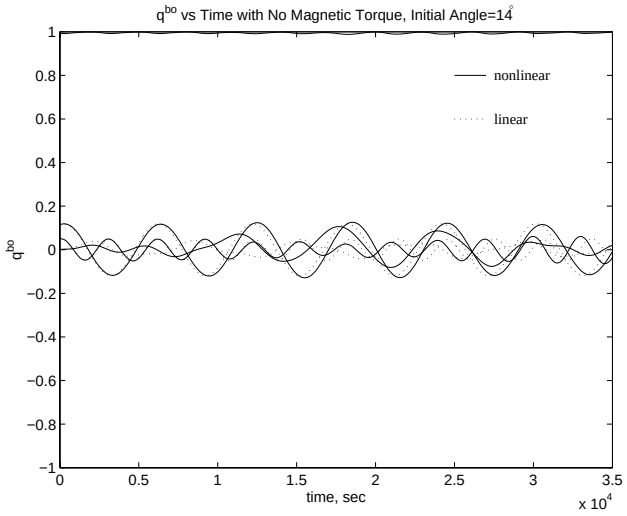

Figure 6.1: Quaternions with No Magnetic Torque, Initial Angle=14°

The linear and nonlinear results are in agreement in the initial times, but drift apart as time progresses.

The simulation was also performed with the initial conditions closer to the desired position. In this case, the initial conditions were

$$\bar{\mathbf{q}}^{bo} = \begin{bmatrix} 0.01990 \\ 0.04584 \\ 0.00550 \\ 0.99875 \end{bmatrix} \qquad \boldsymbol{\omega}^{bo} = \begin{bmatrix} 3.306 \times 10^{-3} \\ 6.851 \times 10^{-3} \\ 1.171 \times 10^{-3} \end{bmatrix} \tag{6.4}$$

which corresponds to an initial rotation of approximately 6° from desired. The linear and nonlinear results are plotted in Figure 6.2.

Figures 6.1 and 6.2 suggest that when the initial conditions are closer to the desired position, there is less error between the linear and nonlinear results, and thus the linearization is a good estimation. As the initial angle from desired is increased, the linearization becomes less reliable.

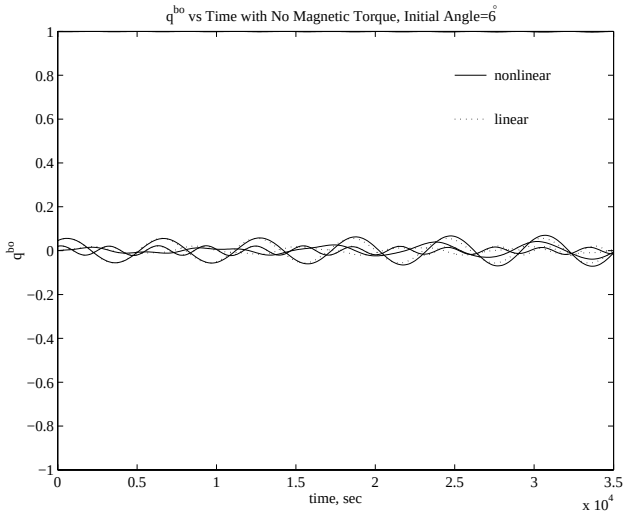

Figure 6.2: Quaternions with No Magnetic Torque, Initial Angle=6°

6.3 Magnetic Control with Gravity Gradient Stability

The magnetic controller is implemented for the gravity-gradient stable spacecraft. The time it takes to stabilize the spacecraft is examined, as well as the magnetic moment required for the maneuver.

6.3.1 P-D Controller

The following gains are implemented in the linear equations:

$$\mathbf{K}_d = \begin{bmatrix} 0.005 & 0 & 0 \\ 0 & 0.005 & 0 \\ 0 & 0 & 0.005 \end{bmatrix} \qquad \mathbf{K}_p = \begin{bmatrix} 0.0001 & 0 & 0 \\ 0 & 0.0001 & 0 \\ 0 & 0 & 0.0001 \end{bmatrix} \tag{6.5}$$

where both $\mathbf{K}_d$ and $\mathbf{K}_p$ are diagonal matrices for simplicity .

The quaternion for the linear equations using the above gains is shown in Figure 6.3 in a close-up view.

As the magnitude of the proportional derivative, $\mathbf{K}_p$ is decreased, the frequency of oscillations decreases. If the derivative gain, $\mathbf{K}_d$ is increased, the system damps faster.

The P-D gains are implemented in the nonlinear equations for a gravity-gradient stable system. These gains also stabilize this system. The quaternion is shown in Figure 6.4 in a close-up view.

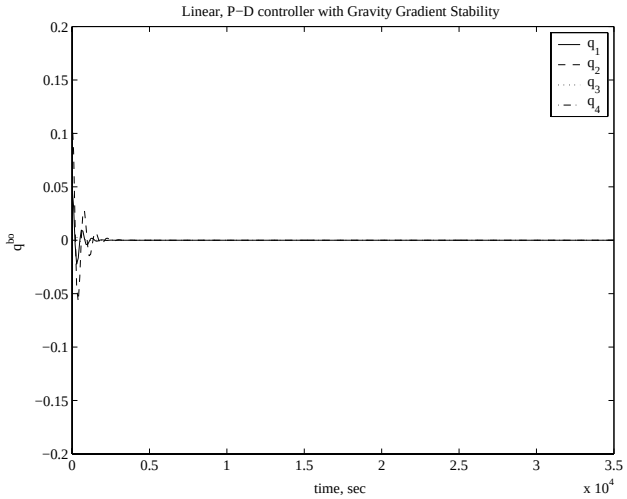

Figure 6.3: Quaternion for Linear, P-D Controller with Gravity-Gradient Stability

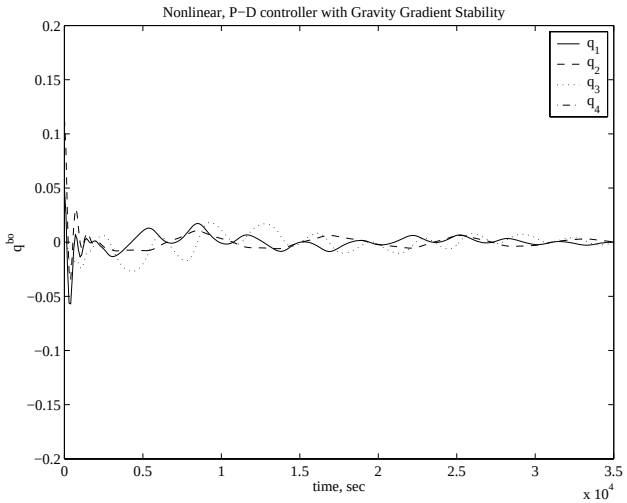

Figure 6.4: Quaternion for Nonlinear, P-D Controller with Gravity-Gradient Stability

6.3.2 Constant Coefficient Linear Quadratic Regulator

For the constant coefficient linear quadratic regulator, the value of the weight matrix, $\mathbf{Q}$, for the gravity-gradient stable equations is set equal to

$$\mathbf{Q} = \begin{bmatrix} 0.001 & 0 & 0 & 0 & 0 & 0 \\ 0 & 0.001 & 0 & 0 & 0 & 0 \\ 0 & 0 & 0.001 & 0 & 0 & 0 \\ 0 & 0 & 0 & 1 & 0 & 0 \\ 0 & 0 & 0 & 0 & 1 & 0 \\ 0 & 0 & 0 & 0 & 0 & 1 \end{bmatrix} \tag{6.6}$$

This leads to a gain matrix, $\mathbf{K}$, of

$$\mathbf{K} = \begin{bmatrix} 0.0014 & 0 & -0.0038 & 16.1206 & -0.1190 & -1.1532 \\ -0.0001 & 0.0051 & 0 & -0.0688 & 29.7242 & -0.0501 \\ 0.0121 & 0 & 0.0056 & -0.7335 & 0.0334 & 32.8568 \end{bmatrix} \tag{6.7}$$

With these gains, the eigenvalues of the $\mathcal{X}(\mathcal{T})$ matrix are located inside the unit circle, as shown in Figure 6.5.

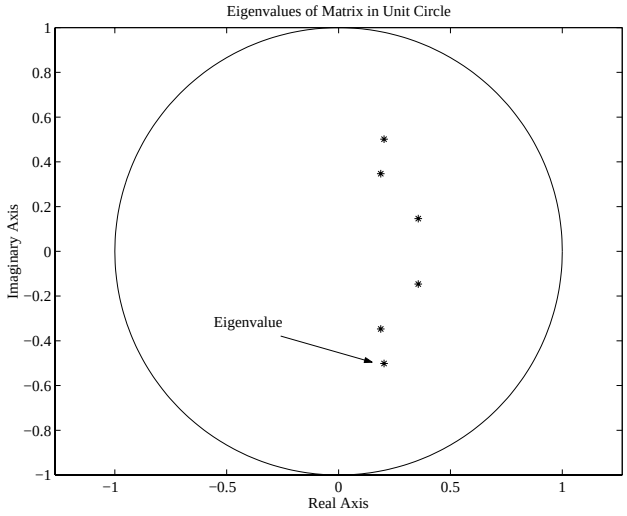

Figure 6.5: Eigenvalues of $\mathcal{X}(t)$ with Gravity-Gradient Stability

Since the eigenvalues are all inside of the unit circle, the linear equations are stable over time, as shown in Figure 6.6.

These values for the gains also stabilize the nonlinear system, as shown in Figure 6.7.

The amount of magnetic moment required to stabilize the nonlinear equations is shown in Figure 6.8.

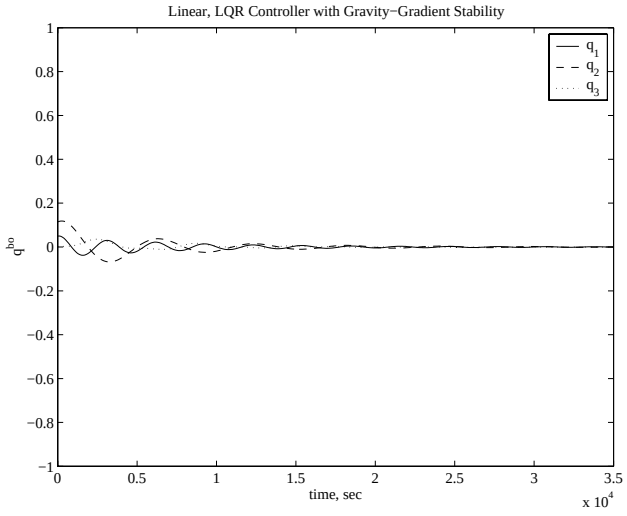

Figure 6.6: Quaternion for Linear, LQR Controller with Gravity-Gradient Stability

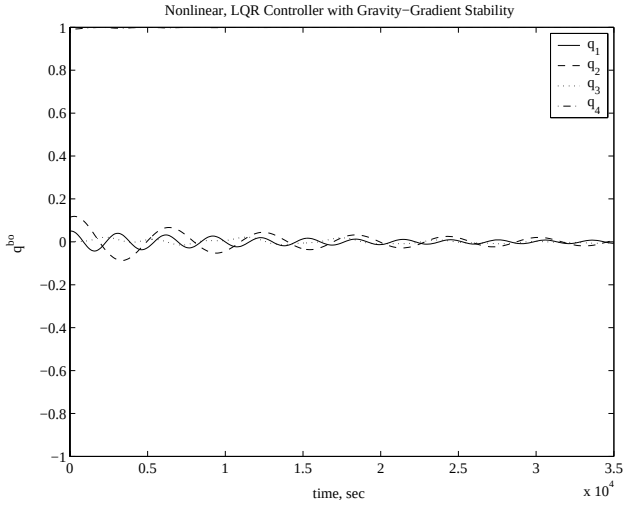

Figure 6.7: Quaternion for Nonlinear, LQR Controller with Gravity-Gradient Stability

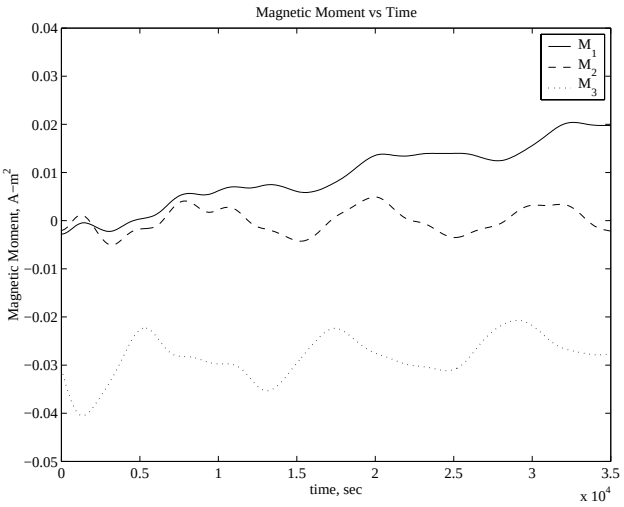

Figure 6.8: Magnetic Moment for Gravity-Gradient Stable Spacecraft

The magnetic moment required experiences long period oscillations over time. These oscillations are evident when the magnetic moment is plotted over a long period of time in Figure 6.9. In this case, one period is equal to approximately six days, and this periodic nature occurs because of the relative rotation between the Earth and the magnetic field, coupled with the orbital position. These long period oscillations exist in all of the cases examined.

6.4 Magnetic Control Without Gravity Gradient Stability

The magnetic controller is also implemented for the non gravity-gradient stable spacecraft. The results from both the P-D controller and linear quadratic regulator are examined.

6.4.1 P-D Controller

The P-D controller becomes much more complicated when the spacecraft is not gravity-gradient stable. The same $\mathbf{K}_d$ and $\mathbf{K}_p$ gains are implemented as in Section 6.3.1 in the non gravity-gradient stable spacecraft, but the resulting motion is different.

The quaternion for the linear equations of motion is shown in Figure 6.10 in a close-up view. Here, the linear system obtains the desired equilibrium using the P-D controller.

The nonlinear system, however, does not stabilize, as shown in a shortened view of Figure 6.11.

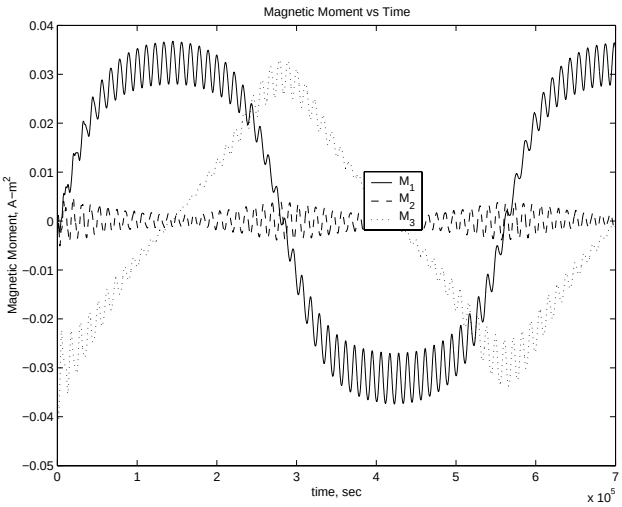

Figure 6.9: Magnetic Moment for Gravity-Gradient Stable Spacecraft Over a Long Period of Time

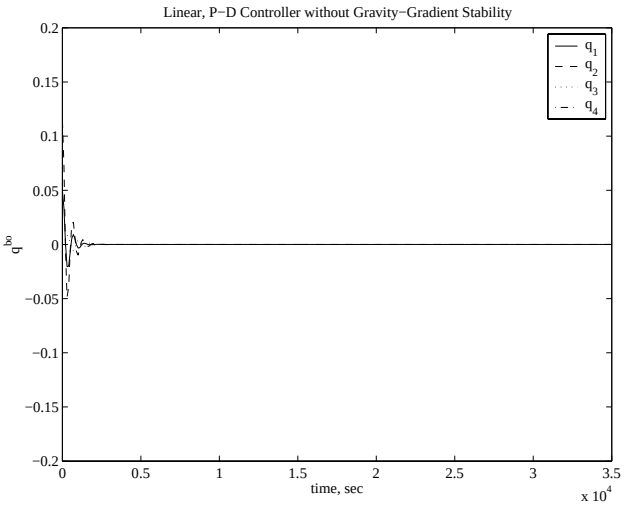

Figure 6.10: Quaternion for Linear, P-D Controller without Gravity-Gradient Stability

The nonlinear system can not be stabilized by changing the values of the gain matrices on the diagonal. Instead, it is necessary to make the off-diagonal elements non-zero. Without a method of reasonably choosing values, this method is tedious. For this reason, it is desirable to use the linear quadratic regulator method to choose the gains.

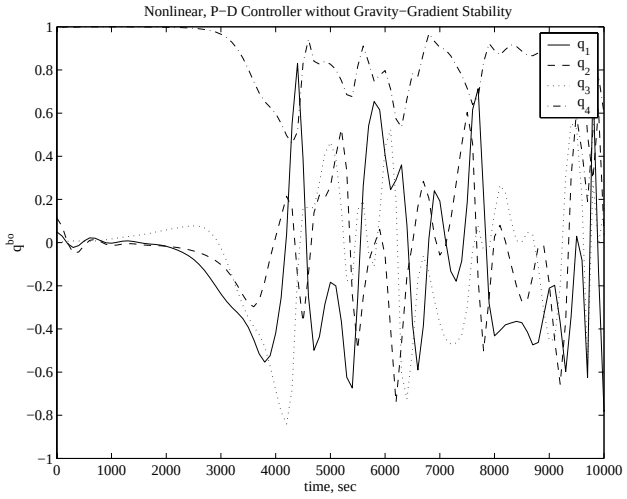

Figure 6.11: Quaternion for Nonlinear, P-D Controller without Gravity-Gradient Stability

6.4.2 Constant Coefficient Linear Quadratic Regulator

The linear quadratic regulator is beneficial when the spacecraft is not gravity-gradient stabilized. It can overcome the shortcomings of the P-D controller by determining elements in the gain matrix that are off-diagonal.

The non gravity-gradient stable spacecraft is examined with the following $\mathbf{Q}$ matrix:

$$\mathbf{Q} = \begin{bmatrix} 0.01 & 0 & 0 & 0 & 0 & 0 \\ 0 & 0.01 & 0 & 0 & 0 & 0 \\ 0 & 0 & 0.01 & 0 & 0 & 0 \\ 0 & 0 & 0 & 1 & 0 & 0 \\ 0 & 0 & 0 & 0 & 1 & 0 \\ 0 & 0 & 0 & 0 & 0 & 1 \end{bmatrix} \tag{6.8}$$

which leads to a gain matrix of

$$\mathbf{K} = \begin{bmatrix} 0.1272 & 0.0001 & -0.0916 & 154.2954 & 0.1902 & -22.4310 \\ 0.0006 & 0.1268 & 0.0001 & 0.2020 & 125.3893 & 0.7256 \\ 0.1110 & 0 & 0.0668 & -8.7619 & 0.1873 & 146.5544 \end{bmatrix} \tag{6.9}$$

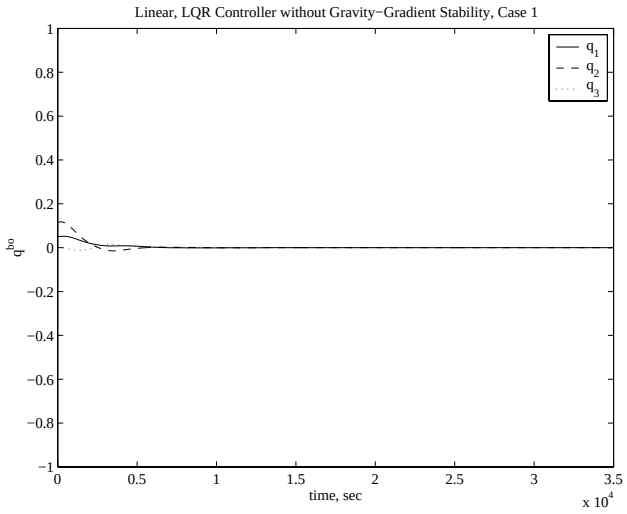

Figure 6.12: Quaternion for Linear, LQR Controller Without Gravity-Gradient Stability, Case 1

The linear equations are stable over time, as shown in Figure 6.12.

Unlike the nonlinear P-D controller, the nonlinear LQR controller without gravity-gradient stability is also stable over time. This is shown in Figure 6.13.

The amount of magnetic moment required with the nonlinear stabilization is shown in Figure 6.14.

However, it is important to note that if the linear system is stable, the nonlinear system is not necessarily also stable. This is apparent with a $\mathbf{Q}$ value of

$$\mathbf{Q} = \begin{bmatrix} 0.001 & 0 & 0 & 0 & 0 & 0 \\ 0 & 0.001 & 0 & 0 & 0 & 0 \\ 0 & 0 & 0.001 & 0 & 0 & 0 \\ 0 & 0 & 0 & 1 & 0 & 0 \\ 0 & 0 & 0 & 0 & 1 & 0 \\ 0 & 0 & 0 & 0 & 0 & 1 \end{bmatrix} \tag{6.10}$$

and gains of

$$\mathbf{K} = \begin{bmatrix} 0.0605 & 0 & -0.0377 & 90.2200 & 0.0687 & 0.7348 \\ 0.0007 & 0.0636 & 0 & 0.1110 & 88.8296 & 0.7348 \\ 0.0785 & 0.0001 & 0.0157 & 2.4290 & 0.2100 & 87.1211 \end{bmatrix} \tag{6.11}$$

The linear quaternion over time is stable, and shown in Figure 6.15. The nonlinear quaternion, shown in Figure 6.16 in an extended view, is not. It oscillates about the desired position, but does not damp.

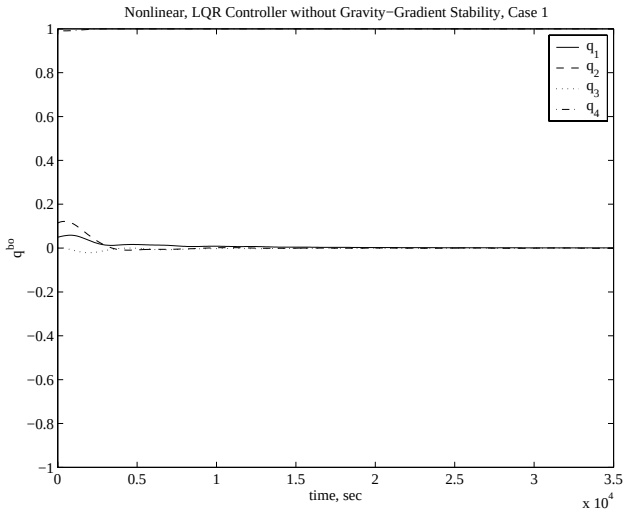

Figure 6.13: Quaternion for Nonlinear, LQR Controller Without Gravity-Gradient Stability, Case 1

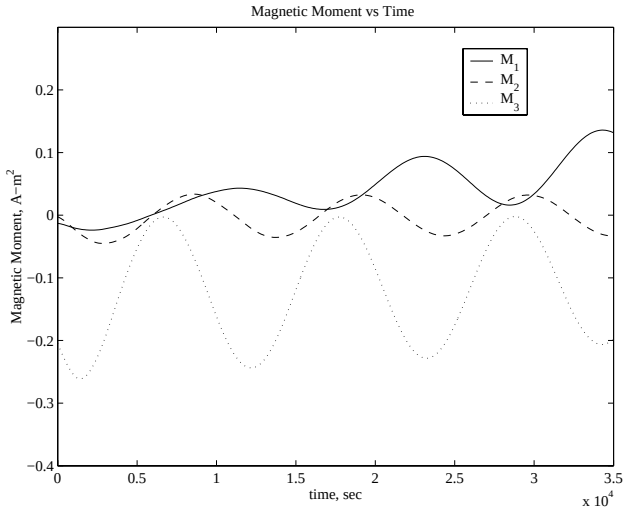

Figure 6.14: Magnetic Moment for Non Gravity-Gradient Stable Spacecraft

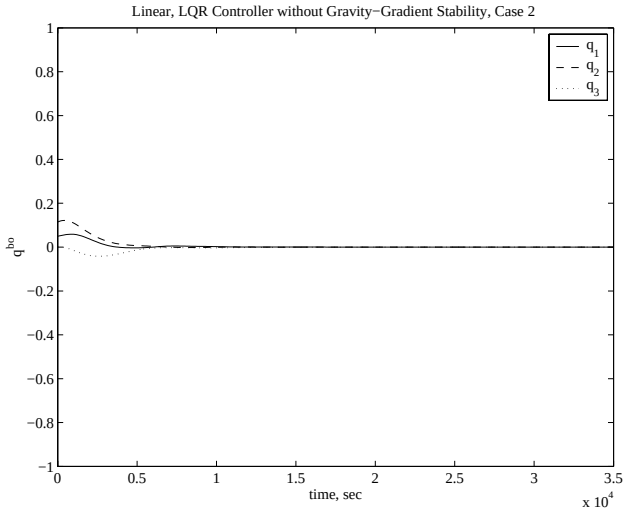

Figure 6.15: Quaternion for Linear, LQR Controller Without Gravity-Gradient Stability, Case 2

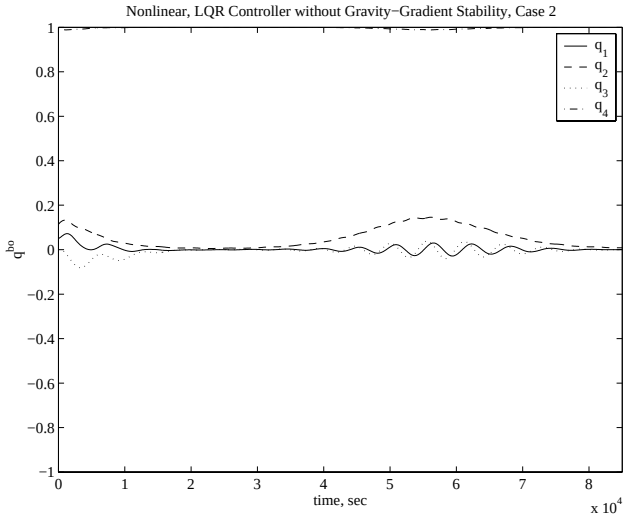

Figure 6.16: Quaternion for Nonlinear, LQR Controller Without Gravity-Gradient Stability, Case 2

6.5 Optimization of Q

With the linear quadratic regulator, if the eigenvalues of $\mathcal{X}(t)$ are located outside the unit circle, the linear system is unstable. One simple method of obtaining stable $\mathbf{Q}$ values that can be implemented involves examining the eigenvalues and their eigenvectors. The largest eigenvalue is identified, and the corresponding eigenvector is isolated. The $\mathbf{Q}$ element corresponding to the largest value in the isolated eigenvector is altered. This method consists of trial and error and does not always provide favorable results. For this reason, an optimization technique is implemented.

The Nelder-Mead Simplex[24] is used to find the optimum value of $\mathbf{Q}$ that minimizes the eigenvalues of $\mathcal{X}(t)$ for the linear quadratic regulator.

6.5.1 Gravity-Gradient Stable

The $\mathbf{Q}$ values for the gravity-gradient stable spacecraft is optimized and the results are compared with the non-optimized case. A $\mathbf{Q}$ value of

$$\mathbf{Q}_1 = \begin{bmatrix} 0.001 & 0 & 0 & 0 & 0 & 0 \\ 0 & 0.001 & 0 & 0 & 0 & 0 \\ 0 & 0 & 0.001 & 0 & 0 & 0 \\ 0 & 0 & 0 & 1 & 0 & 0 \\ 0 & 0 & 0 & 0 & 1 & 0 \\ 0 & 0 & 0 & 0 & 0 & 1 \end{bmatrix} \tag{6.12}$$

was examined in Section 6.3.2. An optimized $\mathbf{Q}$ with $\mathbf{Q}_1$ as an initial condition is equal to

$$\mathbf{Q}_2 = \begin{bmatrix} 0.0131 & 0 & 0 & 0 & 0 & 0 \\ 0 & 0.0065 & 0 & 0 & 0 & 0 \\ 0 & 0 & 0.0062 & 0 & 0 & 0 \\ 0 & 0 & 0 & 0.2206 & 0 & 0 \\ 0 & 0 & 0 & 0 & 9.047 & 0 \\ 0 & 0 & 0 & 0 & 0 & 2.9558 \end{bmatrix} \tag{6.13}$$

with

$$\mathbf{K} = \begin{bmatrix} 0.0209 & 0 & -0.0085 & 55.7854 & -0.1676 & -3.4864 \\ -0.0004 & 0.0294 & -0.0001 & -0.1466 & 71.5140 & -0.0617 \\ 0.0223 & 0 & 0.0305 & -2.3105 & 0.1207 & 77.1279 \end{bmatrix} \tag{6.14}$$

The optimized linear equations are stable over time, as shown in Figure 6.17. When comparing Figure 6.6 with no optimization to Figure 6.17, it is noted that using the optimization technique causes the quaternion to damp faster. This faster damping is because the eigenvalues are further inside the unit circle.

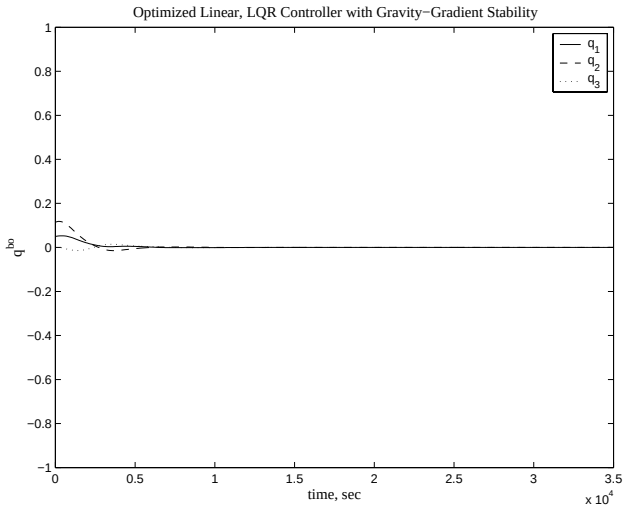

Figure 6.17: Optimized Linear Gravity-Gradient Stable Quaternion

The nonlinear equations are also stable over time with these $\mathbf{Q}$. These are shown in Figure 6.18. The quaternions with no optimization in Figure 6.7 do not damp as fast as the optimized ones.

The amount of magnetic moment required is shown in Figure 6.19. While the optimized equations damp faster, they require more magnetic moment, which is shown in the comparison of Figures 6.8 and 6.19.

6.5.2 Non Gravity-Gradient Stable

The non gravity-gradient stable configurations were discussed in Section 6.4.2. There, it was shown that even if the linear converges to the desired orientation, the nonlinear does not necessarily do the same.

When $\mathbf{Q}$ is equal to

$$\mathbf{Q}_1 = \begin{bmatrix} 0.001 & 0 & 0 & 0 & 0 & 0 \\ 0 & 0.001 & 0 & 0 & 0 & 0 \\ 0 & 0 & 0.001 & 0 & 0 & 0 \\ 0 & 0 & 0 & 1 & 0 & 0 \\ 0 & 0 & 0 & 0 & 1 & 0 \\ 0 & 0 & 0 & 0 & 0 & 1 \end{bmatrix} \tag{6.15}$$

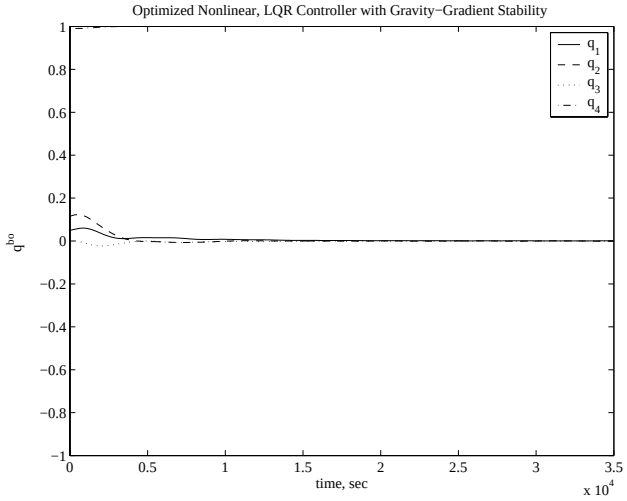

Figure 6.18: Optimized Nonlinear Gravity-Gradient Stable Quaternion

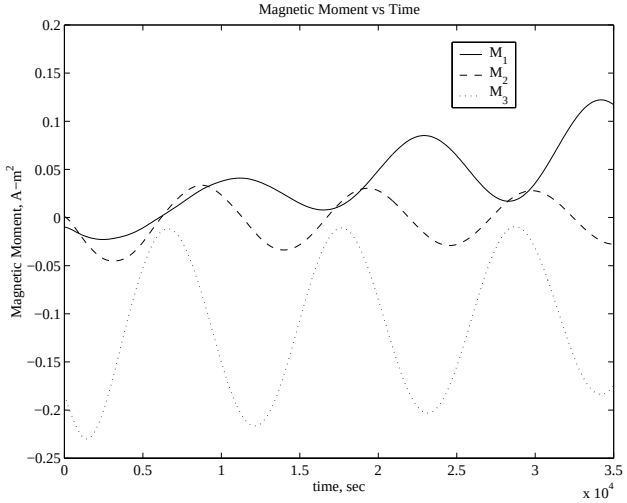

Figure 6.19: Optimized Nonlinear Gravity-Gradient Stable Magnetic Moment

it optimizes to

$$\mathbf{Q}_2 = \begin{bmatrix} 0.0062 & 0 & 0 & 0 & 0 & 0 \\ 0 & 0.0042 & 0 & 0 & 0 & 0 \\ 0 & 0 & 0.0108 & 0 & 0 & 0 \\ 0 & 0 & 0 & 0.9929 & 0 & 0 \\ 0 & 0 & 0 & 0 & 3.9543 & 0 \\ 0 & 0 & 0 & 0 & 0 & 0.7642 \end{bmatrix} \tag{6.16}$$

with gains of

$$\mathbf{K} = \begin{bmatrix} 0.1149 & 0.0001 & -0.0973 & 151.3005 & 0.1872 & -27.7954 \\ 0.0006 & 0.0930 & 0.0001 & 0.1293 & 107.4339 & 0.7625 \\ 0.0985 & 0.0001 & 0.0636 & -10.8590 & 0.2085 & 137.1822 \end{bmatrix} \tag{6.17}$$

The quaternion for the linear equations with $\mathbf{Q}_2$ is shown in Figure 6.20. This damps faster than the quaternion in Figures 6.12 and 6.15.

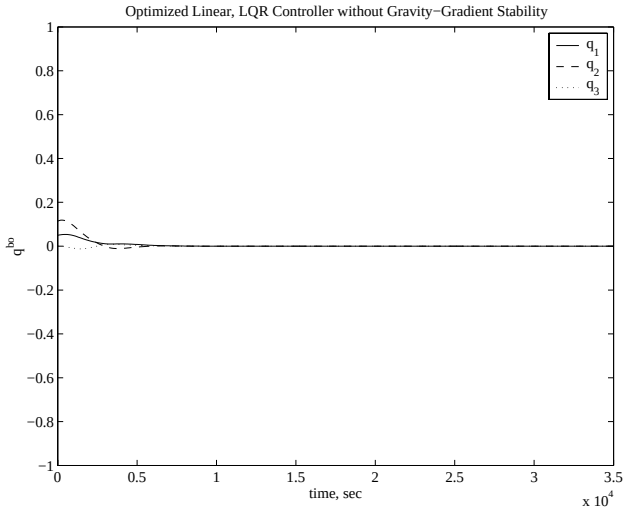

Figure 6.20: Optimized Linear Non Gravity-Gradient Stable Quaternion

The eigenvalues for the optimized system are closer to the center of the unit circle, as shown in Figure 6.21.

The quaternion for the nonlinear system is shown in Figure 6.22. Unlike Figure 6.16, this system is stable around the desired equilibrium point.

The amount of magnetic moment required is shown in Figure 6.23. When compared to Figure 6.14, it is noted that the magnitude of the magnetic moments is approximately equal.

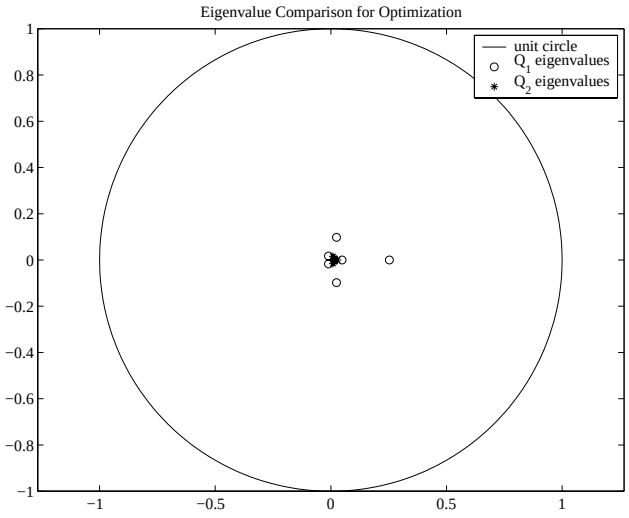

Figure 6.21: Eigenvalue Comparison for Optimization

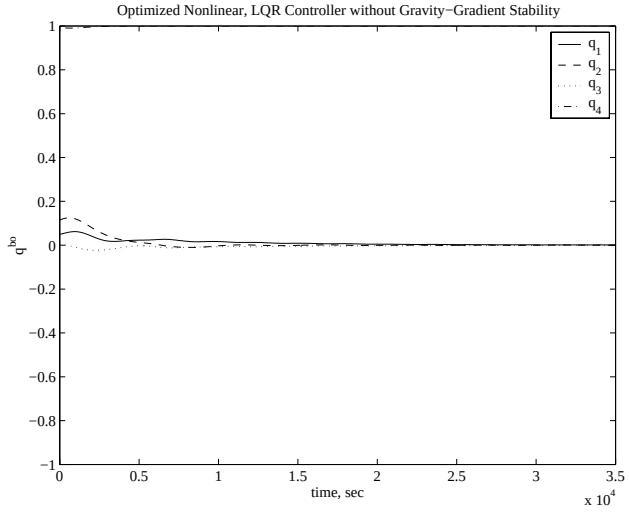

Figure 6.22: Optimized Nonlinear Non Gravity-Gradient Stable Quaternion

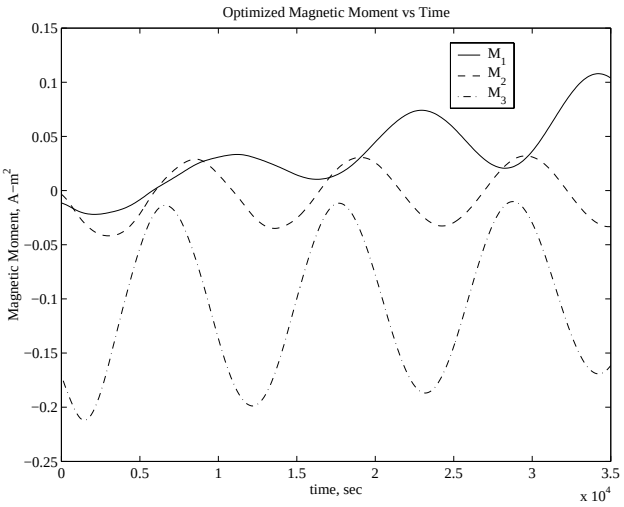

Figure 6.23: Optimized Nonlinear Non Gravity-Gradient Stable Magnetic Moment

The nonlinear equations are not always stable with optimization, however. With a non gravity-gradient stable moment of inertia matrix of

$$\mathbf{I} = \begin{bmatrix} 1 & 0 & 0 \\ 0 & 0.6 & 0 \\ 0 & 0 & 1.4 \end{bmatrix} \tag{6.18}$$

and a $\mathbf{Q}$ value of

$$\mathbf{Q}_1 = \begin{bmatrix} 1 & 0 & 0 & 0 & 0 & 0 \\ 0 & 1 & 0 & 0 & 0 & 0 \\ 0 & 0 & 1 & 0 & 0 & 0 \\ 0 & 0 & 0 & 1 & 0 & 0 \\ 0 & 0 & 0 & 0 & 1 & 0 \\ 0 & 0 & 0 & 0 & 0 & 1 \end{bmatrix} \tag{6.19}$$

both the linear and nonlinear systems are unstable because the eigenvalues of $\mathcal{X}(t)$ are outside the unit circle. Optimizing, the following $\mathbf{Q}$ matrix is obtained:

$$\mathbf{Q}_2 = \begin{bmatrix} 0.0327 & 0 & 0 & 0 & 0 & 0 \\ 0 & 1.7620 & 0 & 0 & 0 & 0 \\ 0 & 0 & 1.1213 & 0 & 0 & 0 \\ 0 & 0 & 0 & 1.5065 & 0 & 0 \\ 0 & 0 & 0 & 0 & 0.8573 & 0 \\ 0 & 0 & 0 & 0 & 0 & 1.1942 \end{bmatrix} \tag{6.20}$$

with

$$\mathbf{K} = \begin{bmatrix} 0.5392 & -0.0030 & -0.7248 & 346.2718 & -0.1119 & -243.0317 \\ 0.0026 & 1.4267 & 0.0001 & 1.0490 & 325.7985 & 0.7905 \\ 0.2346 & -0.0026 & 0.8619 & -73.5638 & -0.2331 & 520.8340 \end{bmatrix} \tag{6.21}$$

With this optimization, the linear system is stable, and is shown in Figure 6.24.

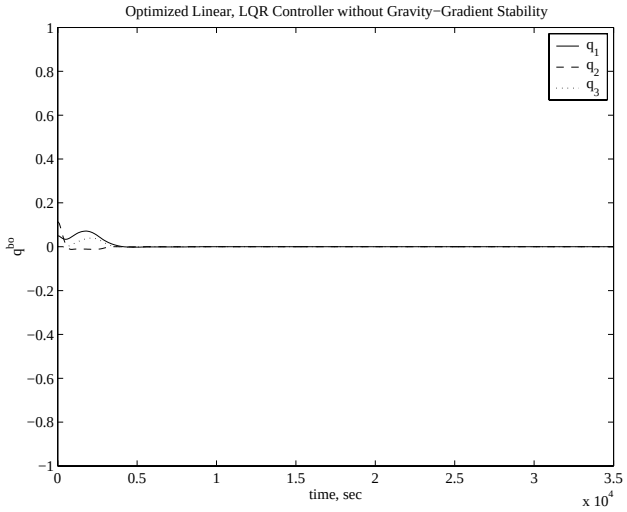

Figure 6.24: Optimized Linear Non Gravity-Gradient Stable Quaternion

The nonlinear system, however, is unstable and does not converge. Instead of using the Nelder-Mead simplex optimization, the technique of examining eigenvalues and eigenvectors from Section 5.2.4 is used to obtain a $\mathbf{Q}$ of

$$\mathbf{Q}_3 = \begin{bmatrix} 0.1 & 0 & 0 & 0 & 0 & 0 \\ 0 & 1000 & 0 & 0 & 0 & 0 \\ 0 & 0 & 0.005 & 0 & 0 & 0 \\ 0 & 0 & 0 & 1 & 0 & 0 \\ 0 & 0 & 0 & 0 & 1 & 0 \\ 0 & 0 & 0 & 0 & 0 & 1 \end{bmatrix} \tag{6.22}$$

and

$$\mathbf{K} = \begin{bmatrix} 0.5 & -0.1 & -0.1 & 261.3 & -5.1 & 42.1 \\ 0 & 31.7 & 0 & 1.1 & 1536.2 & 0.7 \\ 0.3 & -0.1 & 0.2 & 12.6 & -2.3 & 285.5 \end{bmatrix} \tag{6.23}$$

With this value of $\mathbf{Q}$, the eigenvalues are located inside the unit circle. An extended view of the quaternion implementing $\mathbf{Q}_3$ with the nonlinear equations is shown in Figure 6.25.

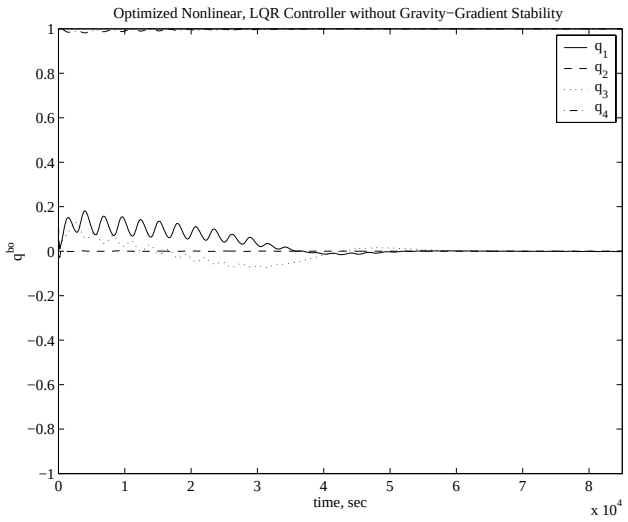

Figure 6.25: Optimized Nonlinear Non Gravity-Gradient Stable Quaternion

6.6 Inverted Spacecraft

Spacecraft occasionally become inverted upon deployment from their launch vehicles, so knowing if the attitude control system can flip the satellite is desirable. To test this case, a non gravity-gradient stabilized spacecraft is examined with the nonlinear controller. With a moment of inertia matrix of

$$\mathbf{I} = \begin{bmatrix} 1.1 & 0 & 0 \\ 0 & 1 & 0 \\ 0 & 0 & 1.2 \end{bmatrix} \tag{6.24}$$

and a rotation of 179° from desired, or

$$\bar{\mathbf{q}}^{bo} = \begin{bmatrix} 0.9999 \\ 0 \\ 0 \\ 0.0087 \end{bmatrix} \tag{6.25}$$

an initial rotation of

$$\boldsymbol{\omega}^{bo} = \begin{bmatrix} 0 \\ 1.135 \times 10^{-3} \\ 0.020 \times 10^{-3} \end{bmatrix} \tag{6.26}$$

and an initial $\mathbf{Q}$ of

$$\mathbf{Q} = \begin{bmatrix} 0.01 & 0 & 0 & 0 & 0 & 0 \\ 0 & 0.01 & 0 & 0 & 0 & 0 \\ 0 & 0 & 0.01 & 0 & 0 & 0 \\ 0 & 0 & 0 & 10 & 0 & 0 \\ 0 & 0 & 0 & 0 & 10 & 0 \\ 0 & 0 & 0 & 0 & 0 & 10 \end{bmatrix} \tag{6.27}$$

This leads to gains of

$$\mathbf{K} = \begin{bmatrix} 0.1272 & 0.0001 & -0.0916 & 154.2954 & 0.1902 & -22.4310 \\ 0.0006 & 0.1268 & 0.0001 & 0.2020 & 125.3893 & 0.7256 \\ 0.1110 & 0 & 0.0668 & -8.7619 & 0.1873 & 146.5544 \end{bmatrix} \tag{6.28}$$

The resulting quaternion over time is shown in Figure 6.26.

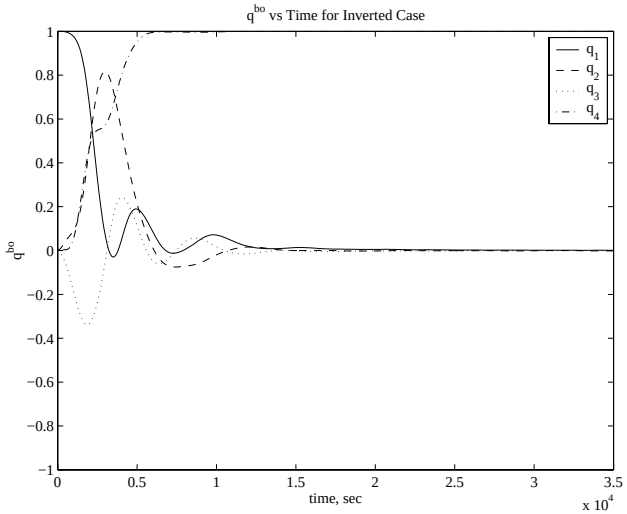

Figure 6.26: Nonlinear Quaternions for Non Gravity-Gradient Stable Inverted Spacecraft

The magnetic moment required for this maneuver with nonlinear equations is shown in Figure 6.27.

These results show that it is possible to recover an inverted spacecraft using the magnetic control laws and a finite amount of magnetic moment.

6.7 Summary

In this chapter, the control laws of Chapter 5 were implemented for various spacecraft configurations. The difference between linear and nonlinear equations was examined for gravity-

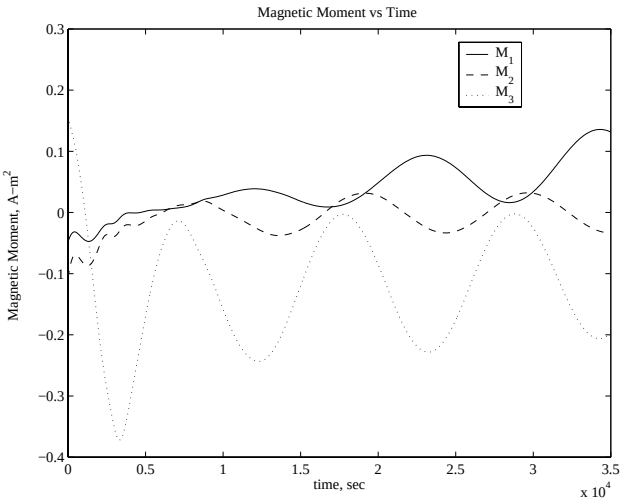

Figure 6.27: Magnetic Moment for Inverted Spacecraft

gradient and non gravity-gradient spacecraft. An optimization technique was implemented, and those results were compared with non-optimized results.

Chapter 7

Conclusion

A magnetic controller was implemented in the equations of motion of a satellite. Results are summarized below, along with recommendations for further work in this subject.

7.1 Summary

Magnetic control laws were developed to bring a spacecraft to the desired equilibrium. This was accomplished by using either a proportional-derivative controller or a constant coefficient linear quadratic regulator controller.

For the P-D controller, the proportional and derivative gains were varied in an attempt to stabilize the system.

For the LQR controller, linear time invariant equations were obtained by using the average value of the periodic variables. These equations were implemented in a linear quadratic regulator and the eigenvalues of the monodromy matrix were examined to determine stable gains for the linear time variant equations. The gains obtained from the LQR were implemented in the linear and nonlinear equations.

Simulations were performed with different spacecraft configurations and initial conditions. The gains were varied to obtain a solution for each case which damped to the desired equilibrium. These simulations lead to a procedure for designing control gains.

7.2 Contributions

In this thesis, it was determined that spacecraft can be stabilized with magnetic control, whether the configuration is gravity-gradient stable or not. This stabilization is possible by

applying magnetic moments which have magnitudes that are reasonable for small satellites.

The linear equations are only a good approximation of the nonlinear system when the initial conditions of the system are close to the desired equilibrium. In addition, the check for stability using Floquet theory is only valid for the linear equations, so linear equation stability does not necessarily imply nonlinear equation stability.

In the implementation of a P-D controller, there are two gain matrices, $\mathbf{K}_d$ and $\mathbf{K}_p$, leading to a total of 18 elements that can be varied to check for stability. Both gain matrices are assumed to be diagonal to reduce the amount of elements that can be altered to six. This assumption causes non gravity-gradient stable spacecraft to be unstable with a P-D magnetic controller.

When a LQR controller is used, the $\mathbf{Q}$ matrix determines the input gain matrix. Since this 6×6 matrix is defined as diagonal, there are only six elements that can be altered, but a gain matrix with 18 elements is created from $\mathbf{Q}$. These additional off-diagonal terms make it possible to stabilize a non gravity-gradient stable spacecraft using magnetic control.

The special case of an inverted satellite poses no difficulty for the magnetic controller. Although it may take a few additional orbits to reach the desired position, it is able to do this with a finite amount of applied magnetic moment.

Using the Nelder-Mead optimization technique with the LQR is not necessarily the best way to obtain the optimum controller performance, but it does work well for select cases. Since the optimizer brings the eigenvalues of the monodromy matrix closer to zero, the linear system always damps to the desired position faster, but also requires more magnetic moment. As stated previously, linear stability does not always imply nonlinear stability, so even after optimization, the system may not be stable.

While the Nelder-Mead optimization may not always produce a stable system, it is also possible to vary the values of $\mathbf{Q}$ by examining the magnitude of the eigenvalues and eigenvectors of the $\mathcal{X}(t)$ matrix and changing select elements. Through iterations, it is possible to find a set of gains that provides three-axis stabilization for various spacecraft configurations.

7.3 Recommended Future Work

Further research on magnetic control would be beneficial in the selection of system gains. The P-D controller could be more effective if all 18 elements of the gain matrices were used, and this would most likely result in damped systems. An optimization technique that accepted constraints could be desirable for the LQR controller because the amount of applied magnetic torque could be monitored and constrained to a maximum value. In addition, a method to quantify how stable a set of gains is for the nonlinear equations would make choosing nonlinear gain values easier.

Appendix A

HokieSat ADCS

The magnetic control laws derived in this thesis are being implemented on the HokieSat satellite designed at Virginia Tech. Here, a description of the spacecraft attitude determination and control system is described.

A.1 Project Background

There has been interest in examining the practicality of using small, distributed spacecraft systems to perform the missions of larger single satellites. The University Nanosatellite Program was funded by the Department of Defense, NASA, and the Air Force Research Labs and provided ten universities with funds to design, build, and launch nanosatellites. Virginia Tech's (VT) university nanosatellite is called HokieSat, and is participating in a joint mission with spacecraft from the University of Washington (UW) and Utah State University (USU).

A.1.1 ION-F

The stack of satellites from VT, UW, and USU are known as the Ionospheric Observation Nanosatellite Formation, or ION-F. The three spacecraft will be launched from the space shuttle in a stack, and then separate to perform the mission. The ION-F mission includes performing formation flying maneuvers, using advanced hardware such as pulsed plasma thrusters and an internet-based operations center, and demonstrating distributed satellite capabilities. For this mission, the distributed capabilities are ionospheric measurements.

A.1.2 HokieSat

HokieSat is located on the bottom of the ION-F stack. It is hexagonal, with an 18-inch diameter and 13-inch height. Solar cells provide power and charge the batteries. HokieSat possesses a GPS receiver, and can communicate with the other two nanosatellites through a crosslink antenna. Uplinks and downlinks are available when the satellite passes over ground stations located at the universities. Orbital maneuvers are performed using pulsed plasma thrusters, and attitude maneuvers are performed using magnetic torque coils.

A.2 ADCS System Requirements

The HokieSat Attitude Determination and Control System (ADCS) is required to maintain a three-axis stabilized orientation of the spacecraft, with the bottom satellite face in the nadir direction. This requirement is fulfilled by first using the attitude determination hardware to get the current spacecraft attitude. These values are compared with the desired attitude, and the difference is computed. The attitude control hardware is then implemented to make adjustments to the spacecraft attitude.

An additional requirement of the ADCS involves yaw steering. Sets of thrusters are used for orbit maneuvering, and it is necessary to position the thrusters in the correct direction. The ADCS has the ability to yaw the spacecraft into the correct orientation prior to thrusting.

A.3 Attitude Determination

The orientation of HokieSat is determined by examining position vectors such as Sun and Earth nadir vectors. The spacecraft uses many types of determination hardware, such as cameras, a magnetometer, and rate gyros. Measurements from these devices are implemented in a Kalman filter, which outputs the spacecraft attitude measurement.

A.3.1 Magnetometer

A magnetometer is used to take measurements of the local magnetic field around the spacecraft. This measurement is compared with the calculated magnetic field for the orbital position to determine a vector from the spacecraft to the Earth.

The magnetometer is a Honeywell HMC2003 three-axis magnetic sensor,[19] and is shown in Figure A.1. It has a measurement range of 40 μGauss to ± 2 Gauss. A set/reset circuit is used to achieve the highest measurement resolution by using an on-chip current strap to reset the sensor characteristics.

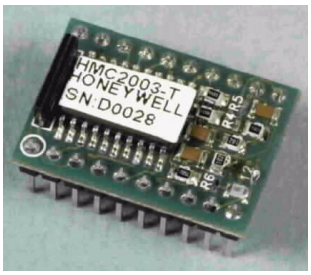

Figure A.1: HMC2003 Honeywell Magnetometer[19]

A.3.2 Cameras

Four Earth-Sun sensing cameras are used to determine a horizon and a Sun vector. The cameras are located on alternating side panels 120° apart, as well as on the top surface of the satellite.

The cameras, shown in Figure A.2, are Fuga 15d CMOS cameras,[45] and take black and white digital pictures with a 512×512 pixel resolution. The pictures are analyzed by scanning for horizon lines, as well as the Sun. The field of view of the lenses is 67°, so there are some gaps in coverage around the spacecraft. These gaps do not degrade the quality of the measurements, however, since each camera is used to detect separate data points and a full representation of the horizon is not required. At the initial spacecraft altitude of 380 km, the horizon is in view of all three side cameras even when the satellite is rotated up to 15° from nadir pointing, and is in view of at least one camera for all other orientations.

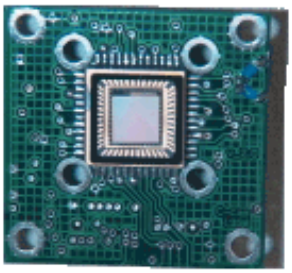

Figure A.2: Fuga 15d Camera[45]

The algorithms for Sun vector and horizon vector determination are complicated because when the Earth is partially shadowed, the terminator instead of the horizon is detected. In addition, distinguishing between the Sun and horizon is a challenge. Further information on the implementation and use of the camera for horizon and Sun sensing is detailed by Meller, Sripruetkiat, and Makovec.[28]

A.3.3 Rate Gyro

Rate gyros are used to determine the angular spin rate of the spacecraft. The gyros, shown in Figure A.3, are QRS11 GyroChips from BEI Systron Donner Inerial Division.[5] They have a range of 10°/s and are made of crystalline quartz.

Figure A.3: QRS11 Systron Donner Rate Gyro[5]

The three gyros are mounted orthogonal to each other so that the angular rate can be determined in three-axis applications.

A.3.4 Sun Sensor

Measurements from solar cells mounted on the outer panels of the spacecraft are used for a coarse sun vector estimate. This estimate is based on the analog sun sensors, or cosine Sun detectors, described by Sidi.[38] It uses the theory that if the angle between the direction to the Sun and the normal vector of the sun detector is 0°, the full intensity of the Sun, K, is detected. At other angles, only the intensity times the cosine of the angle is detected, as shown in Figure A.4.

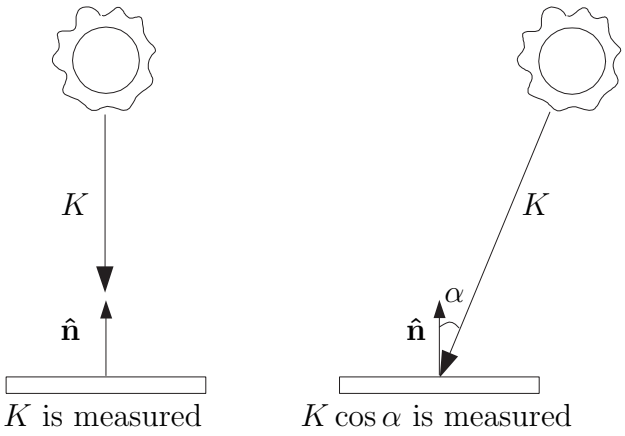

Figure A.4: Sun Sensor Detection

Sidi develops a two-axis Sun sensor, as well as a three-axis Sun sensor which assumes two sets of two sensors placed at 90° to each other. The geometry of HokieSat does not allow this technique to be directly applied, but the basic idea is expanded.

On HokieSat, a Sun sensor can be implemented by examining the characteristics of solar cells on three adjoining panels, *i.e.* a corner, of the spacecraft. A Sun vector can be determined for each set of adjacent panels in which solar cells on all three faces of the corner detect the Sun. The angle between the Sun vector and the normal vector to the spacecraft panel is determined by examining the measured current from the solar panels and determining the cosine relation. Once the angle is known, the possible locations of the Sun vector trace out the shape of a cone on each panel. This is shown in Figure A.5. The location of intersection of the three cones on adjoining sides represents the direction of the Sun vector. This calculation uses the assumption that the Sun is located at a far distance so that the distance between the spacecraft panels can be neglected.

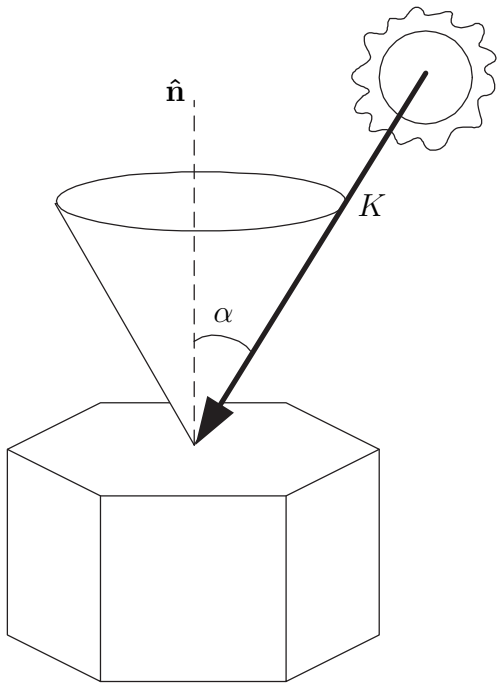

Figure A.5: Sun Sensor Cone of Possibilities

A.4 Attitude Control

HokieSat uses three orthogonal torque coils for attitude control. Control laws developed in this thesis determine the amount of magnetic moment required for stabilization or three-axis

control. This magnetic moment is converted to current values for each torque coil based on the coil characteristics.

A.4.1 Torque Coil Sizing

The torque coils are sized in a tradeoff between minimizing the power and mass, and maximizing the magnetic moment output. These three characteristics are related through the equation for magnetic moment in a coil of wire from Section 4.1.1, which is repeated here for one coil as

$$M = INA \tag{A.1}$$

where I is the applied current, N is the number of turns of wire, and A is the area of the coil. The amount of current applied is dependent on the power, and the magnetic moment output depends on the mass by way of the coil area and number of turns. For HokieSat, the possible area of the coils was known. In addition, computer simulations determined the maximum required magnetic moment for stabilization.

The power required was determined by

$$P = I^2R \tag{A.2}$$

where R is the resistance determined by

$$R = \frac{\ell_w \hat{R}}{A_w} \tag{A.3}$$

The resistivity of copper wire, $\hat{R}$, is 1.70×10^{-8} $\Omega-$m. The cross-sectional area of the wire is A_w, and the length of the wire, ℓ_w, is determined by

$$\ell_w = N \times p_c \tag{A.4}$$

where p_c is the perimeter of the coil.

The mass of the coil, m_c, is calculated by knowing the mass per unit length of the wire and implementing

$$m_c = (\text{mass/length}) N p_c \tag{A.5}$$

Equations A.1 through A.4 are combined to obtain the number of turns of wire required as a function of magnetic moment, power, coil size, and wire characteristics:

$$N = \frac{4M^2 p_c \hat{R}}{P {A_c}^2 \pi {d_w}^2} \tag{A.6}$$

where d_w is the diameter of the wire.

Table A.1: Magnet Wire Characteristics (Adapted from Ref. 14)

Gauge	Cross-sectional Area mm^2	Diameter mm	Mass/Length kg/km
18	0.823	1.024	7.32
24	0.205	0.511	1.82
30	0.051	0.254	0.45
36	0.013	0.127	0.11

The characteristic of various gauges of copper wire are displayed in Table A.1.

On HokieSat, there is one hexagonal coil on the top face with an inside major radius inscribed in a circle of radius 5.69 inches. There are two rectangular coils located adjacent to side panels, which are mutually orthogonal along with the hexagonal coil. The rectangular coils have inner dimensions of 7×9 inches.

The mass was calculated for varying wire gauge and power inputs. With a required magnetic moment of 0.9 Am^2 and 24 gauge wire, the following results are obtained for a maximum power of 0.25W:

Table A.2: HokieSat Torque Coil Characteristics

	Hexagonal Coil	Rectangular Coil
Number of turns	80	133
Mass, kg	0.128	0.200
Power, W	0.25	0.25

Changing the gauge of the wire has little effect on the mass of the system but it does have significant consequences for the power.

A.4.2 Torque Coil Composition

The HokieSat torque coils are made from windings of 24-gauge magnet wire. This wire size provides a compromise between smaller wire which is easier to wind but requires more turns, and larger wire which does not bend into a shape as easily but requires less turns of wire. In addition, the resistance of the wire is taken into account because with a thinner wire, the resistance is greater, which requires a higher voltage to obtain a similar current.

Magnet wire is copper wire covered with a polyurethane film. The polyurethane insulates each individual wire from the others in the winding.

After the magnet wire is wound on a rigid frame, the torque coil is coated with an epoxy for stiffness, and then a layer of Kapton Tape is wrapped around the finished product.

Appendix B

International Geomagnetic Reference Field

The coefficients from the International Geomagnetic Reference Field from 1900 to 2000 are listed in Table B.1, along with the secular variation terms valid for the years 2000 to 2005.

Table B.1: Spherical Harmonic Coefficients of the IGRF-DGRF models over the 20^{th} Century (Adapted from Ref. 8)

g/h	IGRF 1900	IGRF 1920	IGRF 1940	DGRF 1960	DGRF 1980	DGRF 1985	DGRF 1990	IGRF 1995	IGRF 2000	SV 2000-5
g_1^0	-31543	-31060	-30654	-30421	-29992	-29873	-29775	-29682	-29615	14.6
g_1^1	-2298	-2317	-2292	-2169	-1956	-1905	-1848	-1789	-1728	10.7
h_1^1	5922	5845	5821	5791	5604	5500	5406	5318	5186	-22.5
g_2^0	-677	-839	-1106	-1555	-1997	-2072	-2131	-2197	-2267	-12.4
g_2^1	2905	2959	2981	3002	3027	3044	3059	3074	3072	1.1
h_2^1	-1061	-1259	-1614	-1967	-2129	-2197	-2279	-2356	-2478	-20.6
g_2^2	924	1407	1566	1590	1663	1687	1686	1685	1672	-1.1
h_2^2	1121	823	528	206	-200	-306	-373	-425	-458	-9.6
g_3^0	1022	1111	1240	1302	1281	1296	1314	1329	1341	0.7
g_3^1	-1469	-1600	-1790	-1992	-2180	-2208	-2239	-2268	-2290	-5.4
h_3^1	-330	-445	-499	-414	-336	-310	-284	-263	-227	6
g_3^2	1256	1205	1232	1289	1251	1247	1248	1249	1253	0.9
h_3^2	3	103	163	224	271	284	293	302	296	-0.1
g_3^3	572	839	916	878	833	829	802	769	715	-7.7
h_3^3	523	293	43	-130	-252	-297	-352	-406	-492	-14.2
g_4^0	876	889	914	957	938	936	939	941	935	-1.3
g_4^1	628	695	762	800	782	780	780	782	787	1.6
h_4^1	195	220	169	135	212	232	247	262	272	2.1
g_4^2	660	616	550	504	398	361	325	291	251	-7.3

g/h	IGRF 1900	IGRF 1920	IGRF 1940	DGRF 1960	DGRF 1980	DGRF 1985	DGRF 1990	IGRF 1995	IGRF 2000	SV 2000-5
h_4^2	-69	-134	-252	-278	-257	-249	-240	-232	-232	1.3
g_4^3	-361	-424	-405	-394	-419	-424	-423	-421	-405	2.9
h_4^3	-210	-153	-72	3	53	69	84	98	119	5.0
g_4^4	134	199	265	269	199	170	141	116	110	-3.2
h_4^4	-75	-57	-141	-255	-297	-297	-299	-301	-304	0.3
g_5^0	-184	-221	-241	-222	-218	-214	-214	-210	-217	0.0
g_5^1	328	326	334	362	357	355	353	352	351	-0.7
h_5^1	-210	-122	-33	16	46	47	46	44	44	-0.1
g_5^2	264	236	208	242	261	253	245	237	222	-2.1
h_5^2	53	58	71	125	150	150	154	157	172	0.6
g_5^3	5	-23	-33	-26	-74	-93	-109	-122	-131	-2.8
h_5^3	-33	-38	-75	-117	-151	-154	-153	-152	-134	1.7
g_5^4	-86	-119	-141	-156	-162	-164	-165	-167	-169	-0.8
h_5^4	-124	-125	-113	-114	-78	-75	-69	-64	-40	1.9
g_5^5	-16	-62	-76	-63	-48	-46	-36	-26	-12	2.5
h_5^5	3	43	69	81	92	95	97	99	107	0.1
g_6^0	63	61	57	46	48	53	61	66	72	1.0
g_6^1	61	55	54	58	66	65	65	64	68	-0.4
h_6^1	-9	0	4	-10	-15	-16	-16	-16	-17	-0.2
g_6^2	-11	-10	-7	1	42	51	59	65	74	0.9
h_6^2	83	96	105	99	93	88	82	77	64	-1.4
g_6^3	-217	-233	-249	-237	-192	-185	-178	-172	-161	2.0
h_6^3	2	11	33	60	71	69	69	67	65	0.0
g_6^4	-58	-46	-18	-1	4	4	3	2	-5	-0.6
h_6^4	-35	-22	-15	-20	-43	-48	-52	-57	-61	-0.8
g_6^5	59	44	18	-2	14	16	18	17	17	-0.3
h_6^5	36	18	0	-11	-2	-1	1	4	1	0.0
g_6^6	-90	-101	-107	-113	-108	-102	-96	-94	-91	1.2
h_6^6	-69	-57	-33	-17	17	21	24	28	44	0.9
g_7^0	70	73	74	67	72	74	77	78	79	-0.4
g_7^1	-55	-54	-53	-56	-59	-62	-64	-67	-74	-0.4
h_7^1	-45	-49	-52	-55	-82	-83	-80	-77	-65	1.1
g_7^2	0	2	4	5	2	3	2	1	0	-0.3
h_7^2	-13	-14	-18	-28	-27	-27	-26	-25	-24	0.0
g_7^3	34	29	20	15	21	24	26	29	33	1.1
h_7^3	-10	-13	-14	-6	-5	-2	0	3	6	0.3
g_7^4	-41	-37	-31	-32	-12	-6	-1	4	9	1.1
h_7^4	-1	4	7	7	16	20	21	22	24	-0.1
g_7^5	-21	-16	-9	-7	1	4	5	8	7	-0.2

g/h	IGRF 1900	IGRF 1920	IGRF 1940	DGRF 1960	DGRF 1980	DGRF 1985	DGRF 1990	IGRF 1995	IGRF 2000	SV 2000-5
h_7^5	28	28	29	23	18	17	17	16	15	-0.6
g_7^6	18	19	17	17	11	10	9	10	8	0.6
h_7^6	-12	-16	-20	-18	-23	-23	-23	-23	-25	-0.7
g_7^7	6	6	5	8	-2	0	0	-2	-2	-0.9
h_7^7	-22	-22	-19	-17	-10	-7	-4	-3	-6	0.2
g_8^0	11	11	11	15	18	21	23	24	25	-0.3
g_8^1	8	7	7	6	6	6	5	4	6	0.2
h_8^1	8	8	8	11	7	8	10	12	12	0.1
g_8^2	-4	-3	-3	-4	0	0	-1	-1	-9	-0.3
h_8^2	-14	-15	-14	-14	-18	-19	-19	-20	-22	0.0
g_8^3	-9	-9	-10	-11	-11	-11	-10	-9	-8	0.4
h_8^3	7	6	5	7	4	5	6	7	8	0.0
g_8^4	1	2	1	2	-7	-9	-12	-14	-17	-1.0
h_8^4	-13	-14	-15	-18	-22	-23	-22	-21	-21	0.3
g_8^5	2	4	6	10	4	4	3	4	9	0.3
h_8^5	5	5	5	4	9	11	12	12	15	0.6
g_8^6	-9	-7	-5	-5	3	4	4	5	7	-0.5
h_8^6	16	17	19	23	16	14	12	10	9	-0.4
g_8^7	5	6	9	10	6	4	2	0	-8	-0.7
h_8^7	-5	-5	-5	1	-13	-15	-16	-17	-16	0.3
g_8^8	8	8	7	8	-1	-4	-6	-7	-7	-0.4
h_8^8	-18	-19	-19	-20	-15	-11	-10	-10	-3	0.7
g_9^0	8	8	8	4	5	5	4	4	5	0.0
g_9^1	10	10	10	6	10	10	9	9	9	0.0
h_9^1	-20	-20	-21	-18	-21	-21	-20	-19	-20	0.0
g_9^2	1	1	1	0	1	1	1	1	3	0.0
h_9^2	14	14	15	12	16	15	15	15	13	0.0
g_9^3	-11	-11	-12	-9	-12	-12	-12	-12	-8	0.0
h_9^3	5	5	5	2	9	9	11	11	12	0.0
g_9^4	12	12	11	1	9	9	9	9	6	0.0
h_9^4	-3	-3	-3	0	-5	-6	-7	-7	-6	0.0
g_9^5	1	1	1	4	-3	-3	-4	-4	-9	0.0
h_9^5	-2	-2	-3	-3	-6	-6	-7	-7	-8	0.0
g_9^6	-2	-2	-2	-1	-1	-1	-2	-2	-2	0.0
h_9^6	8	9	9	9	9	9	9	9	9	0.0
g_9^7	2	2	3	-2	7	7	7	7	9	0.0
h_9^7	10	10	11	8	10	9	8	7	4	0.0
g_9^8	-1	0	1	3	2	1	1	0	-4	0.0
h_9^8	-2	-2	-2	0	-6	-7	-7	-8	-8	0.0

g/h	IGRF 1900	IGRF 1920	IGRF 1940	DGRF 1960	DGRF 1980	DGRF 1985	DGRF 1990	IGRF 1995	IGRF 2000	SV 2000-5
g_9^9	-1	-1	-2	-1	-5	-5	-6	-6	-8	0.0
h_9^9	2	2	2	5	2	2	2	1	5	0.0
g_{10}^0	-3	-3	-3	1	-4	-4	-3	-3	-2	0.0
g_{10}^1	-4	-4	-4	-3	-4	-4	-4	-4	-6	0.0
h_{10}^1	2	2	2	4	1	1	2	2	1	0.0
g_{10}^2	2	2	2	4	2	3	2	2	2	0.0
h_{10}^2	1	1	1	1	0	0	1	1	0	0.0
g_{10}^3	-5	-5	-5	0	-5	-5	-5	-5	-3	0.0
h_{10}^3	2	2	2	0	3	3	3	3	4	0.0
g_{10}^4	-2	-2	-2	-1	-2	-2	-2	-2	0	0.0
h_{10}^4	6	6	6	2	6	6	6	6	5	0.0
g_{10}^5	6	6	6	4	5	5	4	4	4	0.0
h_{10}^5	-4	-4	-4	-5	-4	-4	-4	-4	-6	0.0
g_{10}^6	4	4	4	6	3	3	3	3	1	0.0
h_{10}^6	0	0	0	1	0	0	0	0	-1	0.0
g_{10}^7	0	0	0	1	1	1	1	1	2	0.0
h_{10}^7	-2	-2	-1	-1	-1	-1	-2	-2	-3	0.0
g_{10}^8	2	1	2	-1	2	2	3	3	4	0.0
h_{10}^8	4	4	4	6	4	4	3	3	0	0.0
g_{10}^9	2	3	3	2	3	3	3	3	0	0.0
h_{10}^9	0	0	0	0	0	0	-1	-1	-2	0.0
g_{10}^{10}	0	0	0	0	0	0	0	0	-1	0.0
h_{10}^{10}	-6	-6	-6	-7	-6	-6	-6	-6	-8	0.0

An example of the variation in the IGRF coefficients is shown in the plotting of g_1^0 in Figure B.1. The dotted line represents the secular variation, or projected value for the next five years after the last IGRF.

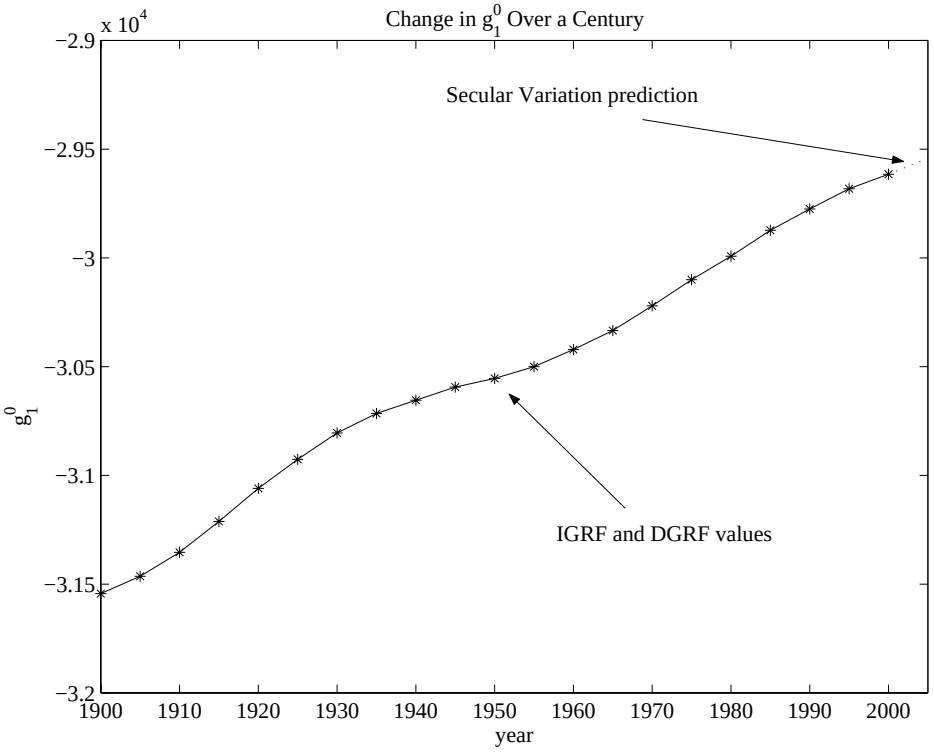

Figure B.1: Variation in the IGRF Coefficient g_1^0

References

[1] Anon. Magnetic Fields - Earth and Extraterrestrial. Technical Report NASA SP-8017, National Aeronautics and Space Administration, March 1969.

[2] Anon. Spacecraft Magnetic Torques. Technical Report NASA SP-8018, National Aeronautics and Space Administration, March 1969.

[3] Carlo Arduini and Paolo Baiocco. Active Magnetic Damping Attitude Control for Gravity Gradient Stabilized Spacecraft. *Journal of Guidance Control and Dynamics*, 20(1):117–122, January-February 1997.

[4] Roger R. Bate, Donald D. Mueller, and Jerry E. White. *Fundamentals of Astrodynamics*. Dover Publications, Inc, New York, 1971.

[5] BEI Syston Donner Inertial Division. *QRS11 Rate Sensor Data Sheet*. http://www.systron.com.

[6] Wallace H. Campbell. *Introduction to Geomagnetic Fields*. Cambridge University Press, Cambridge, 1997.

[7] Vladimir A. Chobotov. *Spacecraft Attitude Dynamics and Control*. Orbit Foundation Series. Krieger Publishing Company, Malabar, Florida, 1991.

[8] Division V, Working Group 8. *International Geomagnetic Reference Field - 2000*. International Association of Geomagnetism and Aeronomy (IAGA), 2000.

[9] E.I. Ergin and P.C. Wheeler. Magnetic Control of a Spinning Satellite. *Journal of Spacecraft and Rockets*, 2(6):846–850, November-December 1965.

[10] Dominic M. Florin. Three Axis Spacecraft Attitude Control and Dynamics with Permanent Magnets. Master's thesis, Utah State University, 2001.

[11] Mike Fuller, C. Laj, and E. Herrero-Bervera. The Reversal of the Earth's Magnetic Field. *American Scientist*, 84(6):552–561, 1996.

[12] Geological Survey of Canada. *National Geomagnetism Program*. http://www.geolab.nrcan.gc.ca/geomag.

[13] William Gilbert. *On the Magnet (De Magnete)*. The Collector's Series in Science. Basic Books, Inc., New York, 1958.

[14] Global Wire Group. *Copper Wires to AWG*. http://www.global-wire.com.

[15] P. S. Goel and S. Rojaram. Magnetic Attitude Control of a Momentum-Biased Satellite in Near-Equatorial Orbit. *Journal of Guidance and Control*, 2(4):334–338, July-August 1979.

[16] Michele Grassi. Attitude Determination and Control for a Small Remote Sensing Satellite. *Acta Astronautica*, 40(9):675–681, 1997.

[17] Christopher Hall. Attitude Determination and Control Course Notes. Virginia Tech.

[18] W.R. Hindmarsh, F.J. Lowes, P.H. Roberts, and S.K. Runcorn, editors. *Magnetism and the Cosmos*. Oliver and Boyd, London, 1967.

[19] Honeywell. *HMC2003 Data Sheet*. http://www.ssec.honeywell.com/magnetic/datasheets/hmc2003.pdf.

[20] Peter C. Hughes. *Spacecraft Attitude Dynamics*. John Wiley and Sons, New York, 1986.

[21] IMAGE Science Center. http://image.gsfc.nasa.gov.

[22] G.E. Schmidt Jr. The Application of Magnetic Attitude Control to a Momentum Biased Synchronous Communications Satellite. *AIAA Guidance and Control Conference, Boston, Massachusetts*, August 20-22 1975.

[23] J.L. Junkins, C.K. Carrington, and C.E. Williams. Time-Optimal Magnetic Attitude Control Maneuvers. *Journal of Guidance and Control*, 4(2):363–368, July-August 1981.

[24] Jeffrey C. Lagarius, James A. Reeds, Margaret H. Wright, and Paul E. Wright. Convergence Properties of the Nelder-Mead Simplex Method in Low Dimensions. *SIAM Journal on Optimization*, 9(1):112–147, 1998.

[25] Steven A. Macintyre. *The Measurement, Instrumentation and Sensors Handbook*, chapter Magnetic Field Measurement. CRC Press LLC, 1999.

[26] Francois Martel, Parimal K. Pal, and Mark Psiaki. Active magnetic control system for gravity gradient stabilized spacecraft. *Proceedings of the Second Annual AIAA/USU Conference on Small Satellites*, pages 1–19, September 1988.

[27] Leonard Meirovitch. *Methods of Analytical Dynamics*. McGraw-Hill, Inc., New York, 1988.

[28] David Meller, Prapat Sripruetkiat, and Kristin Makovec. Digital CMOS Cameras for Attitude Determination. *Proceedings of the 14th AIAA/USU Conference on Small Satellites, Logan, Utah*, pages 1–12, August 2000. SSC00-VII-1.

[29] Ronald T. Merrill and Michael W. McElhinny. *Earth's Magnetic Field*. Academic Press, New York, 1983.

[30] Keith L. Musser and Ward L. Ebert. Autonomous spacecraft attitude control using magnetic torquing only. *Flight Mechanics/Estimation Theory Symposium*, pages 23–38, May 23-24 1989. NASA Conference Publication.

[31] National Geophysical Data Center. *The Geomagnetic Field*. http://www.ngdc.noaa.gov.

[32] Carl R. Nave. *HyperPhysics*. Georgia State University, 2000. http://hyperphysics.phy-astr.gsu.edu/hbase/hframe.html.

[33] Mark L. Renard. Command Laws for Magnetic Attitude Control of Spin-Stabilized Earth Satellites. *Journal of Spacecraft and Rockets*, 4(2):156–163, February 1967.

[34] Francis W. Sears, Mark W. Zemansky, and Hugh D. Young. *University Physics*. Addison-Wesley Publishing Company, Reading, Massachusetts, fifth edition, 1979.

[35] Ye Shi-hui. *Magnetic Fields of Celestial Bodies*. Kluwer Academic Publishers, Dordrecht, 1994.

[36] Masamichi Shigehara. Geomagnetic Attitude Control of an Axisymmetric Spinning Satellite. *Journal of Spacecraft and Rockets*, 9(6):391–398, June 1972.

[37] M.D. Shuster and S.D. Oh. Three Axis Attitude Determination From Vector Observations. *Journal of Guidance, Control and Navigation*, 4(1):70–77, January-February 1981.

[38] Marcel J. Sidi. *Spacecraft Dynamics and Control, A Practical Engineering Approach*. Cambridge Aerospace Series. Cambridge University Press, Cambridge, 1997.

[39] John A. Sorenson. A Magnetic Attitude Control System for an Axisymmetric Spinning Spacecraft. *Journal of Spacecraft and Rockets*, 8(5):441–448, May 1971.

[40] A. Craig Stickler and K. T. Alfriend. Elementary Magnetic Attitude Control System. *Journal of Spacecraft and Rockets*, 13(5):282–287, May 1976.

[41] Sunspot Index Data Center. *World Data Center for the Sunspot Index*. Brussels. http://sidc.oma.be.

[42] Roy Thompson and Frank Oldfield. *Environmental Magnetism*. Allen and Unwin, London, 1986.

[43] United States Geological Survey. *Geomagnetism*. http://geomag.usgs.gov.

[44] U.S. Naval Observatory. *Web MICA (Multiyear Interactive Computer Almanac)*. http://aa.usno.navy.mil/data/docs/WebMICA_2.html.

[45] Vector International. *Fuga 15d Data Sheet*. http://www.vector-international.be/C-Cam/sensors.html.

[46] James R. Wertz, editor. *Spacecraft Attitude Determination and Control*. Kluwer Academic Publishers, Dordrecht, 2000.

[47] James R. Wertz and Wiley J. Larson, editors. *Space Mission Analysis and Design*. Microcosm Press, El Segundo, California, third edition, 1999.

[48] Phillip C. Wheeler. Spinning Spacecraft Attitude Control Via the Environmental Magnetic Field. *Journal of Spacecraft and Rockets*, 4(12):1631–1637, December 1967.

[49] J. S. White, F. H. Shigemoto, and K. Bourquin. Satellite Attitude Control Utilizing the Earth's Magnetic Field. Technical Report NASA TN-D1068, National Aeronautics and Space Administration, August 1961.

[50] Rafał Wiśniewski. *Satellite Attitude Control Using Only Electromagnetic Actuation*. PhD thesis, Aalborg University, Dec 1996.

[51] Rafał Wiśniewski. Linear time varying approach to satellite attitude control using only electromagnetic actuation. *AIAA Guidance Navigation and Control Conference, New Orleans, LA*, August 11-13 1997.

Vita

Kristin Lynne Makovec grew up in Manchester Township, NJ and graduated from Manchester Township High School in 1995. She then attended Virginia Tech and majored in Aerospace Engineering. During her junior year, she was a member of General Aviation Airplane design team whose design concept, the VicTor, won first place in the 1998 AGATE design competition.

Kristin joined the HokieSat satellite design team during her senior year and was the team lead for the Attitude Determination and Control System for three years.

Kristin received her Bachelor of Science degree in Aerospace Engineering from Virginia Tech in 1999, along with minors in Math and Humanities, Science, and Technology. In 2001, she received her Master of Science degree, also from Virginia Tech, concentrating in dynamics and control. She is now continuing to work with space dynamics in the Flight Dynamics branch of NASA Goddard Space Flight Center.